UNIVERSITA' DEGLI STUDI DI CATANIA

Department of Civil Engineering and Architecture

Doctorate of Philosophy

Ingegneria dei Sistemi, Energetica, Informatica, e delle telecomunicazioni

XXIX Ciclo

===

Dott.ssa GIULIA OGNIBENE

MULTIFUNCTIONAL NANOCOMPOSITES OBTAINED BY HIERARCHICAL STRUCTURES

PhD Supervisor : Prof. G.Cicala

PhD Coordinator: Prof. P. Arena

==

2016

Table of Contents

Introduction

Multifunctional materials are a new class of materials which possess, at the same time, different properties, for examples high electrical conductivity and flame retardancy. The growing interest in this new class of materials is therefore quite clear, since they allow to obtain a material that achieves, simultaneously, to two or more functions or which has different properties depending on which part of it is used.

Based on this considerations, the main goal of this PhD project was the development of novel multifunctional composites based on the use of hierarchical structuring. The obtained multifunctional systems have been used for two different applications. In the first one, hybrid thermoplastic/carbon fabrics, by means of electrospinning, was used in order to manufacture toughened and nanorinforced (by using MWCNT) composite laminates by Resin Transfer Molding (RTM) and other infusion techniques. While in the second application, hybrid inorganic/organic membranes have been used as active membranes for water filtration in order to mitigate the fouling problem.

In the firts application CNTs were selected because, in addition to their outstanding mechanical properties, where the strength, modulus, and resilience are equal or superior to any current materials, CNTs also possess excellent electrical and thermal properties, making them attractive for enhancing a variety of matrices [1-2]. A large number of reports describe the production and characterization of CNT-based polymer [3-5], and to a lesser extent ceramic [6], composites [7]. Furthermore, Interest is, therefore, growing in the development of hierarchical (or hybrid or nanostructured or multiscale) composites, in which a nanoscale CNT reinforcement is utilised alongside traditional microscale reinforcing fibres. Hierarchical structures are widely observed in nature, e.g. in plant cell walls, animal shells and skeletons,

showing that a high mechanical performance can be obtained, even from fairly weak constituents, by structuring matter across a range of length scales [8].

The main motivation for adding CNTs to conventional fibre composites is to alleviate the existing limitations associated with the matrix dominated properties. For example, CNTs could offer both intralaminar and interlaminar reinforcement, thus improving delamination resistance and through-thickness properties, without compromising in-plane performance. The CNTs should be superior to other means of improving through-thickness performance, such as z-pinning, stitching, braiding etc., which tend to reduce the in-plane laminate performance, by disturbing and damaging the primary fibres [9]. In addition, the CNTs may introduce additional damage processes that could enhance the local toughness of the matrix during fracture.

The combination of CNTs with conventional fibre-reinforcements in polymer composites has been achieved predominantly through two different routes: dispersing CNTs entirely throughout the composite matrix or attaching CNTs directly onto primary reinforcing fibres. The most straightforward manufacturing process for hierarchical composites involves shear-mixing the CNTs into the resin system, followed by a conventional infusion/impregnation of the CNT modified resin into the primary fibre assembly. This approach generally has the advantages of simplicity and compatibility with standard industrial techniques, but, is limited to relatively low loading fractions. Moreover, other problems are correlated to the composite production techniques. Resin transfer moulding (RTM) is a typical method used in the resin infusion process for fabricating hierarchical composites [10-13]. Vacuum-assisted resin transfer moulding (VARTM) has been reported as being a more efficient route for manufacturing hierarchical composites [14-17].

One of the main problems in these approaches is that the viscosity of a CNT-modified matrix increases dramatically with increasing CNT content, leading to incomplete matrix infusion. Highly viscous or agglomerated resin systems cannot be infused using conventional composite manufacturing techniques. In addition, the size of the CNTs (or their agglomerates) can lead to filtering effects against the primary fibres, leading both to CNT segregation and depletion; this CNT concentration gradient may significantly degrade the composite performance [10-13].

Alternatives based on preparing hierarchical composite pre-pregs using filament winding via a drum winder [18-19] may have the potential to mitigate some of these issues. However, so far, the reported CNT loading fraction in the resulting hierarchical composites (after lay-up and curing in an autoclave) is in the range of 0.1–2 wt%. It is worth noting that, in all cases, the addition of CNTs, particularly of functionalized CNTs designed to react with the resin, can modify curing rates, the extent of resin conversion, and glass transition temperatures [20-21].

For all the reasons explained before, the innovative idea proposed in this PhD research was the use of filled soluble nanofibers that, placed in the interlaminar regions of the composite before the resin injection, will dissolve when the resin is inject releasing the nanofillers. With this solution, no increase in the resin viscosity is caused and is possible to have higher percentage of nanofillers. In chapter 6 the idea will be discussed in detail.

As regards the second application of multifunctional membranes, it was decided to develop "active" membranes for water filtration. The need to develop "active" membranes is due to their fouling problem. The membrane fouling describes the deposition and accumulation of rejected contaminants from the feed stream on the membrane, which results in low water quality, high operation cost, and short lifespan of membrane. In order to overcome these

limitations different methods were proposed in literature [22-23] for the removal of organic and inorganic pollutants from influents. Most of them uses heterogeneous photo-catalysis with semi-conductors that gradually breaks down the molecules of the pollutants and generates no residual by-products thus zero sludge disposal complication. "Active" membranes, in addition to acting as a mechanical filter, holding back the molecules of the polluting substances present in the water, are able to chemically degrade these molecules transforming them into non-toxic substances and therefore preventing they accumulate over the membrane compromising its efficiency over time.

The idea presented in the second part of this thesis was to develop advanced membranes for active water filtering, characterised by combined sieving, photo-catalytic and antibacterial properties. For this purpose ZnO nanowires was grown on the surface of Polyethersulfone (PES) electrospun fibres. Structured hybrid materials containing ZnO nanowires as secondary functional units grown on primary flexible substrates, exhibit highly sought-after functionalities such as bacterial repellency [24], strong UV absorption [25–29], and high photocatalytic potency in the presence of UV light [30-32]. As seen, the idea to graft inorganic nanoparticles onto organic substrates, in order to obtain flexible materials with photocatalytic properties, has already been proposed in literature, but, the novelty of the approach followed in this PhD project is to obtain these hybrid membranes by using a much simpler and economic method than those used until now. This procedure will be described in detail in Chapter 7.

Introduction References

[1] P. Harris, Int. Mater. Rev., 2004, 49, 31–43.

[2] M. Terrones, Int. Mater. Rev., 2004, 49, 325–377.

[3] M. Shaffer and J. Sandler, Processing and Properties of Nanocomposites, ed. S. G. Advani, World Scientific, New Jersey, NJ, 2007, pp. 1–59.

[4] J. N. Coleman et al., Carbon, 2006, 44, 1624– 1652.

[5] W.Wang et al., Philos. Trans. R. Soc. London, Ser. A, 2008, 366, 1613–1626.

[6] J. Cho et al., J. Mater. Sci., 2009, 44, 1934–1951.

[7] P. Harris, Carbon nanotube science:Synthesis, properties and applications, Cambridge University Press, 2009, pp. 227–246.

[8] J. Aizenberg et al., Science, 2005, 309, 275–278.

[9] L. Tong et al., 3D Fibre Reinforced Polymer Composites, Elsevier Science, Oxford, 2002, pp. 1–12.

[10] Z. H. Fan et al., Carbon, 2004, 42, 871–876.

[11] F. H. Gojny et al., Composites, Part A, 2005, 36, 1525–1535.

[12] Y. Iwahori et al., Composites, Part A, 2005, 36, 1430–1439.

[13] M. H. G. Wichmann et al., Eng. Fract. Mech., 2006, 73, 2346–2359.

[14] J. J. Qiu et al., Nanotechnology, 2007, 18, 275708–275711.

[15] R. Sadeghian et al., Composites, Part A, 2006, 37, 1787–1795.

[16] Y. X. Zhou et al., Mater. Sci. Eng., A, 2006, 426, 221–228.

[17] Y. S. Song, Polym. Compos., 2007, 28, 458–461.

[18] W. Chen et al., Composites, Part A, 2009, 40, 1082–1089.

[19] A. Godara et al., Carbon, 2009, 47, 2914–2923.

[20] J. F. Shen et al., Compos. Sci. Technol., 2007, 67, 3041–3050.

[21] S. G. Prolongo et al., Nanotechnol., 2009, 9, 6181–6187.

[22] J. Thushara et al., RSC Adv., 2013, 3, 21431

[23] X. Dong et al., Materials Letters135(2014)96–98

[24] T. J. Athauda et al., RSC Adv., 2013, 7, 1–4.

[25] B. Xu and Z. Cai, J. Appl. Polym. Sci., 2008, 108, 3781–3786.

[26] G. Qi, H. Zhang and Z. Yuan, Appl. Surf. Sci., 2011, 258, 662–667.

[27] B. Xu et al., Surf. Coat. Technol., 2010, 204, 1556–1561.

[28] L. Wang et al., ACS Appl. Mater. Interfaces, 2011, 3, 1277–1281.

[29] B. Xu and Z. Cai, Appl. Surf. Sci., 2008, 254, 5899–5904.

[30] A. Sugunan et al., J. Am. Ceram. Soc., 2010, 93, 3740–3744.

[31] S. Baruah et al., J. Nanotechnol., 2010, 1, 14–20.

[32] S. Baruah and M. Jaisai, Sci. Technol. Adv. Mater., 2010, 055002.

1. Polymer composites

The term *composite materials* refers to a class of materials having three main constituents: a matrix, a reinforcement, and an interface. The matrix in composite materials transfers load to the reinforcement and protects the reinforcement from environmental degradation. Composites can be classified according to their matrix type. When metal or ceramic matrix materials are used, composites are referred to as *metal matrix composites* (MMCs) or *ceramic matrix composites* (CMCs), respectively. When polymeric matrix materials are used, composites are referred to as *polymeric matrix composites* (PMCs). Composite classification is also often made according to the reinforcement used. Three reinforcement types are usually considered: long continuous fibers, short fibers, and particles (fig. 1.1).
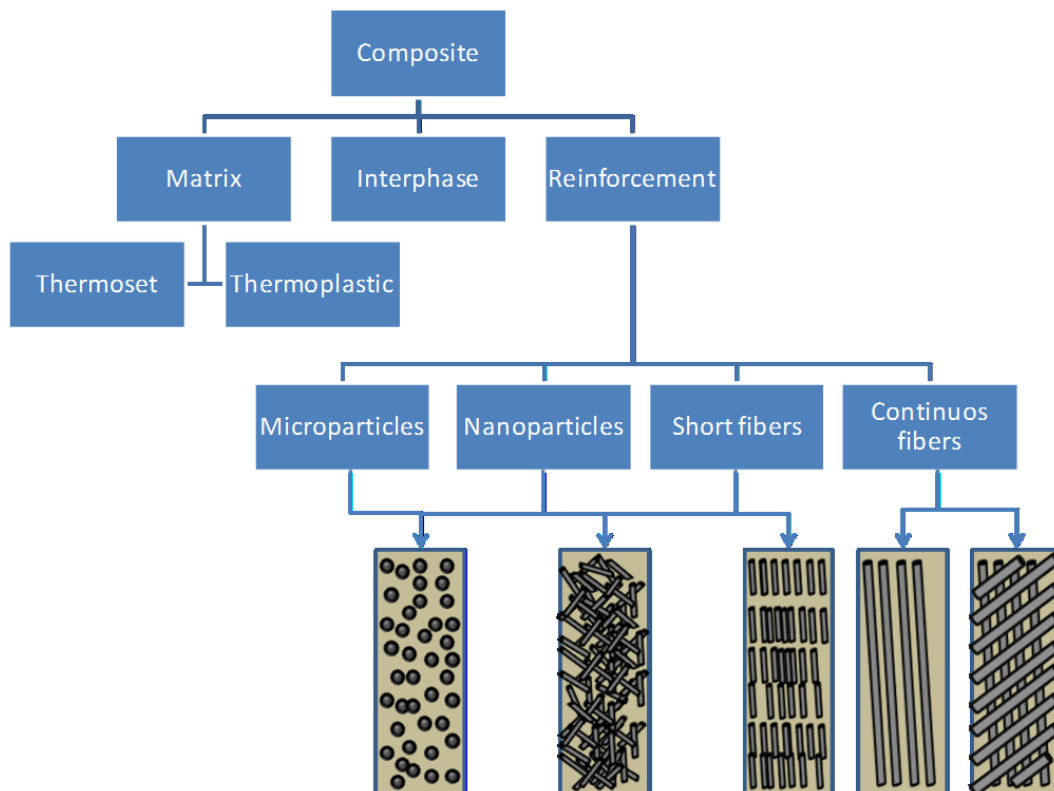
Fig.1.1 Composites classified according to reinforcement types.

Polymeric matrix composites are the focus of this chapter. PMCs present several advantages compared to traditional materials as shown in Figure 1.2 through Figure 1.5.
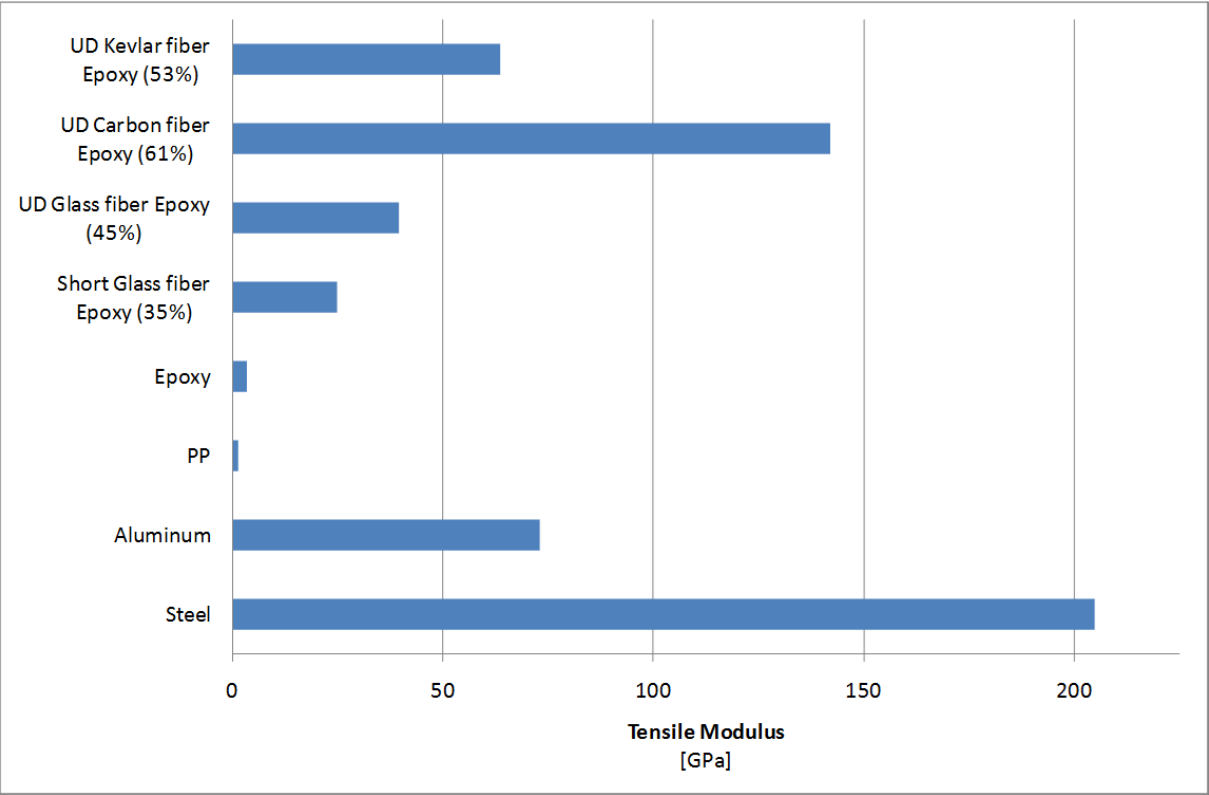
Figure 1.2 Modulus of elasticity
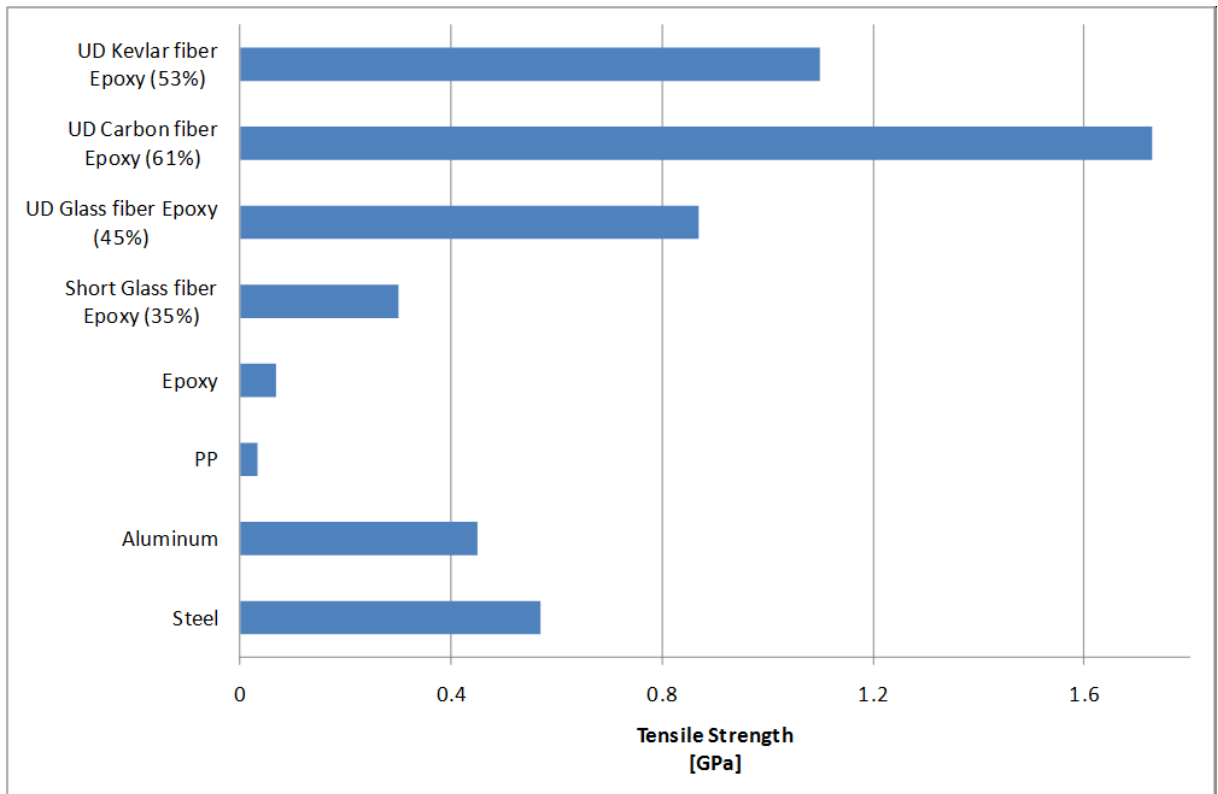
Figure 1.3 Tensile strength

Figure 1.4 Density

13
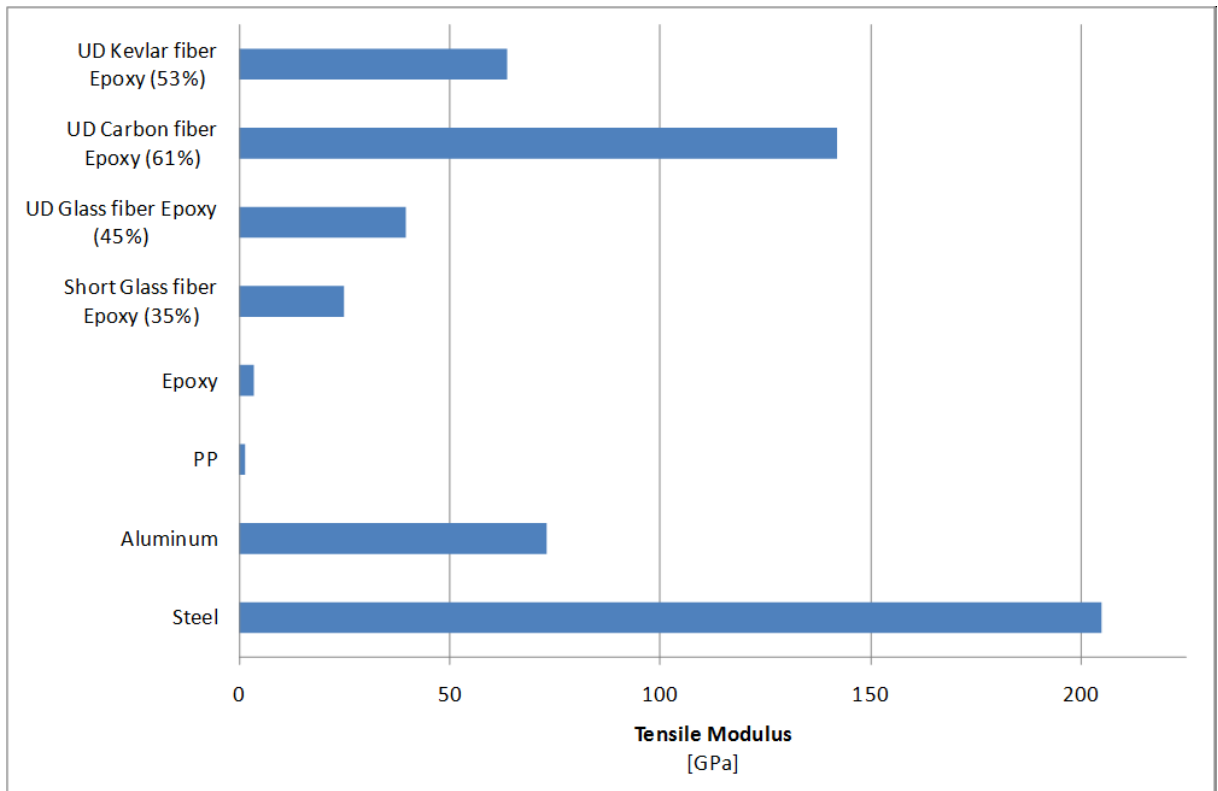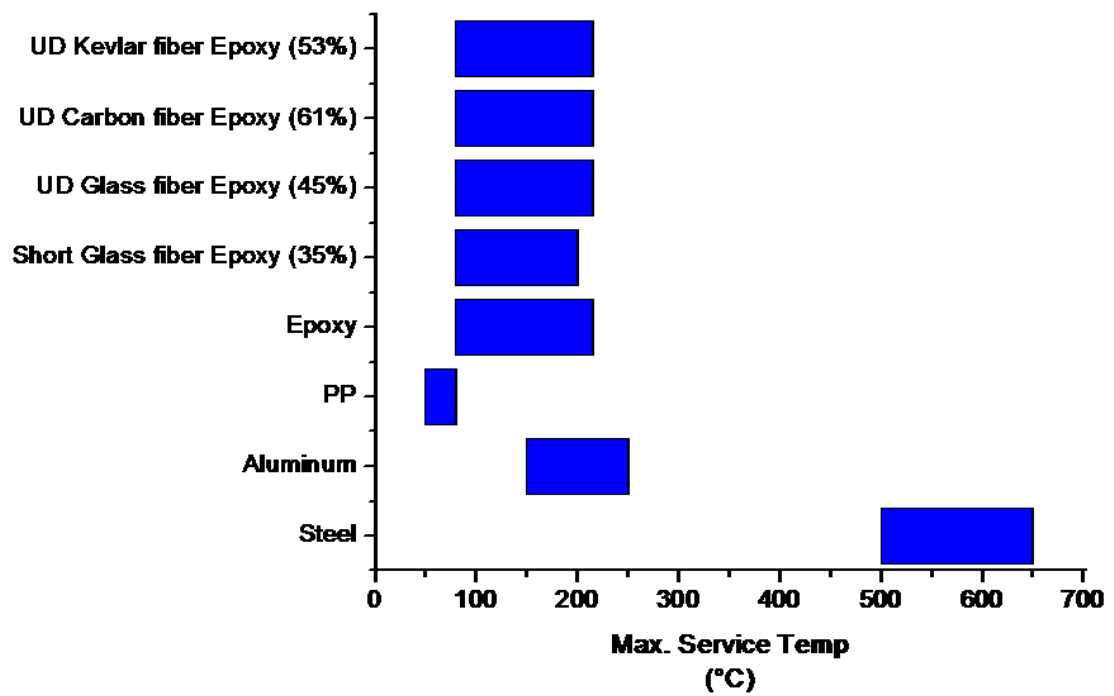
Figure 1.5 Maximum service temperature

Figure 1.6 reports the specific mechanical properties for different materials. This comparison highlights that composite materials outperform traditional materials when weight saving is the driving design factor.
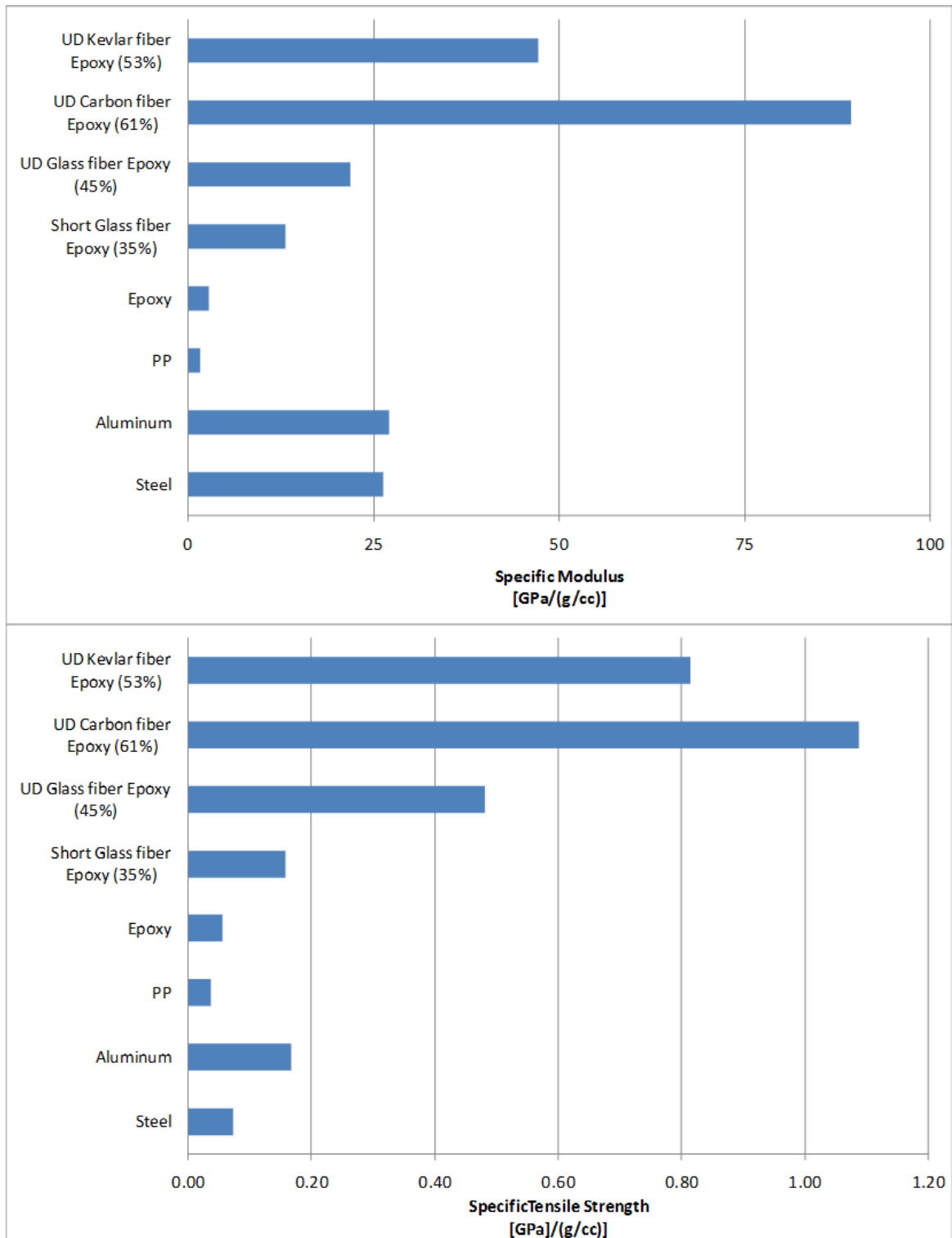
Figure 1.6 Specific mechanical properties

Two types of polymeric matrixes are commonly used: thermoplastics and thermosets. Thermoplastics can be melted by heating and solidified by cooling, which render them capable of repeated reshaping and reforming. Thermoplastics can be either amorphous or

semicrystalline. Thermoset materials, once polymerized, cannot be melted or formed again. The polymerization process is commonly called *curing*. While curing, resin molecules form three-dimensional networks in which they are connected by covalent bonds (cross-links). Owing to these cross-links, thermosets present good thermal stability and chemical resistance but cannot be reshaped after curing.

1.1 Thermoplastics

Thermoplastic resins are increasingly used as matrixes for composites despite the fact that thermosets can be advantageous in terms of processability. Thermoplastics present some advantages over thermosets including the following:

- high delamination resistance and damage tolerance;

- low moisture absorption and excellent chemical resistance if semicrystalline thermoplastics are used;

- low toxicity and infinite storage life due to absence of reactive chemicals;

- recyclability by remelting of used matrixes;

- faster processing because no curing reaction is needed.

The lack of tack of thermoplastics at room temperature is a key disadvantage over thermosets as it requires more sophisticated manufacturing processes for material deposition.

Over the last decade, interest in thermoplastic composites have increased as original equipment manufactures (OEMs) and part fabricators seek new ways to more efficiently produce structural components that have good damage tolerance and environmental performance. Many thermoplastic types can be used as matrixes. A common graph showing classification of thermoplastics consumption versus price and performance is shown in Fig.1.7. Poly(ether ether ketone)s (PEEKs), poly(ether imide)s (PEIs), poly(phenyl sulfide)s

(PPSs), and polysulfones belong to a special class of thermoplastics that can be used as matrixes for niche applications. Commercial prepreg tapes such as carbon fiber/poly(ether ether ketone) (CF/PEEK) and later carbon fiber/poly(phenyl sulfide) (CF/PPS) were introduced in the early 1980s in the aerospace sector [1].
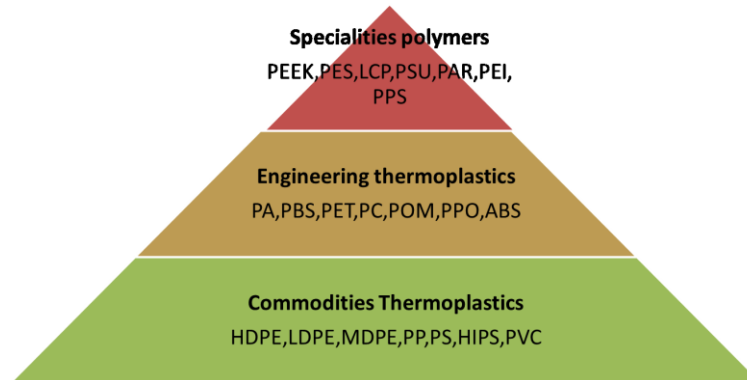
Figure 1.7 Price/performance profile for commercial thermoplastics.

1.2 Thermosets

Thermosets are polymeric materials that form cross-linked networks after curing. These networks render the materials infusible and resistant to chemical agents. Thermosets have good heat retention and maintain their performance over time. They are less susceptible to ageing than thermoplastics. Thermosets present low viscosities in the unreacted state and thus they can be processed manually or at lower pressures compared to thermoplastics. The major limitation of thermosets is their inherent brittleness. Other shortcomings are their limited shelf life due to reactivity, the difficulty of reclaiming scrap material and, for some thermosets, the production of by-products during cross-linking reactions. Typical thermosets used as matrices for composites are reported in Table 1.1.

	Properties	Use Temp. [°C]	Cost	Application	Manufacturing Technique	Examples of Commercial Producers
Polyester	Simplest, room temperature curing, low mechanical properties, good chemical resistance (especially to acids)	60-150	Low	Piping, small boats, automotive, off-shore, civil industry	Hand lay-up, RTM, VARTM, filament winding, pultrusion, spray-up, compression molding	Dow, Ashland, Reichhold, Scott Bader, Cray Valley, DSM, Matrasur, Mapei
Vinyl ester	Better mechanical properties than polyesters, room to medium cure temperature, good chemical resistance (especially to acids)	60-150	Low	Piping, naval, automotive, off-shore, civil industry	Hand lay-up, RTM, VARTM, filament winding, pultrusion, spray-up, compression molding	Dow, Ashland, Reichhold, Scott Bader, Cray Valley.
Phenolic	Needs pressure over curing to avoid bubbling, medium mechanical properties, excellent fire resistance, excellent ablative properties	70-170	Low	Interiors, ablatives, laminates	Compression molding, RTM, filament winding	Dow, J D Lincoln, Gurit, Seal.
Epoxy	Excellent mechanical properties, needs toughening for primary structures, dimensional stability, room to high cure temperature, good chemical resistance (especially to alkalis), very good adhesion to metals	80-215	Medium to high	Piping, profile, automotive, naval, aerospace	Hand lay-up, pultrusion, filament winding, RTM, VARTM, autoclave, compression molding, out-of-autoclave	Gurit, Dow, Huntsman, Reichhold, Hexion, Cray Valley, Cytec, Hexcel, ACG, Toray, Seal, Sika, Mapei
Benzoxazine	Excellent mechanical properties, medium to high cure temperature, excellent fire resistance	80-250	Medium to high	Interiors, aerospace components	autoclave, RTM	Henkel, Huntsman

Table 1.1

1.3 Polymer blends

In most cases of industrial interest, polymer matrices present some deficiencies that limit their use. For example thermosets have good thermal stability, high environmental resistance and high modulus, but they are usually brittle. The poor toughness is largely due to their cross-linked structure and is an intrinsic limit for thermosets. To overcome this limitation many approaches are proposed in the literature (Fig.1.8).
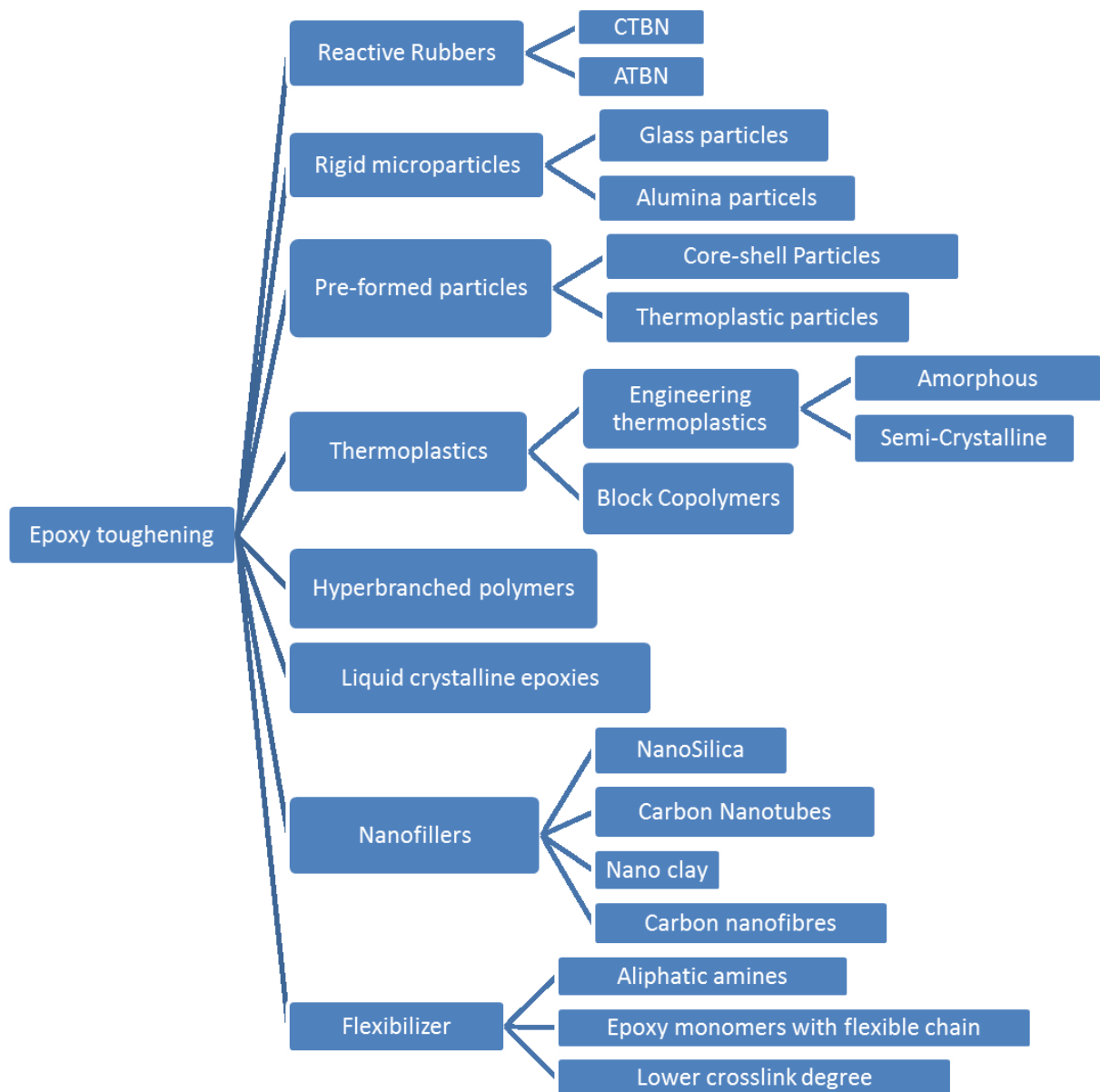
Figure 1.8 Toughening strategies for thermoset resins

The dominant approach has been to add a second phase which precipitates during cure and produces a multiphase morphology able to induce a variety of toughening mechanisms. Many different modifiers have been used: elastomers, polyurethanes, and ductile engineering thermoplastics among others. The use of elastomers typically causes a decrease in mechanical properties, particularly compression strength (due to the reduced resin modulus) and Tg.

Blending thermosets with thermoplastics is one of the most successful approaches because it does not have a significant effect on the balance of properties. Toughness enhancement is typically achieved by phase separation and is driven by many factors including the size and type of morphology, the polymer molecular weight, the backbone structure and end groups and the ductility of the epoxy matrix. A co-continuous morphology is typically desired for the optimum balance of toughness and solvent sensitivity. A toughening technology used to obtain the highest damage tolerance is interlaminar or interleaf toughening. This exploits the concept of increasing the size of the interlaminar region in order to increase the size of the process zone and therefore the fracture toughness and compression after impact (CAI) of the composite. Methods to achieve interlaminar toughening include the additions of particles, films, fibres and veils.

Blending may improve resin or product performance by:

- producing materials having a full set of the desired properties at lowest cost,
- improving product performance, and
- improving processability.

1.4 Filled matrices

Filled matrices are matrices in which a sufficient quantity of a small size of a rigid material (filler) is well dispersed in order to improve certain key properties such as modulus, strength and viscosity or to reduce cost, shrinkage, etc. Conventional loading with traditional fillers typically ranges from 10 to 50wt%. The term filler is used for materials with characteristic dimensions in the range of 100-104 nm. This contrasts with nanofillers which range between

1 and 100nm. Fillers can be classified accordingly to their shape (Fig.1.9), origin and size (Fig.1.10).

| 1D | 2D | 3D |
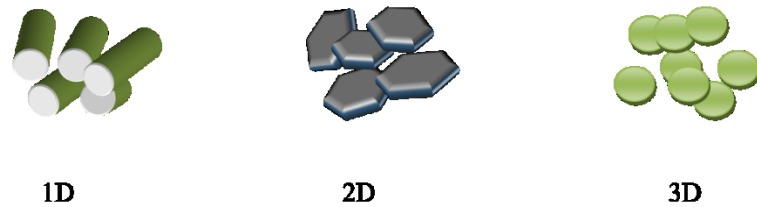
Fig.1.9Filler classification according to shape.
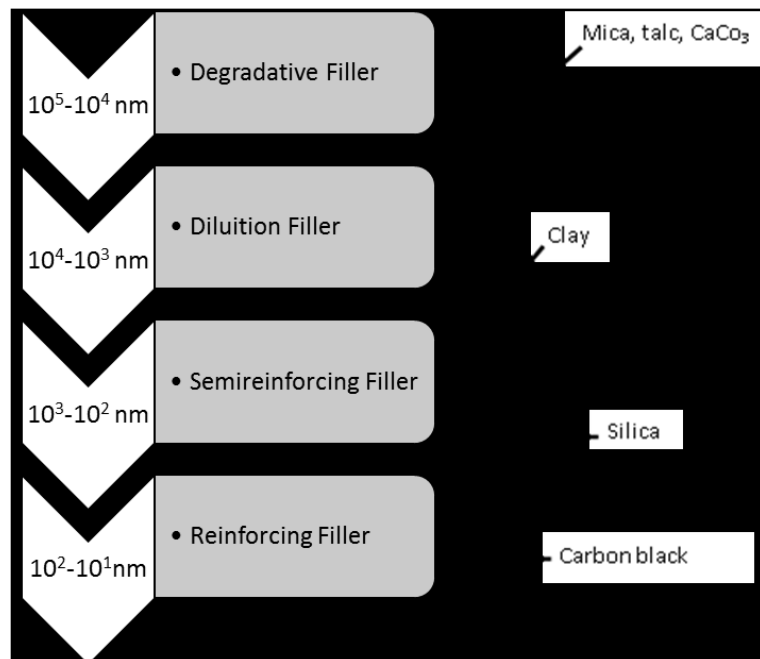
Fig.1.10 Filler classification according to their size.

Some fillers exhibit reinforcing capabilities and others do not [2]. The reinforcing activity of a filler depends on four factors:

- particle size

- particle structure (for most fillers it is more appropriate to speak of aggregate structure)

- specific area

- surface activity.

The term nanofilled matrices refers to polymeric matrices compounded with fillers with characteristic dimensions in the nanometer range. *Polymer nanocomposite* is the most common name used to refer to such matrices. The fillers used for nanocomposites are usually referred to as nanofillers. Several types of nanofillers can be found that present one or more dimension in the nanometer range (Fig.1.11)

1D	2D	3D
Carbon Nanotubes (CNT)	NanoClay	Nanosilica
Carbon Nanofibers (CNF)	Graphene	Fullerene
Cellulose Whiskers		Nano Silver
		POSS.
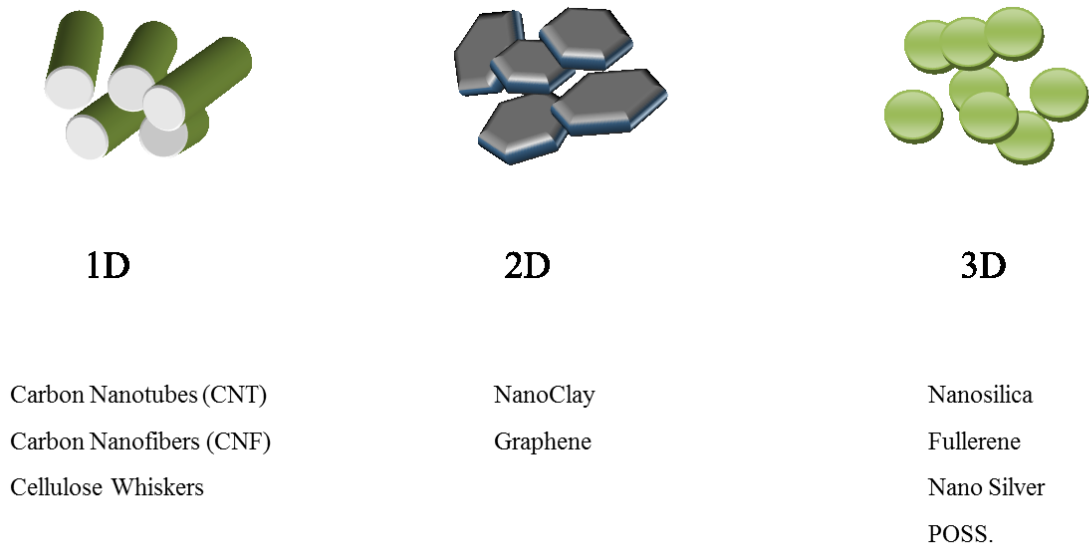
Figure 1.11 Common nanofillers of interest for nanofilled matrices

Traditional filled matrices contain reinforcements with length in micrometers, and the interface of fillers is close to the bulk polymer matrix. In the case of nanocomposites, where the length of the reinforcement is on the nanometer scale, they have ultra-large interfacial area per volume, and the distances between the polymer and filler components are extremely short. Polymer coils are 40 nm in diameter, and the nanofillers are on the same order of magnitude; as a result, molecular interaction between the polymer and the nanofillers are thought to give nanofilled matrices unusual material properties that conventional matrices do not possess [3]. These unpredicted effects are also referred to as "nano-effects". More recent results have, however, indicated that while the property profile is interesting, the nanoclay-based nanocomposites often obey continuum mechanics predictions and, in most cases, reinforcement effects obey composite theories where no "nano-effect" is considered [4]. Nanocomposites offer several advantages over the simple reinforcement effect that makes them of

interest for composite materials. One big advantage is the possibility to realize matrices with sensing and actuation capabilities that can be used for the development of multifunctional composites [5]. Other non-structural functions achieved by nanocomposites include thermal and electrical conductivity, flame resistance and abrasion resistance. Thermal and electrical conductivity are two of the most interesting functions that can be improved by the addition of nanofillers.

When developing nanofilled matrices key factors to achieve optimal reinforcing efficiency are: high dispersion degree to ensure the absence of nanofiller agglomerates in the micrometer range; good adhesion between matrix and nanofiller to ensure adequate stress transfer; and, in some cases (e.g., nanotubes and nanofibers), nanofiller orientation for optimal performance. The most complex and challenging task is to achieve fine and uniform dispersion because of the great interactions between nanofillers and the high matrix viscosity increase due to nanofiller addition.

1.5 Chapter 1 References

[1] L. A. Berglund in S.T. Peters, ed., Handbook of composites, Chapman & Hall, London, 1998, pp.115-130

[2] J.L. Leblanc, Filled Polymers: Science and Industrial Applications, CRC Press, Boca Raton, 2010.

[3] J.H. Koo Polymer Nanocomposites, McGraw Hill, 2006, DOI: 10.1036/0071458212

[4] D.R. Paul, L.M. Robeson, Polymer 49 (2008) 3187–3204

[5] C.Li, E.T. Thostenson, Tsu-Wei Chou, Composites Science and Technology 68 (2008) 1227–1249

2. Multifuntional Material Systems

2.1 Introduction

Multifunctional Material Systems (MFMS) comes from the idea of having materials that are more autonomous and polyvalent than their counterpart monofunctionals.

For example, an electrically conductive material eliminates the need for wires, a shape morphing material may eliminate the need for actuators, a flame retardant material eliminates the need for severe fire protection mechanisms, a renewable material minimizes the need for continuing of extraction of raw materials, and of course a combination of these eliminates the need for all of those and maybe some more, because many times the combination of materials can result in new functions not present in either of the single materials by themselves. Moreover, by using MFMS will be possible to save in number of parts, reducing the need for joining operations. A good integration among materials should be able to eliminate traditional boards, connectors, bulky cables yielding major weight and volume savings (Fig.2.1) increasing system-level efficiency. They should also be vastly more tailorable to the application than current unifunctional materials, because of the wide range of combinations of materials and resulting properties and functions.

Furthermore, in addition to the strong performaces that could be achieved using MFMS, it is good to also take into account the cost saving, at least in the post-production phase, that they could allow (Fig.2.2).
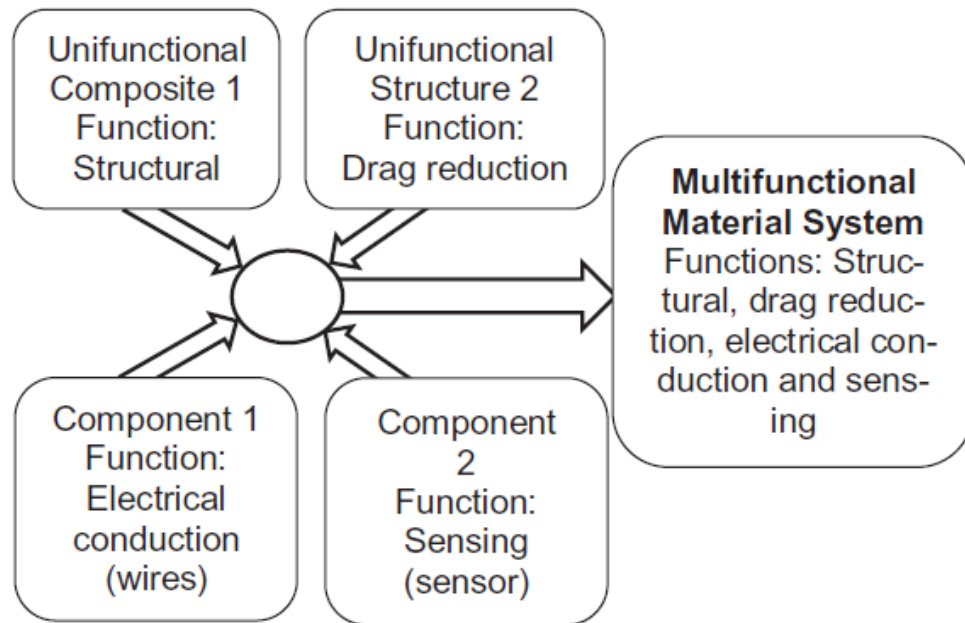
Figure 2.1 A multifunctional material system should integrate in itself the functions of two or more different components.

.

Figure2.2 Cost study: Metal vs Composite vs Multifunctional Composite.

Below is a detailed explanation for each component of the Figure 2.2.

Raw material:

- In most cases different materials will be used in a MFMS, because that's easier than to find a MFM that performs all the desired functions. On the other hand, there are several hierarchical MS being developed, that increase material efficiency, thus using less material to achieve a greater performance. It is then unclear where would MFMSs stand in terms of raw material costs. Some may be cheaper others may be more expensive than current materials, but either way, for the same price it is expected that the performance for each function will increase, so the value will tend to get better.

Fabrication:

- Many methods used in the production of MFMS are expensive and haven't been transferred to industry because of difficulty in achieving scalability. Anyway, since MFMS are of higher complexity than monofunctional ones, it might be expected that their production will also be more expensive and require more expensive tooling. On the other hand, with the increasingly improving 3D-printing technology some of those difficulties may significantly reduce.

Assembly:

- Assembly should be a winner for MFMS. Shape morphing technologies and multifunctionality reduce the number of articulated and external components, which in turn reduce the number of parts and joining complexity. For example, if one part made of a MFMS can do functions that used to need 5 different materials/parts, then it's a 5-fold decrease in joining operations.

Maintenance:

- Because of the increasingly autonomous status of MFMS, self-healing/sensing/regulating (homeostasis)/etc., the need for human control should gradually decrease, and therefore so should maintenance costs.

Non-recurring:

- The design phase for MFMS needs to integrate engineers from several fields as the material itself will satisfy the requirements of several functions of different schools: electrical, mechanical, biological, environmental, chemical, etc. For this reason simulation software and material databases should get more complex and have some impact in the final cost of the material.

2.2 Classification: Nomenclature

The interest of the scientific community in the new class of materials able to perform several functions is increasing, as it's possible to observe by literature data (Fig.2.3) . As the number of people working in a field increases so does the need for clarification. Many terms are used interchangeably with slightly different meanings. For example, the term ''smart material'' is a very lose term whose meaning varies significantly from author to author. Few good suggestions that might be useful was presented by A. Ferreira [1]. He groups Multifunctional materials (MFM), Multifunctional composites (MFC) and multifunctional structures (MFS), will here be group into a broader group named Multifunctional Material Systems (MFMS). The definition of material systems (MS) encompasses materials, composites and structures (Fig.2.4).
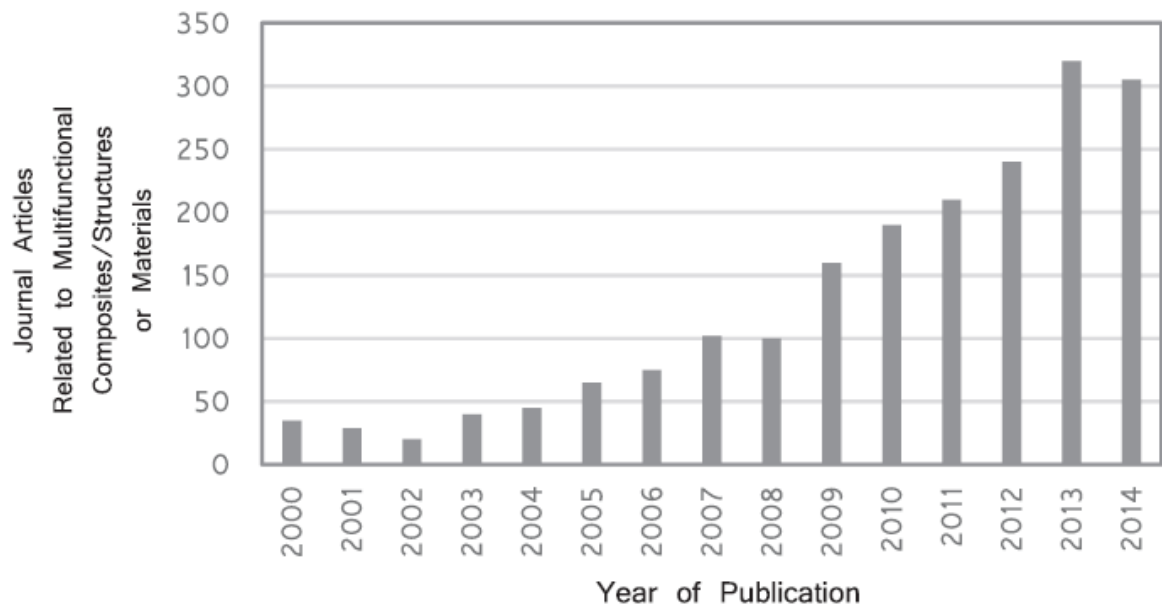
Figure 2.3 Literature survey on journal articles related to multifunctional composites/ structures/materials in Engineering Village, March 2015.
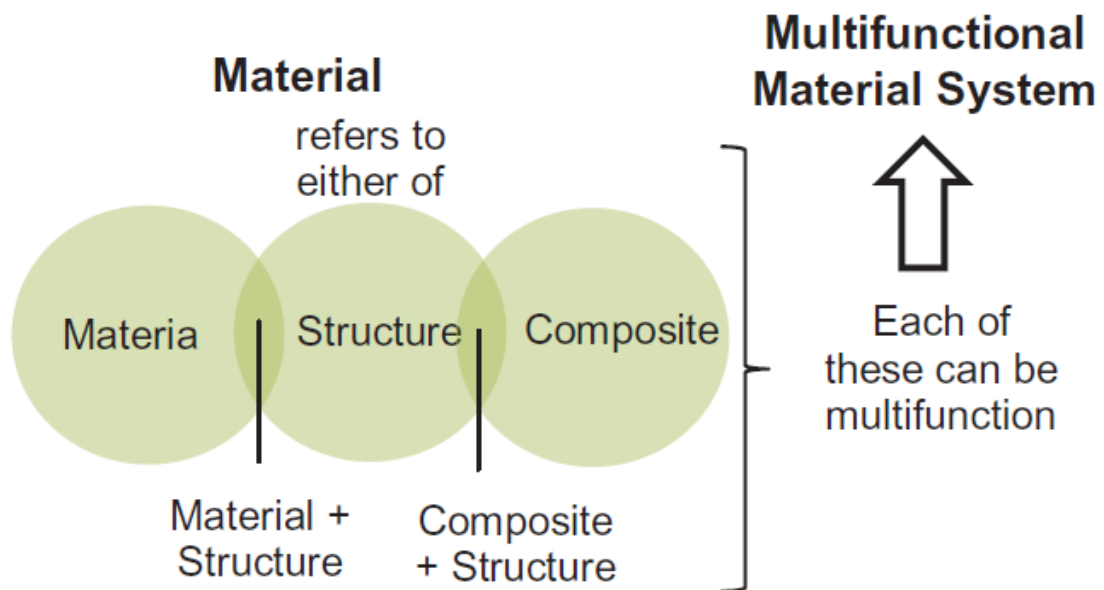
Figure 2.4 Basic nomenclature explanation.

This definition is necessary because one could have, for example, a monofunctional ceramic with a textured surface and an internal structure of a nanolattice. It wouldn't be correct to call it a MFM because the multifunctionality arises both from the material and the structure.

An example of a MFM would be Carbon Nanotubes (CNTs) which inherently have high mechanical strength and electrical conductivity or PZT which can provide both sensing and actuation. An example of a MFC would be epoxy/CF-(Fe powder) (mechanical strength and electrical conductivity), and an example of a MFS would be shark denticles which provide anti-bioufouling and reduce drag. The definition of MFMS, then, encompasses all of these.

Other concepts that are going to be mentioned quite a frequently are 'multiscale' and 'hierarchical' composites (Fig. 2.5). Multiscale composites concern the different sizes of the fillers. For example, a carbon fiber (micromaterial) + carbon nanotube (nanomaterial) reinforcing an epoxy matrix is a multiscale composite. A hierarchical composite concerns the structural organization of the fillers, where fillers/materials are organized in a hierarchical way. For example, filler A is contained inside filler/material B, which is contained inside filler/material C.
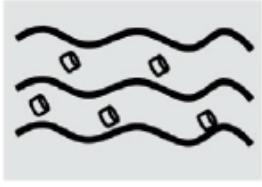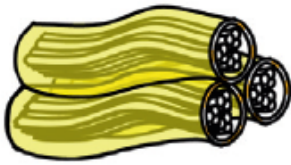
Composite	Multiscale Composite	Hierarchical Composite	Molecular Composite / Hybrid Material
CF/Epoxy, (CF+GF)/ Epoxy, reinforced concrete	(CF+CNT)/ Epoxy	Many biological materials (bone, nacre, wood,…)	Organic-inorganic hybrids, FGMs
One or more fillers	Different fillers at different scale sizes	Fillers at different scale sizes hierarchically organized	Different constituents at a molecular level

Figure 2.5 Classification of multi-materials according to the types, sizes and organizations of constituents

Another useful concept for distinguishing material systems is that of material integration, that is, how well materials are integrated into one another. One can obtain multifunctionality by integrating various functions in multimaterial systems or single materials. In the former, it can be obtained by the addition of fillers at the nano or microscale such as in (nano-) composites, or multilayer constructs. For single materials it can be obtained at the molecular level such as with several functionalized polymers. Matic [2] and Asp and Greenhalgh [3] have proposed slightly different versions of the same division, a three scale system that Ferreira adapted as a combination of both ideas (Fig.2.6).
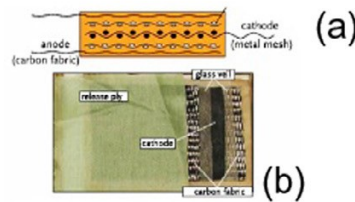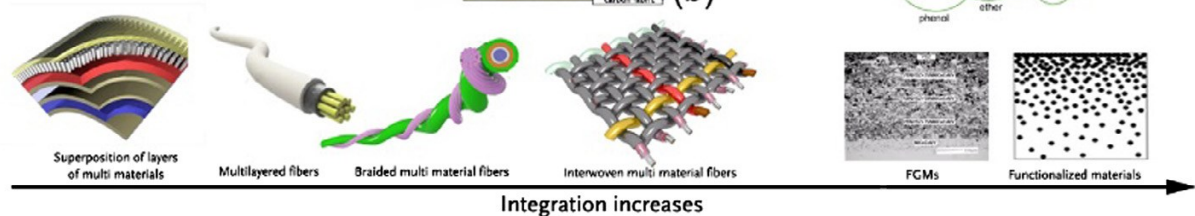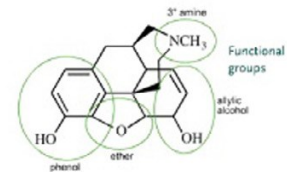
Figure 2.6 Classification of MFMS according to the distinguishing of the constituents: multifunctional structure, multifunctional composite and multifunctional material [1].

The integration of materials goes from not integrated (type I or structure) to integrated but with distinct phases (composite) to fully integrated at the molecular level or type III.

2.3 Current Multifunctional Materials Systems:

2.3.1 Carbon nanomaterials

A lot of research worldwide have recently been focused on Graphene, carbon nano tubes (CNTs) and carbon nanofibers (CNFs). These different spatial configurations of carbon atoms, covalently bonded, (Fig.2.7) combine great mechanical, thermal and electrical properties. Liu et al. [4] have predicted from first principles that this material has the highest specific stiffness and strength of any known material. Many papers had presented the mechanical characterization of these carbon nanomaterials [5–12] which unfortunately have seen highly variable results due to the difficulties in performing the required tests at the nanoscale, forcing many scientists to resort to indirect ways of measuring. If we were to take a few representative values, CNTs would have 1 TPa < E < 1.8 TPa and 11 < σ_r< 150 GPa

[5] and would be best thermal conductors currently known having a maximum thermal conductivity of 6600 W/ mK for an individual SWCNT and >3000 W/mK for an individual MWCNT, which is at least twice of diamond's, and a maximum electrical conductivity of ~300 MS/m for SWNT and >0.1 MS/m for MWNT while revealing superconducting properties at low temperature [13]. Moreover thanks to the fact that CNTs, graphene and CNFs are of a very small size, they are susceptible of reaching far greater surface area to volume ratio (A/V) than micro fillers. Furthermore both CNTs and graphene have either very low (<<1) or very high (>1) aspect ratio which also further increases their A/V ratio (Fig. 2.8). This ratio is one of the main reasons to develop nanocomposites; a high interface region means high adhesion and high efficient transfer of stress across the composite components. This also means that for the same desired effect, a less amount is required of the filler with higher A/V.
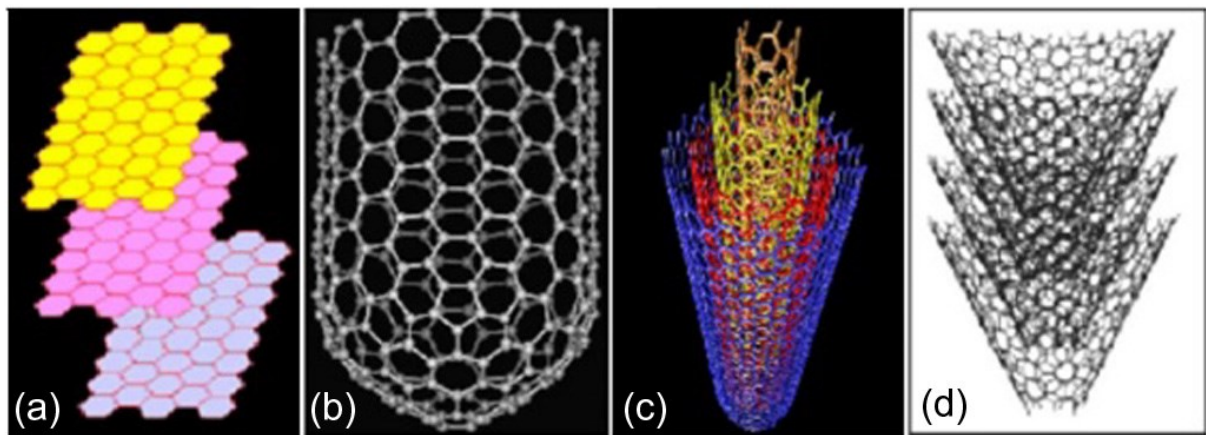
Figure 2.7 (a) carbon nano wall or graphene; (b) single walled CNT; (c) multi walled CNT; (d) carbon nano fiber. Adapted from [14].
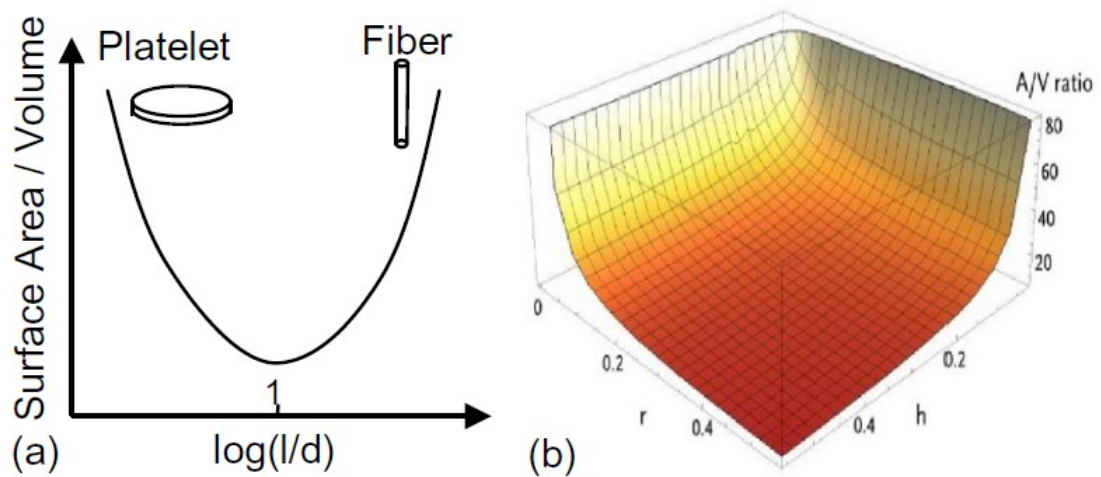
Figure 2.8 Variation of the ratio of surface area/volume (A/V ratio) against aspect ratio l/d and (b) A/V ratio for a cylinder with its radius and height [1].

For the reasons explained before, i.e. extremely good mechanical, electrical and thermal properties and high A/V ratio, there is a strong interest in reinforcing materials with carbon nanomaterials to enhance their properties. This interest can also be attributed to the fact that fiber-reinforced polymer matrix composites, such as glass and carbon fiber, can also be reinforced by these carbon nanomaterials resulting in a multiscale composite with even better properties. Moreover different materials benefit, in different ways, from being reinforced with carbon nanomaterials. Polymers see greatly improved thermal and electrical conductivity as well as increases in strength and elastic modulus when reinforced with graphene, CNTs or CNFs [12,15–18]. Composites of ceramic matrices see an increase in toughness and electrical and thermal conductivity [19]. Metal matrices, most commonly based on Al, Mg, Cu and Ni, have been reported to have increased resistance to corrosion, stiffness and strength [20-22]. Some representative examples can be seen in Fig. 2.9.
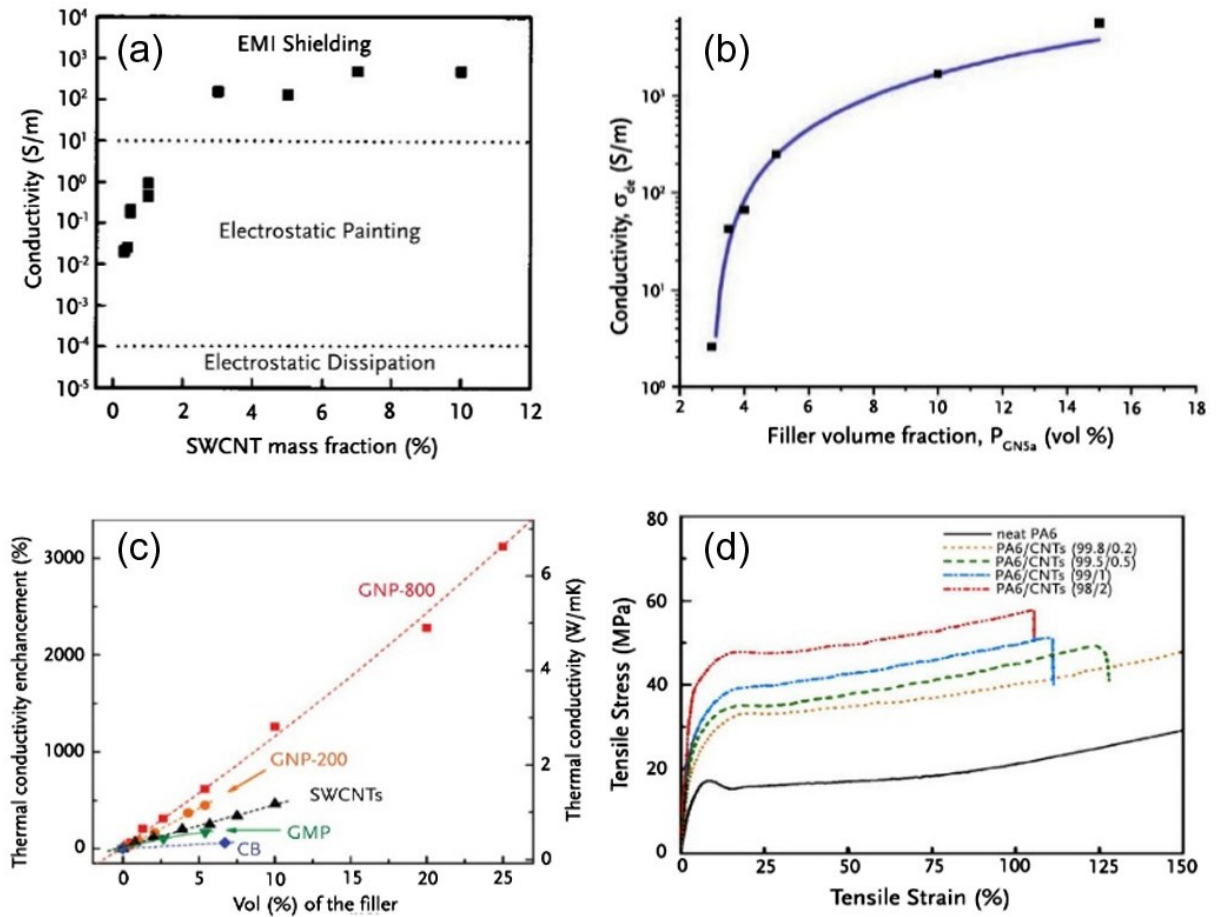
Figure 2.9 Electrical conductivity as a function of SWCNT mass fraction in a SWCNT-polycarbonate composite. The dashed lines represent the minimum conductivity necessary for the specified functions [23]; (b) Electrical conductivity as a function of graphene volume fraction in a graphene-alumina composite. Adapted from [19]; (c) Thermal conductivity of epoxy-based composites as a function of filler volume fraction for carbon black (CB), graphitic micro particles (GMP), nanoplatelets (GNP) and single walled CNTs (SWCNT). Adapted from [24]; (d) Stress–strain curve for a nanocomposite of PA6 polymer matrix and different CNT filler concentrations, adapted from [25].

Given than the most used composites have polymers as matrices, in aircrafts where electrical conductivity is needed in certain parts to transfer electricity from thunders, the poor conductivity of polymers has to be compensated by the addition of more parts, being the sole function is to transfer lightning strikes' electricity. Polymer matrix nanocomposites with carbon-based fillers are being investigated as a possible replacements for regular polymers typically used in composites' matrixes.

2.3.2 Piezoelectrics

Piezoelectric materials are materials that generate an electric potential in response to an applied mechanical stress, the direct piezoelectric effect, which can be used for sensing or energy harvesting. On the other hand, when applied an electric field to the material it will either change shape or generate mechanical stress, inverse piezoelectric effect, which can be used for actuation and shape control. This means that if we apply a force to a piezoelectric material, it will develop a positive charge on one end and a negative charge on the other end. If we connect the two ends, current flows. Piezoelectric materials are capable of actuating or sensing at frequencies from about 1 Hz to the MHz range with relatively linear behavior. Moreover, they have high stiffness which provides them with strong voltage dependent actuation.

The most used piezoelectric materials are polycrystalline ceramic (PZT, PbTiO3, BaTiO3), single crystals (SiO2, LiNbO3, LiTaO) and polymeric (PVDF, co-polymer) and they take the form of monolithic, thin films [26], wafers [27] and (nano)fibers/wires, [28–33] which can be hollow [34–36] and arranged as macro and active fiber composites [37,38] (MFCs1 and AFCs) or 1–3 Composites. The piezoelectric ceramics are more brittle but have larger actuating forces, whereas the piezoelectric polymers withstand higher deformations and so are better fit for shape hanging applications or irregularly shaped parts. Traditionally, the ceramics have been the most used due to low cost, ease of manufacturing, high coupling efficiency, chemically inertness, high operating temperature and high sensitivity (for sensing). However, ceramics are very brittle and therefore requires extra care when being handled. Furthermore they also have poor conformability to curved surfaces generally requiring extra manufacturing steps in order to be used. The fragility of the piezoceramics has been partially overcome, while also increasing the flexibility of the material, by having them in the form of fibers. Typically, crystalline materials have much higher specific strengths in the form of fiber

because the volume fraction of flaws diminishes. Then, by embedding those fibers in a tough polymer-matrix we can increase toughness and flexibility of the composite [39].

A good example was developed by Lin and Sodano [40,41] which create piezoelectric structural fibers that can be laid up in a composite material giving it sensing, actuation and load bearing capacity. The structural fiber was made of a piezoelectric material as an interface between an interior carbon fiber and an exterior piezoelectric material, as illustrated in fig. 2.10a. Guillot et al. [42] also developed a TEFLON-FEP coated PZT hollow fiber for sensing and energy harvesting purposes (fig. 2.10b) revealing a flexibility that wouldn't be possible had it not been coated (Fig.2.10c) and producing twice as much energy density as the current state of the art Multifunctional Composites (MFCs).
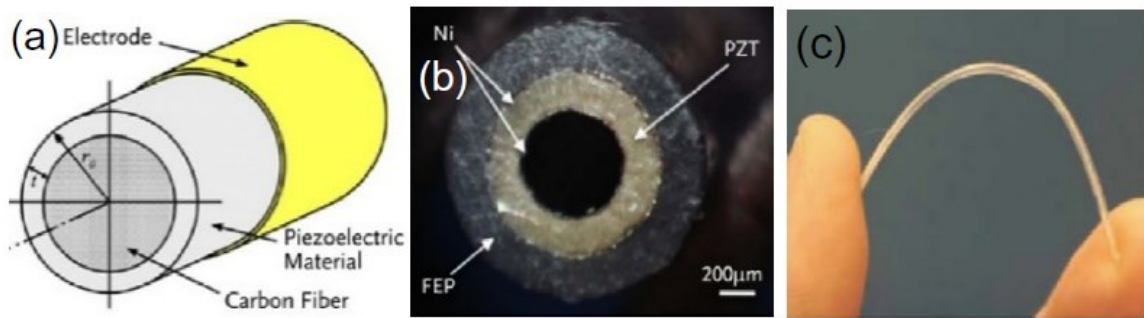
Figure 2.10 (a) Hybrid structural-actuating fiber [40]; (b) one mm diameter hollow PZT fiber coated by Teflon-FEP (c) in bending. Adapted from [42].

Using the inverse piezoelectric effect, it is possible to use piezoelectric materials for actuation. MFCs are composed of unidirectionally aligned rectangular piezoceramic fibers bonded by a polymeric matrix, and sandwiched between interdigitated electrodes (Fig.2.11). This arrangement of electrodes exploits the d33 electromechanical coupling allowing for greater efficiency. Because they are thin and flexible, they can easily be coupled to the surface of other parts, and allow for several actuation types (Fig.2.12).
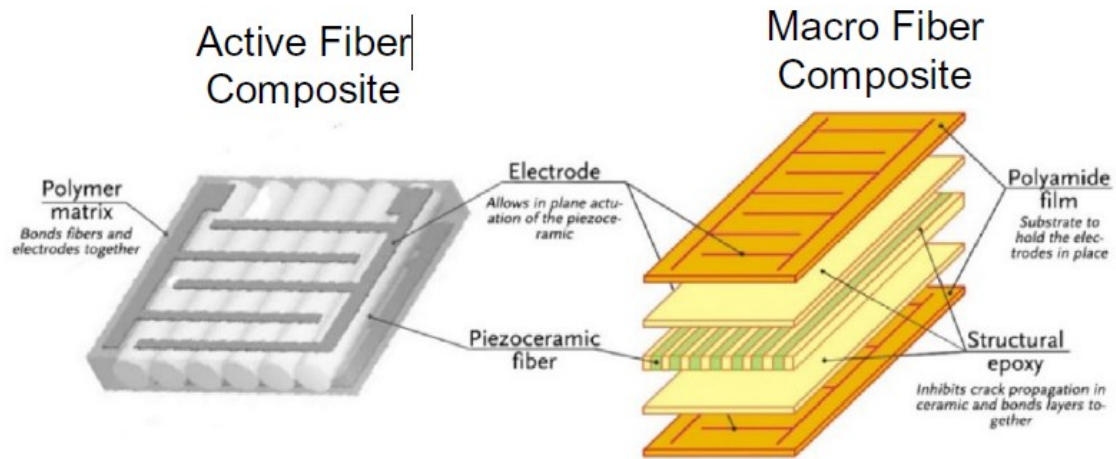
Figure 2.11 Constitution of a typical AFC and a typical MFC. Adapted from [43,44].
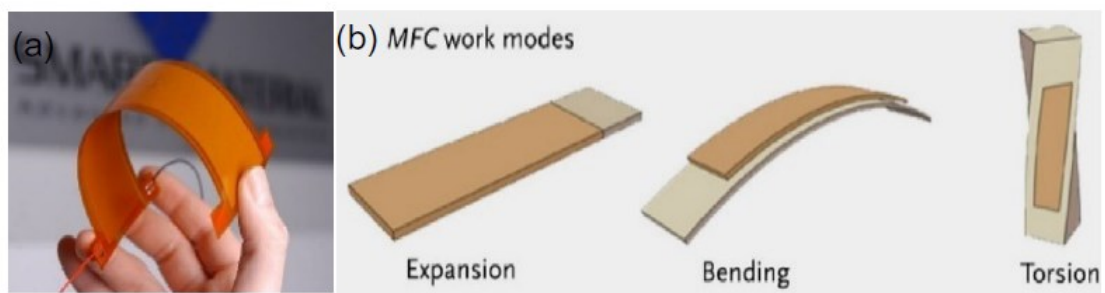
Figure 2.12 (a) Picture of an MFC showing its high flexibility [45]; (b) MFCs' work modes. Adapted from [46].

Li et al. [47] have presented an approach for increasing aerodynamic performance, such as increasing lift, reducing drag and improving roll performance, by using several MFCs distributed on the aircraft wing surface that control the wing's mechanical deformations.

2.3.3 Shape memory materials

Shape memory materials (SMMs) are a type of SRMs that respond to thermal, pressure and magnetic field. For example, Shape memory alloys (SMAs) are metallic alloys that can reversibly recover permanent strains when subjected to a specific stimulus. This recovery occurs when the SMA goes back from the malleable martensite phase to the very stiff austenite phase. SMAs can provide a very lightweight alternative to conventional actuators such as pneumatic, hydraulic or motor-based, since they are outstanding in terms of power/weight ratio over other types of actuators.

SMAs are used in morphing aerospace structures quite extensively [48]. Sofla et al. [49] reviewed aircraft wing morphing technologies while also developing a shape morphing aircraft wing using an antagonistically positioned SMAs material which flex the wing (Fig. 2.13). In the trailing edges of some jet engines chevrons are used for noise reduction. BOEING developed a device known as variable geometry chevron to reduce take-off noise and increase cruise efficiency which is actuated by NiTi SMAs flexures [50] (Fig. 2.14).
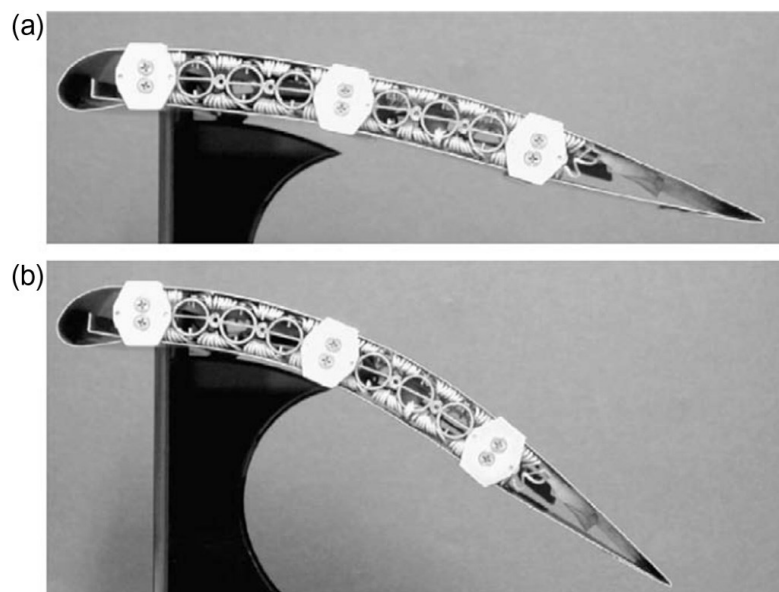
Figure 2.13 Bending achieved in a prototype aircraft wing by heating of SMA strips. (a) Un-morphed and (b) morphed [49].
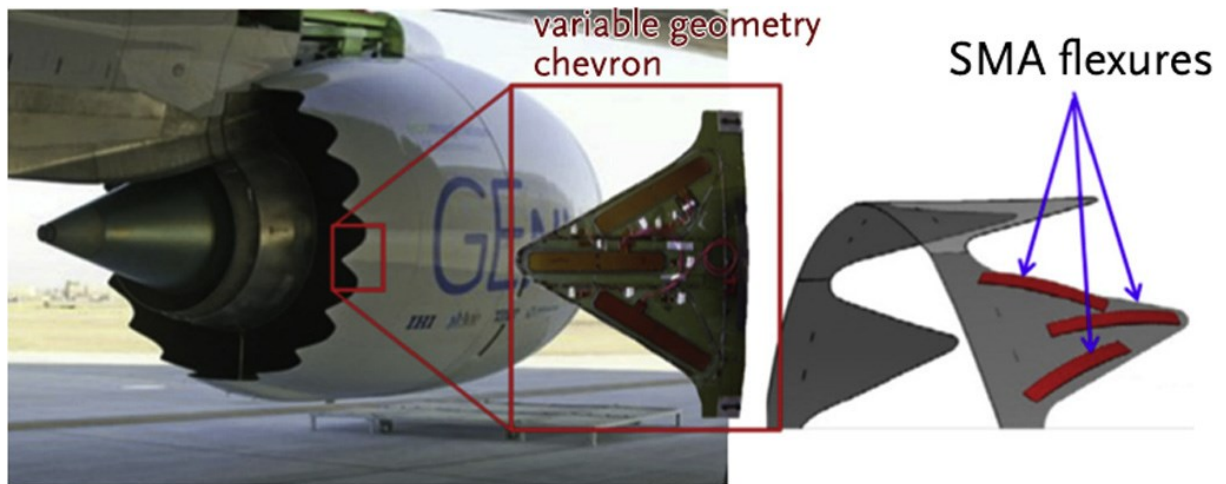
Figure 2.14 Variable geometry chevron developed by Boeing, adapted from [50].

In SMAs, it is also possible to program multiple memory shapes, and this has seen a surge of interest in the recent years. This can be done using a new process known as multiple memory material technology [51] or by combining SMAs with other materials such as SMPs (Shape memory polymers) [52] resulting in a SMH with greater functionality.

Comparatively to SMAs, SMPs have many important advantages such as lower cost, density and easier processing, among others. Most studies concerning SMPs are about the thermoplastics ones, which have relatively poor thermal and mechanical properties (e.g. temperature, moisture and chemical resistance), so they may not be able to meet many requirements for multifunctional structural materials. However, thermosets, as well as thermoplastic SMPs reinforced with CF and CNTs, and other fillers are in development and show promise [53,55].

Like SMAs, SMPs also find applications in aerospace. The aerodynamic performance of aircrafts is designed for specific flight conditions, e.g. cruise for long range airliners, meaning that whenever the plane is not at the condition it was optimized for, efficiency is going to drop. For this reason, there is great interest in expanding the optimal flight conditions, which could be obtained through morphing parts of the aircraft giving it the ability to change its

geometry during flight. There are several attempts at implementing the concept of morphing wings [56]. Two examples concerning the use of SMPs as the actuation mechanism are shown in (Fig.2.15a and b). Due to their shape morphing ability, SMPs are also being studied for use in deployable structures [57]. The main advantage of using SMPs for space applications is that it could greatly reduce the volume, weight, and cost of the structure compared with traditional self-deploying techniques. For example, Keller et al. [58] have developed a deployable radio frequency reflector comprised of SMP-based composites claiming it is much more mechanically simpler and lighter than its conventional competitors (Fig.2.15c–d).
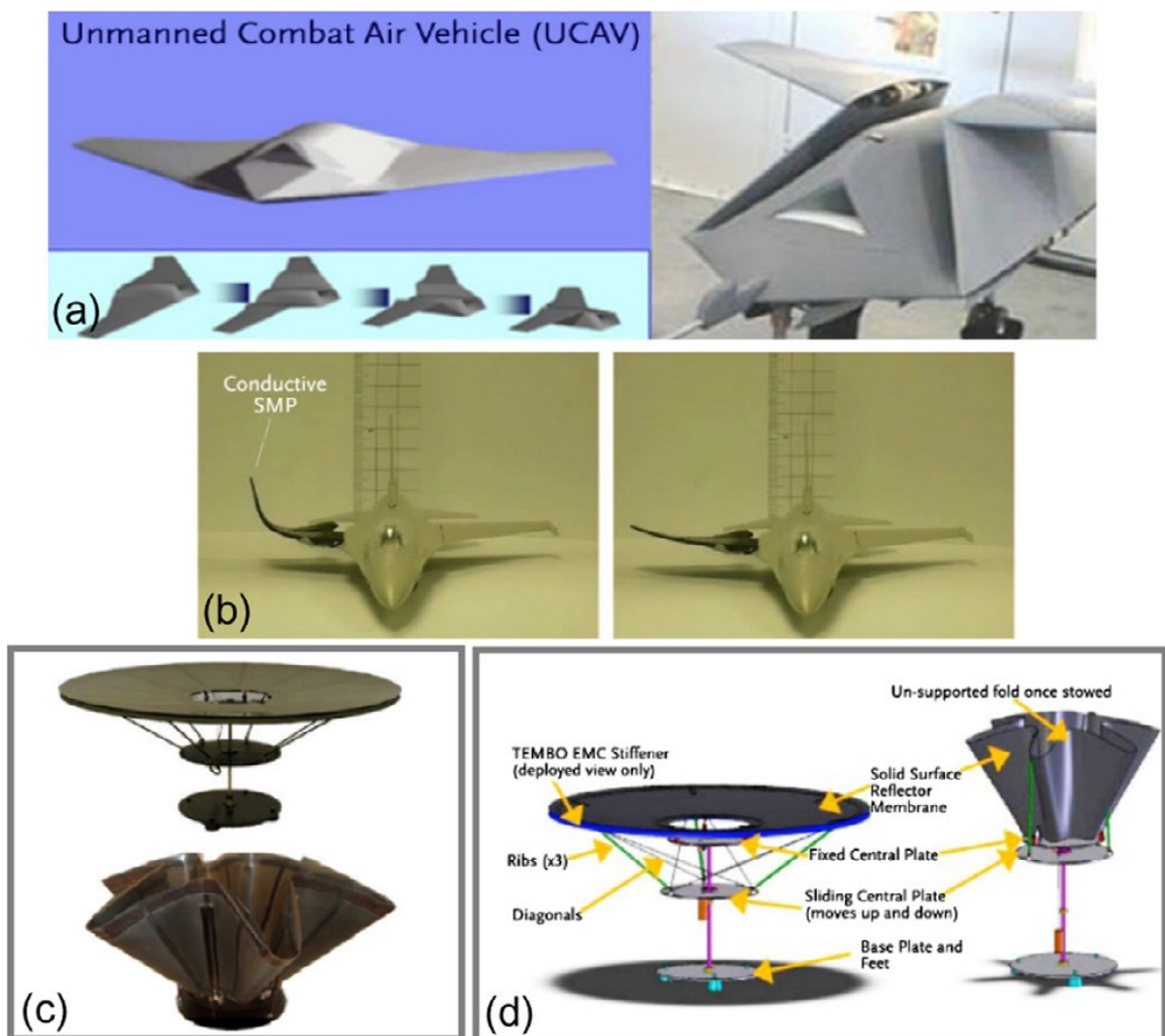
Figure 2.15 SMPs application in aerospace, so far mainly for actuation: (a) Prototype of a morphing wing unmanned combat air vehicle by Lockheed Martin [53]; (b) Conductive SMP for morphing wing, adapted from [58]; (c) A SMP composite reflector in its pre-deformed (up) and recovered (down) shape; (d) illustration of the structure of the reflector [57].

2.3.4 Carbon fiber reinforced composites for energy storage and sensing

The idea of adding energy storage function to high performance structural materials has been gaining increased attention. has the interest in better batteries. Eric Jacques, a researcher in and aerospace engineering at KTH, has mentioned how carbon fiber can fill two functions in an electric car: as a lightweight composite reinforcement material for the car's body, and as an active electrode in lithium ion batteries. He says carbon fiber offers a viable alternative to graphite. Lithium can be inserted into the carbon fiber microstructure and the carbon fiber acts as a good conductor [59].

Drayson Racing Technologies and Lola first presented the Lola Drayson B12/69EV, an electric racing car that uses a composite structural battery to aid the main battery for powering (Fig.2.16) [60]. Even though the way the composite was achieved in the Lola Drayson, and many others, are hidden inside the R&D of industries, other researches might give a hint due to research of their own. Pereira [61] obtained a CF/epoxy with energy storage function by embedding thin film lithium energy cells within the CF layers. The strength and stiffness of the carbon/epoxy laminate was not significantly changed, and there was no abnormalities in the energy cells' charging and discharging processes when the composite was mechanically loaded to up to 50% of its ultimate tensile strength.
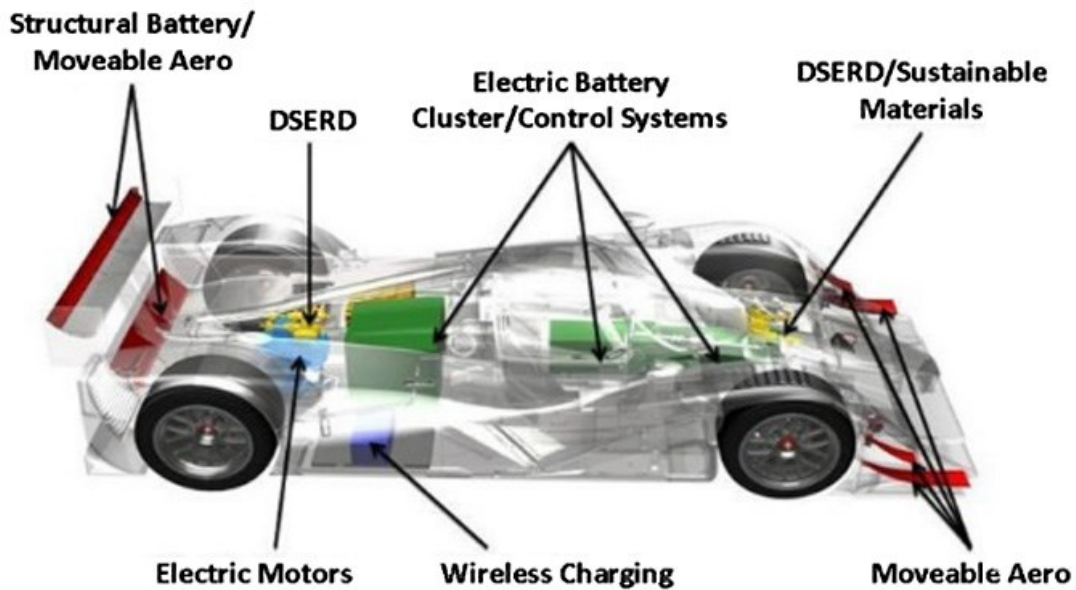
Figure 2.16 Lola Drayson B12/69EV electric racing car with nickel-based and CF structural-batteries [60].

2.3.5 Self-healing materials

Self-healing materials are materials that are capable of selfrepairing damage without human intervention. To help categorize these materials we can divide them into classes (Fig.2.17). The first is related to how the healing mechanism is triggered. If it needs an external stimulus such as light or heat they're called non-autonomic, whereas if the damage itself is enough to trigger the healing they're called autonomic. The second is related to how the healing mechanism is or isn't part of the material. In extrinsic self-healing, the process requires external, specifically brought in by vascules, or embedded in micro or nanocapsules materials for the self-healing to occur. Intrinsic self-healing, on the other hand happens when the matrix itself has the ability to provide healing function. The self-healing ability has been studied in for ceramics, metals and polymers. A way to quickly perceive the difference in difficulty of implementing the self-healing functions on these three material types is through the temperatures at which the mechanism of healing occurs. Low temperatures for polymers and

their composites (<120 °C) and high temperatures for metals (<600 °C) and ceramics (>800 °C).
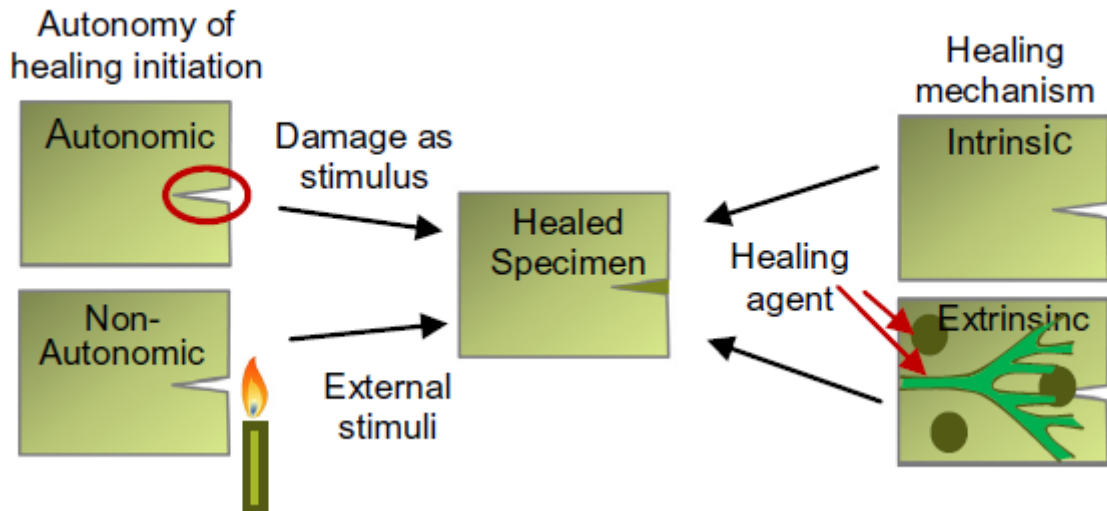
Figure 2.17 Classification of self-healing materials according to their autonomy and healing mechanism integration.

Self-healing finds most interest, by far, in polymer matrix composites. In them, internal micro cracks/damages during their lifetime cycle are very hard to detect and to repair. The current way to deal with this is to adopt conservative designs, which lead to overweight structures that do not utilize the full potential of fiber reinforced polymer matrixes. The development of self-healing in thermosets has followed a distinctly different route than that of thermoplastics. While for thermoplastics healing is generally associated with the high chain mobility which allows a softening and flow of material across a damaged interface that occurs upon heating, for thermosets such is not possible because their typical cross-link network prevents the polymer chains from diffusing through the material when heated above the Tg and instead the material degrades. Because of this, for thermosets most of the methods developed so far are extrinsic, requiring the use of a healing agent to mend the cracks. The research is presently focused on discovering the best distribution method and healing agent as well as the

possibility of mixing with others. As for the distribution method of the healing agent the most well-known are:

- Healing agent sealed in discrete micro-capsules for one time local healing when capsules are ruptured [62] (Fig.2.18a). This only works for micron-sized cracks with limited size and the healing process ceases once the healing agent is used;

- Hollow fiber embedment, generally glass fibers but more recently CNTs have also been researched [63] (Fig.2.18b). This method allows for multiple healing to occur and for larger cracks, and also can increase structural performance as the fibers also have load bearing capacity;

- A bio-inspired network of capillaries in which healing agen flows inside for multiple local healing events (Fig.2.18c) [64,65];

- Brownian motion induced polymer chain crawling has also been applied for self healing but with limited achievement.

Even if self-healing occurs and is shown to totally restore strength, it might be useful to have indications of the location and severity of the damage. Such can be accomplished if the healing agent is mixed with a fluorescent dye like Pang and Bond [70] did.

As the literature review showed, self-healing currently almost exclusively deals with repairing the structural function of materials. When damage occurs in multifunctional composites, several functions can be impaired at the same time, which raises the need for the healing ability to repair them as well.
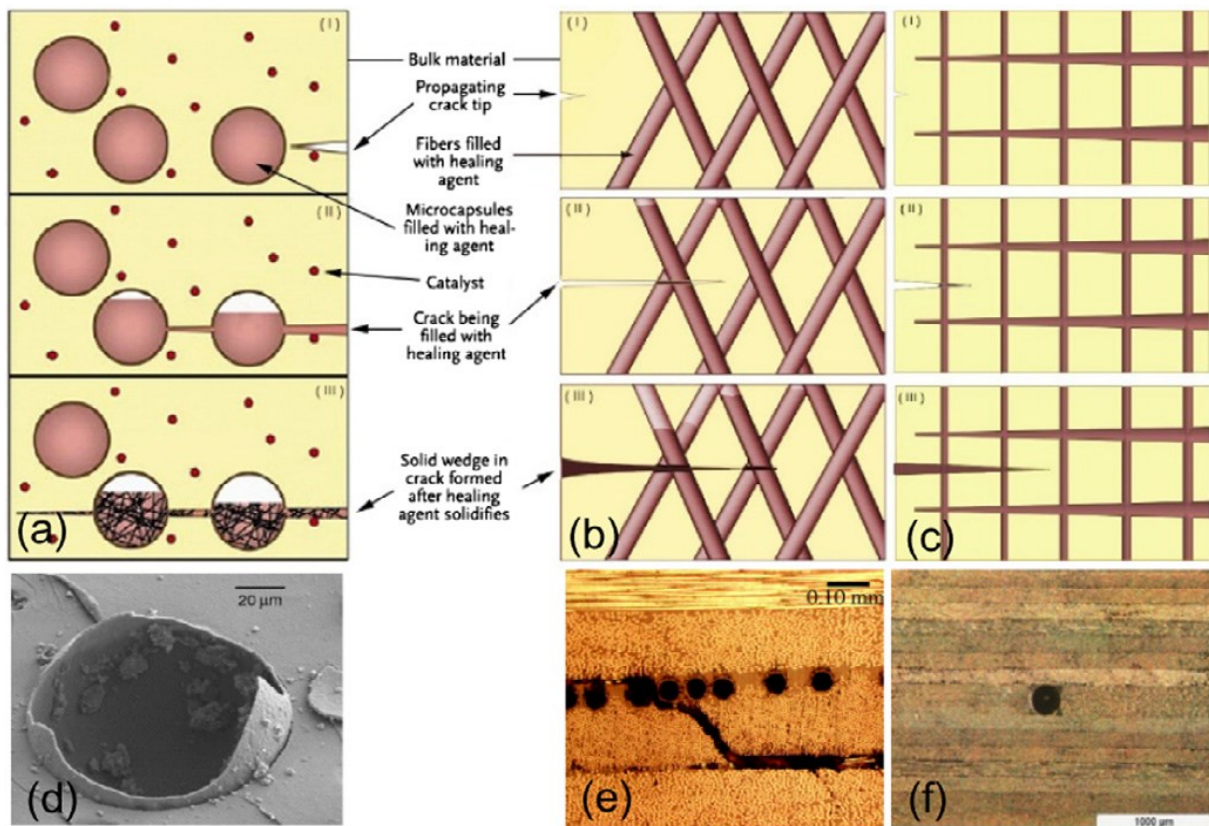
Figure 2.18 Fig. 62. (a) Illustration a self-healing mechanism based on a microencapsulated healing agent embedded in the matrix. When a crack occurs, the healing agent fills it cracks by capillary action, and, mixed with the catalyst, is polymerized and bonds the crack faces together; (b) illustration of self-healing mechanism in hollow fiberbased self-healing composites. Adapted from [66] and [67]; (c) Self-healing mechanism based on distribution by vasculature; (d) ESEM image showing ruptured microcapsule [68] (e) Intra-ply shear cracks intercepting hollow glass fibers in a self-healing CFRP laminate [69]; (f) Vascule in an Epoxy/CF laminate[64].

2.4 Synthesis of multifunctional nanocomposites

Multifunctional nanocomposites received a great deal of attention due to their synergy or enhanced properties compared to their base counterparts. In the field of multifunctional nanomaterials, considerable effort has been centered on the noble metal-based systems by immobilizing noble metal onto diverse inorganic/organic supports to obtain the desired functional nanomaterials. In addition, effort has been made in loading noble metals on semiconductor metal oxides such as TiO_2 and highly conductive nanomaterial such as CNTs using any surfactant or linkers [71].

It is well known that at nanoscale, the physical, chemical, and biological properties of materials are very different from their corresponding bulk counterpart because of the quantum confinement. For instance, gold and silver nanoparticles are characterized by their strong ability to absorb visible light at certain wavelengths, which depend on the size and shape of the nanomaterials. Solids with nanoparticle size cannot be prepared by traditional methods simply because the reactants are not mixed on the atomic scale. For this reason alternative methods, e.g., hydrothermal, sol–gel, Pechini, CVD, electrospinning, and microwave, have been evaluated in order to achieve atomic-scale mixing of reactants, in gas, liquid, or even solid phases. Although these are low-temperature methods, nevertheless, high-temperature processing may be required, especially for ceramic-based nanomaterials. These methods enable the final product to be homogenous nanosized materials with narrow particle size distribution. The appropriate methodologies for the preparation of these multifunctional nanomaterials are depicted in Table 2 [72] and they will be described below.

Phase system	Applications mode	Inherited properties	Applications
Single-phase NF	A composite system with the relevant metal oxides NF/NP	Large surface to weight ratio	High effective energy storage at reduced material cost and improved cycling performance, and
			Improved ion-transporting membranes for fuel cells, tailoring of the nanoarchitecture for thickness, density, porosity, surface area, and conductivity for the breakthrough of the technology
	Combined with polymer matrix to form composite system	High strength and stiffness	High flux and low-energy filtration media for water and air
			Interleave material for improved damage tolerance structural composites
Single-phase NP	A composite system with the relevant metal oxides NF/NP	Large surface area per unit volume	Stronger, corrosion/wear-resistant tunable platform for controlling surface wetting
	Combined with polymer matrix to form composite system	Thermally stable	Aerospace components, housings for electronics
Two-phase NF (composite NF)	A composite system with the relevant metal oxides NF/NP	Multifunctionality	Anti-counterfeiting of drugs, thermal interfaces
	Combined with polymer matrix to form composite system	Thermally and electrically stable, light weight	Smart textiles, coatings
			Thermal interface materials, clothes
Two-phase NP (composite NP)	A composite system with the relevant metal oxides NF/NP	Multifunctionality	Sensors having the ability to detect lower concentrations of biologically important species/detectable analytes
			The coatings having both electric/magnetic properties to effectively shield electromagnetic waves generated from an electric as well as the magnetic source, especially at low frequencies
	Combined with polymer matrix to form composite system	Highly resistant	Smart textiles

Table 2 Methodologies for the preparation of multifunctional nanomaterials

➤ *Hydrothermal synthesis*

Hydrothermal synthesis is one of the prominent methods employed to precipitate single/multiphase metal/semiconductor metal oxides directly from their corresponding homogeneous/heterogeneous solution. Hydrothermal synthesis is a single-step process preferred for preparing several single/multiphase oxides and phosphates [73-76]. Due to its simplicity and versatility, hydrothermal synthesis is also being used to grow single crystals ranging from emeralds, rubies, quartz, to alexandrite. The technique is also being employed to obtain nanomaterial for energy as well as environmental applications ranging from dye-sensitized solar cells to catalysis [77-78].

> *Sol–gel synthesis*

In sol–gel synthesis, a colloidal solution (sol) is being used to prepare a compound consisting of a metal or metalloid element surrounded by appropriate ligands (gel). This process results in the fabrication of variety of nanocrystalline elemental, alloy, and composite metal/semiconductor metal oxides. The sol–gel synthesis provides greater control in the process parameters, resulting in the synthesis of a variety of metal/semiconductor metal oxides [79].

> *Polymerized complex method (Pechini process)*

A wet chemical method using polymeric precursor based on the Pechini process has been employed to prepare a wide variety of ceramic oxides. The process offers several advantages for processing ceramic powders such as direct and precise control of stoichiometry, uniform mixing of multicomponents on a molecular scale, and homogeneity. The method is being widely used for the synthesis of dielectric, fluorescent, magnetic materials, high-temperature superconductors, and catalysts. The method is also preferred for the deposition of oxide films as coatings, for instance, nanostructured electrode in dye-synthesized solar cells and lithium ion battery [80-82].

> *Chemical vapor deposition*

Chemical vapor deposition (CVD) can deposit a film of solid material on a heated surface from a chemical reaction in the vapor phase. The versatile process can result in nano/microstructured coatings, powders, fibers, as well as multiphase compounds from metals, metal oxides, as well as nonmetallic elements such as carbon and silicon [83-85]. The advantage of CVD includes high throughput due to high deposition rate, as well as fabrication of single/multiphase nanomaterials. CVD process has been given enormous attention, owing to the possibility of mass production of nanomaterials; nevertheless, the mechanism of powder synthesis kinetics is still not completely known for this technique.

➤ *Microwave synthesis*

The applicability of microwave processing spans over a number of fields, ranging from food processing to medical and chemical applications. A major area of research in microwave processing includes microwave material interaction, microwave equipment design, new material development, sintering, joining, and modeling. As microwave processing offers uniform heating at a lower temperature, it is being successively utilized in the fabrication of ceramics as well as carbon fibers at low temperature and time [86-87].

2.5 Chapter 2 References

[1] A.D.B.L. Ferreira et al. / Composite Structures 151 (2016) 3–35.

[2] Matic P, 5053. Bellingham, Wash: SPIE; 2003. p. 61–9.

[3] Asp LE, Greenhalgh ES. Multifunctional composite materials for energy storage in structural load paths. [Slide Presentation]; 2012.

[4] Liu M, et al., ACS Nano 2013;7:10075–82.

[5] Page CD. Characterization of multifunctional carbon nanotube yarns: in-situ strain sensing and composite reinforcement 3586178 Ph.D. North Carolina State University, Ann Arbor; 2013.

[6] Zuberi MJS, Esat V., Compos B Eng 2015;71:1–9.

[7] Sakharova NA, et al., Compos B Eng 2015;75:73–85.

[8] Rafiee R, Moghadam RM., Compos B Eng 2014;56:435–49.

[9] Shokrieh MM, Rafiee R., Mech Compos Mater 2010;46:155–72.

[10] Allaoui A, et al., Compos Sci Technol 2002;62(11):1993–8.

[11] Hu Z, Lu X. Chapter 8 – mechanical properties of carbon nanotubes and graphene. In: Iijima KT, editor. Carbon nanotubes and graphene. Oxford: Elsevier; 2014. p. 165–200.

[12] Du JH, Cheng HM., Macromol Chem Phys Jun 2012;213:1060–77.

[13] Zapata-Solvas E, et al., J Eur Ceram Soc Sep 2012;32:3001–20.

[14] Kang I, et al., Compos Part B: Eng 2006;37:382–94.

[15] Wang S, Qiu J., Compos Part B: Eng 2010;41(10):533–6.

[16] Coleman JN, et al., Carbon 2006;44:1624–52.

[17] Tjong SC., Mater Sci Eng: R: Rep 2006;53:73–197.

[18] Lin Y, et al., Compos B Eng 2015;76:31–7.

[19] Porwal H, et al. Appl Ceram Nov 2013;112:443–54.

[20] Ovid'ko IA., Rev Adv Mater Sci 2014;38:190–200.

[21] Tjong SC., Mater Sci Eng: R: Rep 2013;74:281–350.

[22] Bakshi SR, et al., Int Mater Rev 2010;55:41–64.

[23] Moniruzzaman M, Winey KI., Macromolecules 2006;39:5194–205. 2006/08/01.

[24] Yu A, et al., J Phys Chem C 2007;111:7565–9. 2007/05/01

[25] Liu, Phang IY, et al., Macromolecules 2004;37:7214–22. 2004/09/01.

[26] Muralt P, et al., MRS Bull 2009;34:658–64.

[27] Giurgiutiu V, Zagrai AN., J Intell Mater Syst Struct 2000;11:959–76.

[28] Cook AC, Vel SS., Eur J Mech A Solids 2013;40:11–33.

[29] Cook AC, Vel SS., Compos Struct 2012;94:322–36.

[30] Huang T, et al., Nano Energy 2015.

[31] Ramdayal, Balasubramanian K., Defence Sci Journal 2013;63:331–9.

[32] Zhang M, et al., Nano Energy 2015.

[33] Nilsson E, et al., Proc Eng2014;87:1569–72.

[34] Fernandez JF., Sens Actuators A: Phys 1995;51:183–92.

[35] Brei D, Cannon BJ., Compos Sci Technol 2004;64:245–61.

[36] Guillot FM, et al., J Eng Fibers Fabr 2013;8:75–81.

[37] Chen Y, et al., In: SPIE, Smart structures and materials 2006: smart structures and integrated systems, San Diego; 2006.

[38] Bent AA. Active fiber composites for structural actuation [Doctor of Philosophy], Aeronautics and Astronautics, Massachusetts Institute of Technology; 1997.

[39]Lin X-J, et al., Trans Nonferrous Met Soc China 2013;23:98–107.

[40] Lin Y, Sodano HA., Compos Sci Technol 2008;68:1911–8.

[41] Lin Y, Sodano HA., . Adv Funct Mater 2009;19:592–8.

[42] Guillot François M, et al., J Eng Fibers Fabrics 2013;8.

[43] Brett Williams R et all., Modal Analysis Conference; 2002.

[44] Kovalovs A, et al., J Phys: Conf Ser 2007;93:012034.

[45] NASA's Langley Research Center. <https://spinoff.nasa.gov/Spinoff2007/ip_9.html>; 2007.

[46] Smart material. <http://www. smart-material.com/MFC-product-main.html>; 2015.

[47] Li M., Sci China Ser E: Technol Sci 2011;54:395–402.

[48] Calkins FT, Mabe JH., J Mech Des 2010;132:111012.

[49] Sofla AYN, et al., Mater Des 2010;31:1284–92.

[50] Oehler SD, et al., Smart Mater Struct 2012;21:094016.

[51] Khan MI, et al., Adv Eng Mater 2013;15:386–93.

[52] Ghosh P, et al., Mater Des 2013;44:164–71.

[53]Leng J, et al., Prog Mater Sci 2011;56:1077–135.

[54] Meng H., Polymer 2013;54:2199–221.

[55] Lu HB, et al., Nanosci Nanotechnol Lett Sep 2014;6:772–86.

[56] Thill C, et al., Aeronaut J 2008;112:117–39.

[57] Leng J-S, et al., Yuhang Xuebao/J Astronaut 2010;31:950–6.

[58] K. Philip, et al., 47th AIAA/ASME/ASCE/AHS/ASC Structures, Structural Dynamics, and Materials Conference, American Institute of Aeronautics and Astronautics, 2006.

[59] <http://www.kth.se/en/aktuellt/nyheter/de-gor-batterier-avkolfiber-1.480780>

[60] The Conservative Thinkers Blogspot. Lola Drayson B12/69EV electric racing car launched, available: Lola Drayson B12/69EV electric racing car launched; 2014.

[61] Pereira AM. Energy-storage multifunctional composites 3405614 Ph.D. University of California, Los Angeles, Ann Arbor; 2009.

[62] Kirkby EL, et al., Polymer 2009;50:5533–8.

[63] Lanzara G, et al., Nanotechnology 08/19 2009;20:5533–8. p. 335704 (7 p.).

[64] Norris CJB, et al. Healing of low-velocity impact damage in vascularised composites. vol. 44; 2013. p. 85.

[65] Hugo RST, et al., first international conference on self healing materials, Noordwijk aan Z ee,The Netherlands; 2007

[66] White RS, et al., Nature 2001;409:794–7. 02/15/print.

[67] Wu DY, et al., Prog Polym Sci 2008;33:479–522.

[68] Trask RS, et al., Bioinspiration Biomimetics Mar 2007;2:P1–9.

[69] Trask RS, et al., J R Soc Interface 2007;4:363–71.

[70] Pang JWC et al., Compos Part A Appl Sci Manuf 2005;36:183–8.

[71] Jose et al., Journal of the American Ceramic Society (2009), 92(2), 289–301.

[72] Sahay et al. International Journal of Mechanical and Materials Engineering 2014, 9:25

[73] Dai et al., Nano Letters (2009), 9(6), 2455–2459

[74] Fang et al., Small (2006), 2(5), 612–615.

[75] Ye et al., Small (2010), 6(2), 296–306.

[76] Ji et al., Research Bulletin (2009), 44(4), 768–774.

[77] Hsu et al., Applied Physics Letters (2008), 92(13), 133507.

[78] Zhou et al., European Journal of Inorganic Chemistry (2010), 5, 729–734.

[79] Leventis et al., Journal of the American Chemical Society(2009), 131(13), 4576–4577.

[80] Sahay et al., Journal of Solid State Chemistry (2012a), 186, 261–267.

[81] Sahay et al., Journal of Physical Chemistry C (2012b), 116(34), 18087–18092.

[82] Suresh Kumar et al., J. Phys. D: Appl. Phys. (2012), 45(26), 265302 (1-5).

[83] Hitchman and Tian, Journal of Electroanalytical Chemistry (2002), 538, 165–172.

[84] Iguchi et al., Topics in Catalysis (2009), 52(6–7), 563–570.

[85] Mills et al., Journal of Photochemistry and Photobiology A-Chemistry (2002), 151(1–3), 171-179.

[86] Reddy et al., Catalysis Letters (2009), 130(1–2), 227–234.

[87] Chae et al., Journal of Nanoscience and Nanotechnology (2010), 10(5), 3534–3537.

3. Electrospinning: Process and Applications

3.1 Introduction

It has been view that when the diameters of polymer fiber materials are shrunk from micrometers to submicrons or nanometers, there appear several amazing characteristics such as very large surface area to volume ratio (this ratio for a nanofiber can be as large as 103 times of that of a microfiber), flexibility in surface functionalities, and superior mechanical performance (e.g. stiffness and tensile strength) compared with any other known form of the material. These outstanding properties make the polymer nanofibers to be optimal candidates for many important applications. A number of processing techniques such as drawing, template synthesis, phase separation, self-assembly, electrospinning, etc. have been used to prepare polymer nanofibers in recent years.

The drawing is a process similar to dry spinning in fiber industry, which can make one-by-one very long single nanofibers. However, only a viscoelastic material that can undergo strong deformations while being cohesive enough to support the stresses developed during pulling can be made into nanofibers through drawing. The template synthesis, as the name suggests, uses a nanoporous membrane as a template to make nanofibers of solid (a fibril) or hollow (a tubule) shape. The most important feature of this method may lie in that nanometer tubules and fibrils of various raw materials such as electronically conducting polymers, metals, semiconductors, and carbons can be fabricated. On the other hand, the method cannot makeone-by-one continuous nanofibers. The phase separation consists of dissolution, gelation, extraction using a different solvent, freezing, and drying resulting in a nanoscale porous foam. The process takes relatively long period of time to transfer the solid polymer into the nano-porous foam.

The self-assembly is a process in which individual, pre-existing components organize themselves into desired patterns and functions. However, similarly to the phase separation the self-assembly is time-consuming in processing continuous polymer nanofibers. Thus, the electrospinning process seems to be the only method which can be further developed for mass production of one-by-one continuous nanofibers from various polymers. Electrospinning has emerged as a powerful technique for producing high strength fibers due to its versatility, ease of use, ability to align structures and control fiber diameters. Some of these unique features cannot be otherwise achieved by conventional fiber processing techniques mentioned above. Another merit is that under the influence of an electric field, electrospinning self-assembles dispersed fillers along the axial direction such that composites can be formed by imposing additional spatial confinement to the polymer chains. These reinforced fibers display superior properties and function as basic building blocks for the fabrication of high strength structures using a bottom-up approach. For example, carbon nanotubes (CNTs) and carbon black (CB) particles are among the commonly used fillers which are dispersed within the fibers to mimic the functionality of silk fibers for high strength and toughness applications.

3.2 History of electrospinning

The origin of electrospinning as a viable fiber spinning technique can be traced back to the early 1930s. In 1934, Formhals patented his first invention relating to the process and the apparatus for producing artificial filaments using electric charges [1]. Though the method of producing artificial threads using an electric field had been experimented with for a long time, it had not gained importance until Formhals's invention due to some technical difficulties in earlier spinning methods, such as fiber drying and collection. Formhals's spinning process consists of a movable thread collecting device to collect the threads in a stretched condition, like that of a spinning drum in the conventional spinning. Formhals's process was capable of

producing threads aligned parallel on to the receiving device in such a way that it can be unwound continuously. The first spinning method adopted by Formhals had some technical disadvantages. It was difficult to completely dry the fibers after spinning due to the short distance between the spinning and collection zones, which resulted in a less aggregated web structure. Formhals refined his earlier approach to overcome the aforementioned drawbacks.

Subsequently in 1940, Formhals patented another method [1] for producing composite fiber webs from multiple polymer and fiber substrates by electrostatically spinning polymer fibers on a moving base substrate. In the 1960s, fundamental studies on the jet forming process were initiated by Taylor [36]. In 1969, Taylor studied the shape of the polymer droplet produced at the tip of the needle when an electric field is applied and showed that it is a cone and the jets are ejected from the vertices of the cone.7 This conical shape of the jet was later referred to by other researchers as the "Taylor Cone" in subsequent literature. By a detailed examination of different viscous fluids, Taylor determined that an angle of 49.3 degrees is required to balance the surface tension of the polymer with the electrostatic forces. The conical shape of the jet is important because it defines the onset of the extensional velocity gradients in the fiber forming process. In subsequent years, focus shifted to studying the structural morphology of nanofibers [1]. Researchers were occupied with the structural characterization of fibers and the understanding of the relationships between the structural features and process parameters. Wide-angle X-ray diffraction (WAXD), scanning electron microscopy (SEM), transmission electron microscopy (TEM), and differential scanning calorimetry (DSC) have been used by researchers to characterize electrospun nanofibers.

In 1987, Hayati et al. [2] studied the effects of electric field, experimental conditions, and the factors affecting the fiber stability and atomization. They concluded that liquid conductivity plays a major role in the electrostatic disruption of liquid surfaces. Results showed that highly conducting fluids with increasing applied voltage produced highly unstable streams that

whipped around in different directions. Relatively stable jets were produced with semi conducting and insulating liquids, such as paraffinic oil. Results also showed that unstable jets produce fibers with broader diameter distribution.

After a hiatus of a decade or so, a major upsurge in research on electrospinning took place due to increased knowledge on the application potential of nanofibers in different areas, such as high efficiency filter media, protective clothing, catalyst substrates, and adsorbent materials.

Research on nanofibers gained momentum due to the work of Doshi and Reneker [3]. They studied the characteristics of polyethylene oxide (PEO) nanofibers by varying the solution concentration and applied electric potential. Jet diameters were measured as a function of distance from the apex of the cone, and they observed that the jet diameter decreases with the increase in distance.

Deitzel et al.[4] showed that an increase in the applied voltage changes the shape of the surface from which the jet originates and the shape change has been correlated to the increase in the bead defects. They tried to control the deposition of fibers by using a multiple field electrospinning apparatus that provided an additional field of similar polarity on the jets.

Warner et al. [5] and Moses et al. [6] pursued a rigorous work on the experimental characterization and evaluation of fluid instabilities, which are crucial for the understanding of the electrospinning process. Shin et al. designed a new apparatus that could give enough control over the experimental parameters to quantify the electrohydrodynamics of the process.

Gibson et al. [7] studied the transport properties of electrospun fiber mats, and they concluded that nanofiber layers give very less resistance to the moisture vapor diffusional transport.

3.3 The process

Electrospinning, uses high voltage (about 10–20 kV) to electrically charge the polymer solution for producing ultra-fine fibers. The basic electrospinning setup, consists of a pipette or a syringe filled with polymer solution, a high voltage source and a grounded conductive collector screen. In addition, a metering syringe pump can be used to control the flow rate of the polymer solution. The needle of the syringe typically serves as an electrode to electrically charge the polymer solution and the counter-electrode is connected to the conductive collector screen. Under the influence of a strong electrostatic field, charges are induced in the solution and the charged polymer is accelerated towards the grounded metal collector. At low electrostatic field strength, the pendant drop emerging from the tip of the pipette is prevented from dripping due to the surface tension of the solution. As the intensity of the electric field is increased, the induced charges on the liquid surface repel each other and create shear stresses. These repulsive forces act in a direction opposite to the surface tension, which results in the extension of the pendant drop into a conical shape and serves as an initiating surface.

A schematic of the process is shown in Figure 3.1. When the critical voltage is reached, the equilibrium of the forces is disturbed and a charged jet emanates from the tip of the conical drop. The discharged jet diameter decreases in size with concomitant increase in length before being deposited on the collector. This process can be explained by the three types of physical

instabilities experienced by the jet. These instabilities influence the size and geometry of the deposited fibers. The first instability, also known as the Rayleigh instability is axisymmetric and occurs when the strength of electric field is low or when the viscosity of the solution is below the optimum value. Use of very low viscosity solutions causes jet break-up and leads to the bead-on-fiber morphology. It is attributed to the poor chain entanglement density in the solution and insufficient resistance to the electrostatic field. Rayleigh instability is suppressed

at high electric fields (high charge densities) or when using higher concentration of polymer in the solution.
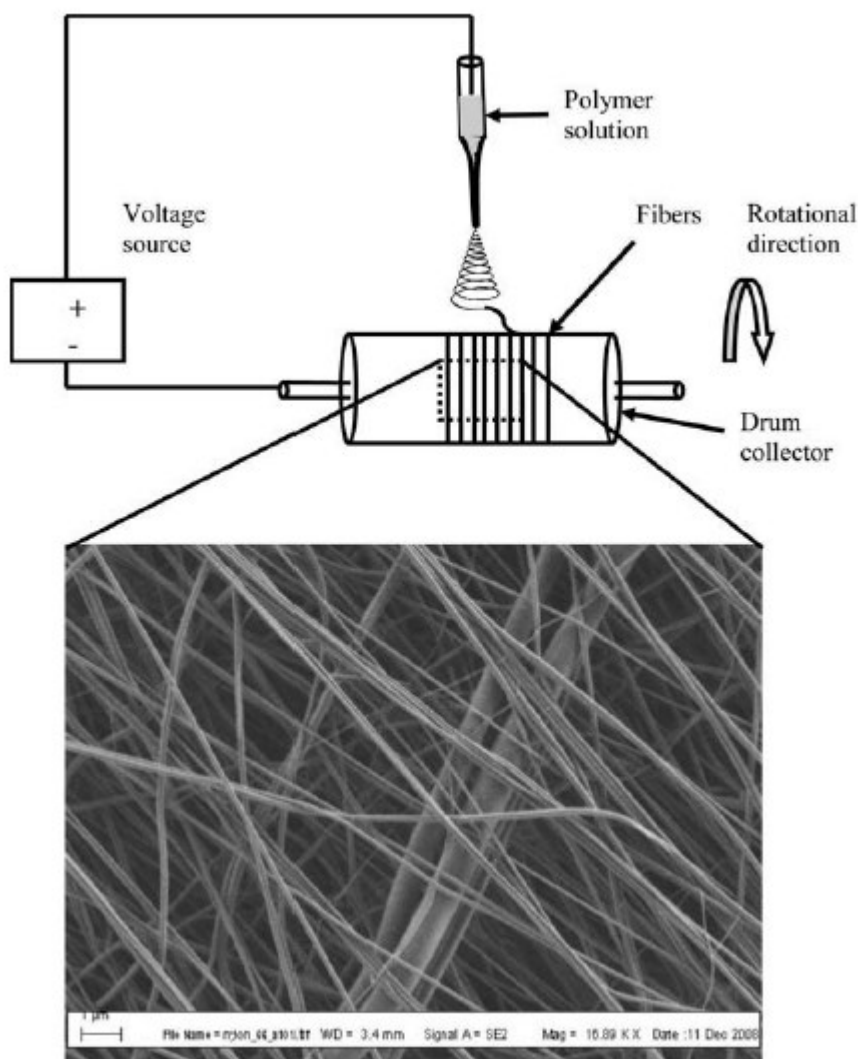
Figure 3.1 Schematic of the rotating drum used for fiber collection. The inset SEM micrograph shows the aligned fibers obtained using the rotating drum

Following the initial straight path of the jet, which is controlled by the Rayleigh instability, the polymer jet is influenced by two other instabilities: the bending and whipping instabilities. These instabilities arise owing to the charge-charge repulsion between the excess charges present in the jet which encourages the thinning and elongation of the jet. At high electric forces, the jet is dominated by bending (axisymmetric) and whipping instability (non-

axisymmetric), causing the jet to travel in an ''inverse cone'' manner. It produces wave or dumb-bell shaped patterns in the jet . At higher electric fields and at sufficient charge density in the jet, the axisymmetric (i.e., Rayleigh and bending) instabilities are suppressed and the non-axisymmetric instability is enhanced. The whipping instability produces a bending force on the jet, resulting in a high degree of elongation of the jet. During these processes, the solvent evaporates and finally leads to the deposition of ultra-fine fibers on the conductive ground electrode.

3.4 Spinning of Polymeric Nanofibres

Research activity on the electrospinning of nanofibers has been successful in spinning submicron range fibers from different polymeric solutions and melts.

Polymers with attractive chemical, mechanical, and electrical properties like high conductivity, high chemical resistance, and high tensile strength have been spun into ultrafine fibers by the electrospinning process, and their application potential in areas like filtration, optical fibers, drug delivery system, tissue scaffolds, and protective textiles have been examined [4-7].

3.4.1 Structure and morphology of polymeric nanofibres

As theoretical studies on the electrospinning process have been conducted by various groups [6-8] for a while to understand the electrospinning process, there have been some simultaneous efforts to characterize the structure and morphology of nanofibers as a function of process parameters and material characteristics. rocess is influenced both by the electrostatic forces and the viscoelastic behavior of the polymer. Process parameters, like solution feed rate, applied voltage, nozzle-collector distance, and spinning environment, and

material properties, like solution concentration, viscosity, surface tension, conductivity, and solvent vapor pressure, influence the structure and properties of electrospun nanofibers.

3.4.1.1 Process parameters and fiber morphology

Applied Voltage

Various instability modes that occur during the fiber forming process are expected to occur by the combined effect of both the electrostatic field and the material properties of the polymer. It has been suggested that the onset of different modes of instabilities in the electrospinning process depend on the shape of the jet initiating surface and the degree of instability, which effectively produces changes in the fiber morphology [4]. In electrospinning, the charge transport due to the applied voltage is mainly due to the flow of the polymer jet towards the collector, and the increase or decrease in the current is attributed to the mass flow of the polymer from the nozzle tip.

Deitzel et al. [4] have inferred that the change in the spinning current is related to the change in the instability mode. They experimentally showed that an increase in applied voltage causes a change in the shape of the jet initiating point, and hence the structure and morphology of fibers. Earlier in 1971, Baumgarten while carrying out experiments with acrylic fibers observed an increase in fiber length of approximately twice with small changes in fiber diameter with an increase in applied voltage [9].

Generally, it has been accepted that an increase in the applied voltage increases the deposition rate due to higher mass flow from the needle tip.

Nozzle collector distance

The structure and morphology of electrospun fibers is easily affected by the nozzle to collector distance because of their dependence on the deposition time, evaporation rate, and whipping or instability interval.

Buchko et al. [1] examined the morphological changes in SLPF and nylon electrospun fibers with variations in the distance between the nozzle and the collector screen. They showed that regardless of the concentration of the solution, lesser nozzle-collector distance produces wet fibers and beaded structures. SLPF fiber morphology changed from round to flat shape with a decrease in the nozzle collector distance from 2cm to 0.5cm. This result shows the effect of the nozzle collector distance on fiber morphology. The work also showed that aqueous polymer solutions require more distance for dry fiber formation than systems that use highly volatile organic solvents.

Polymer flow rate

The flow rate of the polymer from the syringe is an important process parameter as it influences the jet velocity and the material transfer rate. In the case of PS fibers, Megelski et al. [36] observed that the fiber diameter and the pore diameter increased with an increase in the polymer flow rate. As the flow rate increased, fibers had pronounced beaded morphologies and the mean pore size increased from 90 to 150 nm.

Spinning environment

Environmental conditions around the spinneret, like the surrounding air, its relative humidity, vacuum conditions, surrounding gas, etc., influence the fiber structure and morphology of electrospun fibers. Baumgarden [1] observed that acrylic fibers spun in an atmosphere of relative humidity more than 60% do not dry properly and get entangled on the surface of the

collector. The breakdown voltage of the atmospheric gases is said to influence the charge retaining capacity of the fibers.

3.4.1.2 Solution parameters and fiber morphology

Solution concentration

Solution concentration decides the limiting boundaries for the formation of electrospun fibers due to variations in the viscosity and surface tension. Low concentration solution forms droplets due to the influence of surface tension, while higher concentration prohibits fiber formation due to higher viscosity. Previously published literature has documented the difficulties in the electrospinning of polymers like PEO, PAN, and PDLA in certain concentration levels [1].

Solution conductivity

Polymers are mostly conductive, with a few exceptions of dielectric materials, and the charged ions in the polymer solution are highly influential in jet formation. The ions increase the charge carrying capacity of the jet, thereby subjecting it to higher tension with the applied electric field. Baumgarden [1] showed that the jet radius varied inversely as the cube root of the electrical conductivity of the solution.

Volatility of solvent

As electrospinning involves rapid solvent evaporation and phase separations due to jet thinning, solvent vapor pressure critically determines the evaporation rate and the drying time. Solvent volatility plays a major role in the formation of nanostructures by influencing the phase separation process.

Lee et al. [1] evaluated the effect of volume ratio of the solvent on the fiber diameter and morphology of electrospun PVC fibers. Average fiber diameters decreased with an increase in the amount of DMF in the THF/DMF mixed solvent. Lee et al. found the electrolytic nature of the solvent to be an important parameter in electrospinning. Megelski et al. [1] studied the characteristics of electrospun fibers with respect to the physical properties of solvents. The influence of vapor pressure was evident when PS fibers spun with different THF/DMF combinations resulted in micro and nanostructure morphologies at higher solvent volatility and a much-diminished microstructure at lower solvent volatility.

3.4.2 Properties of nanofibers

As briefly discussed, a major upsurge in research on nanofibers has taken place most recently due to its high surface area and nanostructure surface morphologies that enable a myriad of advanced applications [1]. Nanofibers have been reported to have marked differences in their thermal and mechanical properties compared to regular fibers and bulk polymers.

3.4.2.1 Thermal properties

There are a few published reports on the thermal properties of nanostructured materials. Thermal analysis has been carried out on a number of electrospun polymeric materials to understand the relationship between nanostructure and thermal properties. DSC studies have indicated that electrospun PLLA fibers have lower crystallinity, glass transition temperature (T_g), and melting temperature (T_m) than semicrystalline PLLA resins [1]. Zong et al. attributed the decrease in the T_g to the large surface to volume ratio of nanofibers with air as the plasticizer [1]. The high evaporation rate followed by rapid solidification at the final stages of electrospinning is expected to be the reason for the low crystallinity. The T_g and the peak crystallization temperature (T_c) of the electrospun polyethylene terephthalate (PET) and

polyethylene naphthalate (PEN) decreased significantly, while the heat of crystalline melting increased. The decrease in Tg and Tm, and the increase in the heat of melting were attributed

to the increase in the segmental mobility. The melting temperature of the PET and PEN electrospun fibers remained almost constant, without any significant variations compared to that of regular fiber forms. PEO nanofibers have shown a lower melting temperature and heat of fusion than the PEO powder, which is attributed to the poor crystallinity of the electrospun fibers. The crystallinity of the PLLA fibers was observed to be completely retarded by electrospinning, and the WAXD patterns of the electrospun PLLA fibers confirmed highly oriented fibers. This decrease in crystallinity has been shown to be a general phenomenon and has been observed in poly (*meta*-phenylene isophthalamide), poly (glycolide), and polyacrylonitrile. Deitzel et al. [4] inferred that PEO nanofibers retained the same crystal structure as PEO powders, while there is a clear indication of reduced crystalline order in nanofibers. Bognitzki et al. concluded with the help of a DSC thermogram that the degree of crystallinity of electrospun PLLA fibers was in the order of 40%.

Thermal degradation of PET and PEN before and after electrospinning was analyzed by Kim and Lee [1] using the TGA thermogram, and they found that on electrospinning the intrinsic viscosities of both PET and PEN reduced significantly. The thermal degradation and hence the decrease in intrinsic viscosities (i.e., decrease of molecular weight) were postulated to be the reasons for the decrease in Tg and Tc caused by reduced entanglements.

3.4.2.2 Mechanical properties

Electrospun fibers have nanostructured surface morphologies with tiny pores that influence mechanical properties like tensile strength, Young's modulus, etc. Gibson et al. [7] have

found that there is no significant change in the Young's modulus of electrospun Pellethane thermoplastic elastomers. When compared with cast films, electrospun elastomers have shown a 40% reduction in the peak tensile strength and 60% reduction in elongation at maximum applied stress. The decrease in the tensile strength has also been reported by Buchko et al. [1] with SLPF fibers. Nanofiber reinforced polymer composites have shown more highly enhanced mechanical properties than the unfilled or carbon/glass fiber filled composites. Young's modulus of a nanofiber composite has been found to be 10-fold greater than the pure Styrene-Butadiene rubber. As is evident, there is less information available on the mechanical properties of nanofibers and nanofiber composites. Research on the mechanical properties of nanofibers and their composites from a variety of polymers is essential for a greater understanding on the contributions of nanofibers to the mechanical and performance related characteristics of nanofiber composites.

3.5 Application of electrospun nanofibres

Nanomaterials have been attracting the attention of global materials research these days primarily due to their enhanced properties required for application in specific areas like catalysis, filtration, NEMS, nanocomposites, nanofibrous structures, tissue scaffolds, drug delivery systems, protective textiles, storage cells for hydrogen fuel cells, etc. (Fig.3.2). A brief discussion on some of the applications (excluding nanocomposites application that will be discussed later) is given in this section.
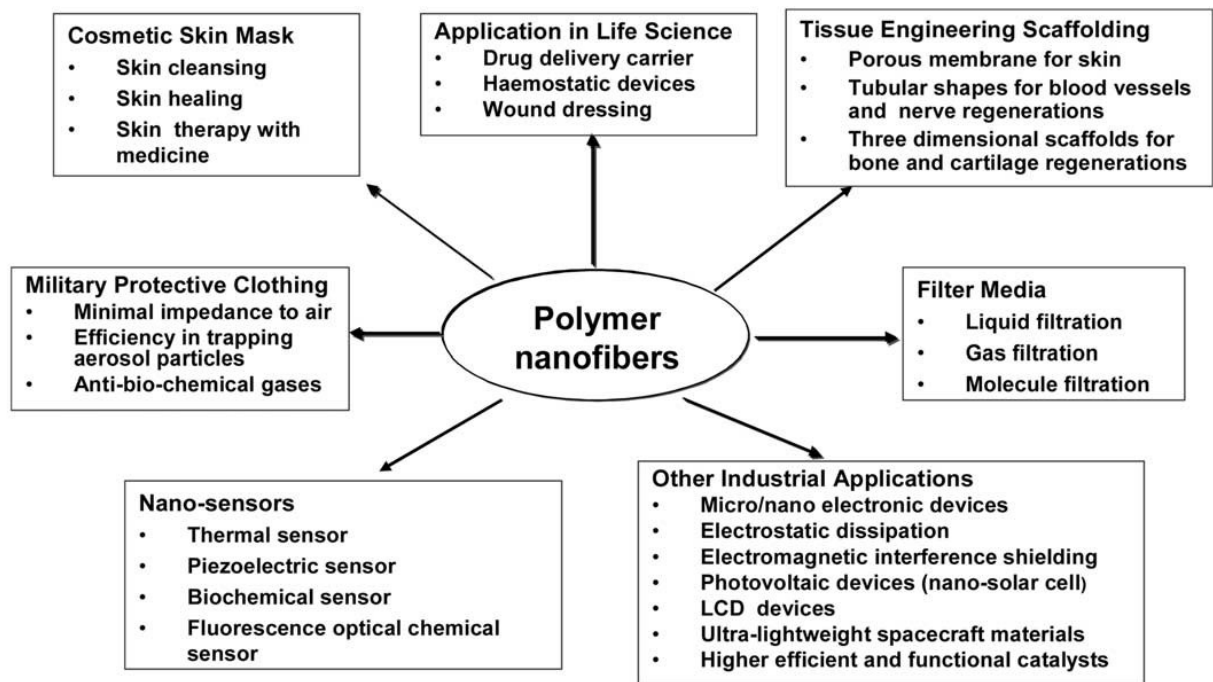
Cosmetic Skin Mask
- Skin cleansing
- Skin healing
- Skin therapy with medicine

Application in Life Science
- Drug delivery carrier
- Haemostatic devices
- Wound dressing

Tissue Engineering Scaffolding
- Porous membrane for skin
- Tubular shapes for blood vessels and nerve regenerations
- Three dimensional scaffolds for bone and cartilage regenerations

Military Protective Clothing
- Minimal impedance to air
- Efficiency in trapping aerosol particles
- Anti-bio-chemical gases

Polymer nanofibers

Filter Media
- Liquid filtration
- Gas filtration
- Molecule filtration

Nano-sensors
- Thermal sensor
- Piezoelectric sensor
- Biochemical sensor
- Fluorescence optical chemical sensor

Other Industrial Applications
- Micro/nano electronic devices
- Electrostatic dissipation
- Electromagnetic interference shielding
- Photovoltaic devices (nano-solar cell)
- LCD devices
- Ultra-lightweight spacecraft materials
- Higher efficient and functional catalysts

Figure 3.2 Potential applications of electrospun polymer nanofibers

3.5.1 Biomedical application

From a biological viewpoint, almost all of the human tissues and organs are deposited in nanofibrous forms or structures. Examples include: bone, dentin, collagen, cartilage, and skin. All of them are characterized by well organized hierarchical fibrous structures realigning in nanometer scale. As such, current research in electrospun polymer nanofibers has focused one of their major applications on bioengineering. We can easily find their promising potential in various biomedical areas. Some examples are listed later.

3.5.1.1 Medical prostheses

Polymer nanofibers fabricated via electrospinning have been proposed for a number of soft tissue prostheses prostheses applications such as blood vessel, vascular, breast, etc (Fig.3.3). In addition, electrospun biocompatible polymer nanofibers can also be deposited as a thin porous film onto a hard tissue prosthetic device designed to be implanted into the human

body. This coating film with gradient fibrous structure works as an interphase between the prosthetic device and the host tissues, and is expected to efficiently reduce the stiffness mismatch at the tissue/device interphase and hence prevent the device failure after the implantation.
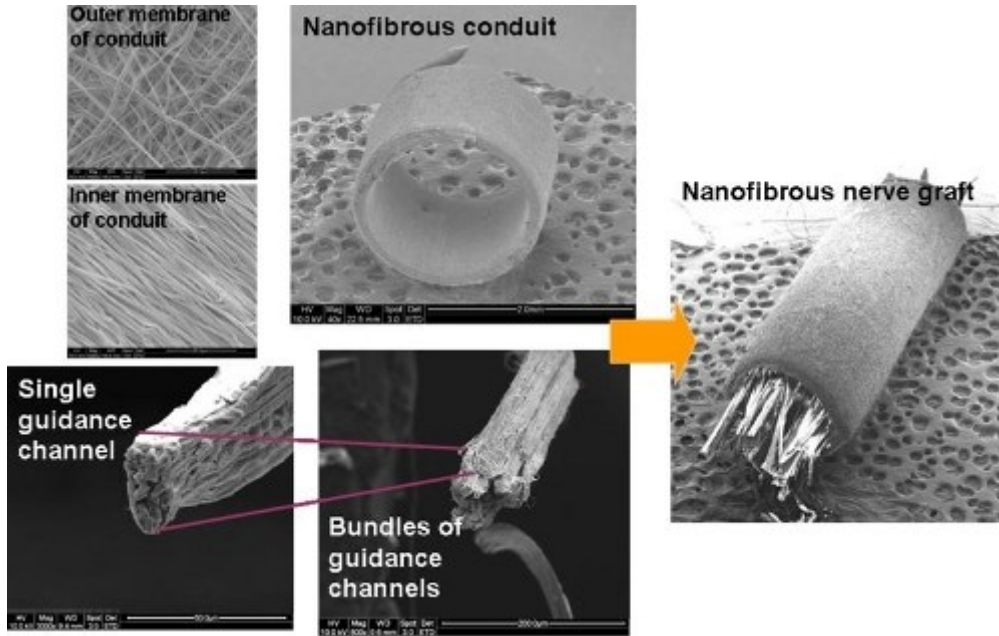

Figure 3.3 Structural organization of nerve guidance conduit (H S Koh et al. J. Neural Eng. 2010; 7: 046003

3.5.2 Electrical and optical application

Conductive nanofibers are expected to be used in the fabrication of tiny electronic devices or machines such as Schottky junctions, sensors and actuators. Due to the well-known fact that the rate of electrochemical reactions is proportional to the surface area of the electrode, conductive nanofibrous membranes are also quite suitable for using as porous electrode in developing high performance battery (Fig.3.4). Conductive (in terms of electrical, ionic and photoelectric) membranes also have potential for applications including electrostatic dissipation, corrosion protection, electromagnetic interference shielding, photovoltaic device, etc..
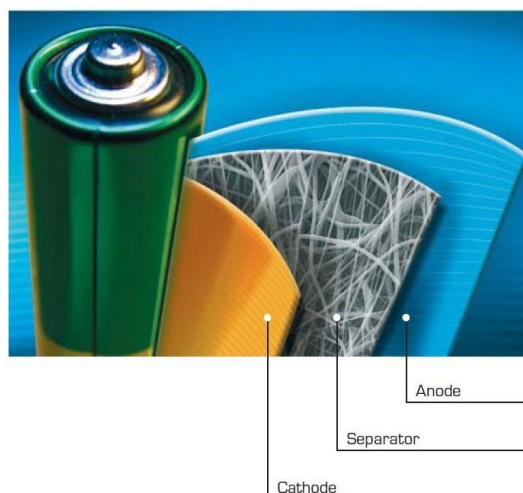
Figure 3.4 battery with superior parameters by Elmarco's Nanospider™ technology.

Waters et al. [10] reported to use electrospun nanofibers in the development of a liquid crystal device of optical shutter which is switchable under an electric field between a state in which it is substantially transparent to incident light and a state in which it is substantially opaque. The main part of this liquid crystal device consisted of a layer of nanofibers permeated with a liquidcrystal material, having a thickness of only few tens microns. The layer was located between two electrodes, by means of which an electric field could be applied across the layer to vary the transmissivity of the liquid crystal/nanofiber composite. It is the fiber size used that determines the sensitivities of the refractive index differences between the liquid crystal material and the fibers, and consequently governs the transmissivity of the device. Obviously nanoscale polymer fibers are necessary in this kind of devices.

One dimensional (1D) nanostructures displaying luminescence i.e. photoluminescence, electroluminescence have attracted strong attention in recent years in particular in view of potential applications in light emitting diodes, full colour displays, lasers, data storage. The

number of papers on electrospun light emitting nanofibers has correspondingly increased strongly with the last years. In principle three concepts were used to prepare such nanofibers based on (a) conjugated polymers frequently in combination with polymer blend components, (b) polymers into which functional components such as quantum dots or rare earth complexes were incorporated (here the argument is that such an approach allows to combine the favorable properties of the organic materials – flexibility, processibility, light weight – with the ones of the inorganic materials – hardness, thermal stability, chemical resistance, optical function), (c) inorganic materials doped among others also with rare earth complexes.ù

3.6 References Chapter 3

[1] T. Subbiah et al., Wiley InterScience, (2004).

[2] Hayati, I et al., T. F. J Colloid Interface Sci 1987, 117, 205.

[3] Doshi, J.; Reneker, D. H. J Electrostatics 1995, 35, 151.

[4] Deitzel, J. M. et al.; N. C Polymer 2001, 42, 261.

[5] Warner, S. et al., Shin, M. Y. National Textile Center Annu Report November 1998, 83.

[6] Moses, M. et al.; Phys Fluids 2001, 13, 2201

[7] Gibson, P. W. et al.; Rivin, D. AIChe J 1999, 45, 190.

[8] Yarin A. L et al., D. H. J Appl Phys 2001, 89, 5.

[8] Baumgarten, P. K. JColloid Interface Sci 1971, 36, 71.

[10] Waters CM, Noakes TJ, Pavery I, Hitomi C. US patent 5088807, 1992.

4. Electrospun nanofibres reinforced composites

Composite products are used practically in every type of advanced structural applications including civil infrastructures, mechanical industry, land, sea and air transport vehicles, space exploration, military equipment and defense, healthcare and sporting items.

Fiber reinforced polymer (FRP) composites are commonly designed with the primary aim of obtaining superior mechanical properties (higher modulus and strength to weight ratio) with respect to existing materials for advanced structural applications, but they are also promising candidates as functional materials. The fiber component can also provide the possibility of modifying other functional properties of the plain polymer matrix, such as its optical and thermal properties, as well as its conductivity and dielectric constant.

With the aim of designing advanced and innovative FRP composites, the idea of further engineering the material through the incorporation of reinforcing nanofibers have attracted an increasing amount of interest. This research area has emerged starting from the consideration that either the use of nanofibers in place of the presently used micro-size fibers, or a suitable combination of micro- and nanofibers might further improve FRP composites mechanical properties.

4.1 Why nanofibres as composite reinforcement?

In traditional FRP composites, different configuration of the reinforcing fibers can be used, each leading to different mechanical performances. There are two principal fibres configurations within the matrix: in the first one short fibres are randomly oriented while the other are represented by layers of long unidirectional fibers. Composites reinforced with short random fibers display isotropic mechanical properties while long unidirectional fibers are used when an orthotropic and strong reinforcing effect is desired.

In the field of FRP two main types of structural composites architectures can be distinguished:

> bulk composite structures,

> laminate composites.

In the first type of composites, the efficiency of the stress transfer from the polymer matrix to the filler governs the effectiveness of the reinforcement, thus the possibility to obtain improved mechanical properties with respect to those of the unfilled matrix. It has been widely demonstrated that fibers can carry out the reinforcing function, when they fulfill the following requirements: (a) suitable mechanical properties in terms of strength and stiffness with respect to the matrix; (b) large aspect ratio; (c) high surface area to volume ratio; (d) good fiber-matrix adhesion; (e) good dispersion and embedding in the polymer matrix; (f) proper orientation with respect to the applied external load. Since it is expected that nanofibers have the potentiality to greatly satisfy all the above listed characteristics, it can be easily understood why the engineering idea of using nanofibers to fabricate high-performance FRP composite structures, with further enhanced structural properties, is attracting growing interest nowadays.

Figure 4.1 sketches the potentialities of using nanofibers in place of microfibers for designing bulk composite structures.
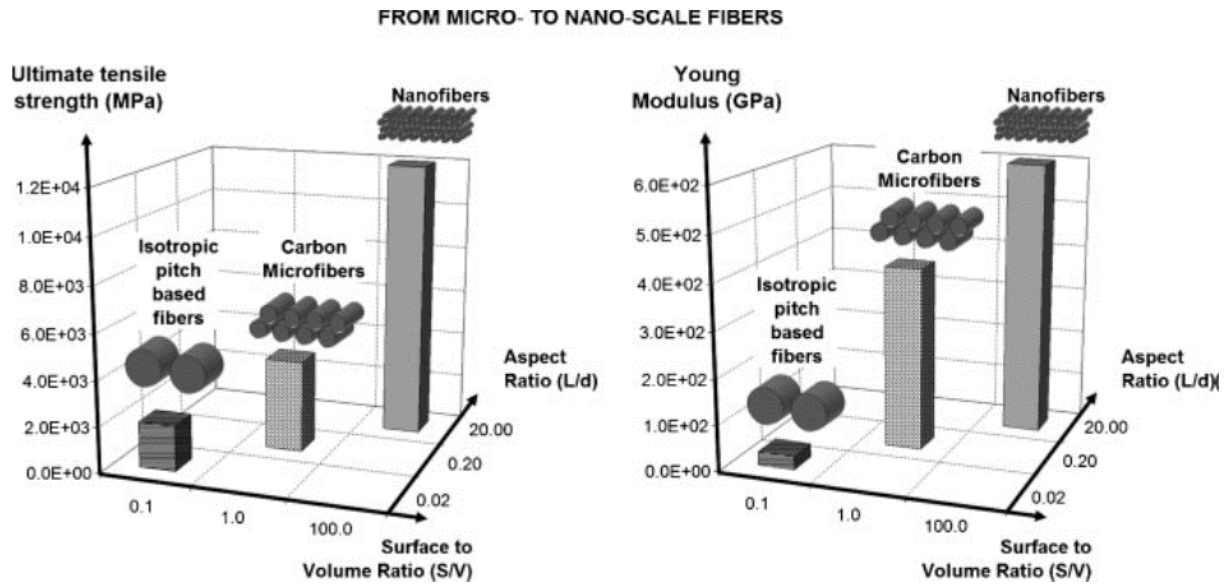
Figure 4.1 From micro- to nano-scale fibers as reinforcement of bulk composites

In terms of fiber mechanical properties, going from micro- down to nano-dimensions, fibers are expected to show an improved elastic modulus and strength at break, thanks to their internal structure consisting of highly aligned macromolecular chains, especially in the case of fibers fabricated through spinning technologies.

Another advantage of using nanofibers in composites arises from the possibility to achieve high aspect ratios. Finally, since nanofibers possess very high surface area to volume ratio, that is a key factor in improving nanofiber-matrix interphase adhesion, an effective load-transfer from the matrix to the nanofibers is expected.

In the case of laminate composites the susceptibility to delamination along interlaminar planes is an intrinsic and severe problem, due to the ply-by-ply nature of such materials. Interlaminar stresses due to mismatch of anisotropic mechanical and thermal properties of plies occur at free edges, joints, and under out-of-plane loading. Delamination is often the dominating failure mode in laminates subjected to impact and fatigue loading. It is believed that nanofibers, being characterized by a diameter typically in the range of few hundreds

nanometers, can be small enough to reinforce regions of the matrix located in between adjacent plies of the laminate, as schematically illustrated in Figure 4.2. The idea of using nanofibers to reinforce small-scale places, such as the regions at the interfaces of laminated composites, arises from the consideration that, in such composites, structural failures mainly occur in small critical areas, in particular in matrix-rich micro-volumes, where the matrix is not reinforced and it experiences high stress concentration.
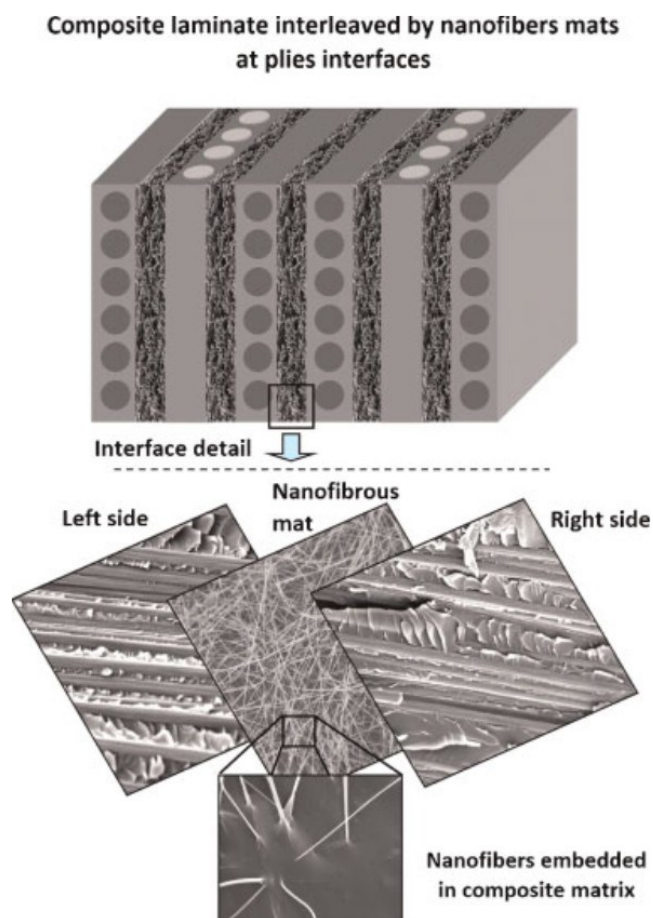
Composite laminate interleaved by nanofibers mats at plies interfaces

Interface detail

Left side   Nanofibrous mat   Right side

Nanofibers embedded in composite matrix

Figure 4.2 Composite laminate interleaved by nanofibrous mats at plies interfaces.This figure is available in colour online at wileyonlinelibrary.com

Nanofibers fabricated by electrospinning technology are considered as promising candidates for composite reinforcement. They are continuous, long fibers that, differently from

78

nanofibers with finite length produced by other techniques, display an extremely high aspect ratio and do not present fiber edges that can act as stress concentration points. Moreover, the high stretching rate (estimated 10 s-1) and the high elongation (draw ratio up to 104) of the solidifying jet enables the spontaneous orientation of the macromolecular chains along fiber direction, thus contributing to increase the modulus and the strength of the single fiber. In addition, electrospun fibers are usually obtained in the form of non-woven mats that can be easily dispersed in the polymer matrix and fiber alignment and highly ordered fiber architectures can be fabricated by means of proper collectors.

4.2 Polymer composites reinforced with electrospun nanofibres: Literature review

4.2.1 Electrospun nanofibers as bulk reinforcement of polymer matrix

Most of the works currently available in the literature on electrospun nanofibers as reinforcement of polymer composites aim at improving physical and chemical properties, as well as mechanical performances, of the polymer matrix.

One of the first papers about the fabrication and the structure property relationships of such composite materials was published by Kim and Reneke in 1999 [1]. They investigated the reinforcing effect of polybenzimidazole (PBI) electrospun nanofibers (fiber diameter around 500 nm) both in a diglycidyl ether of bisphenol-A (DGEBA) epoxy matrix and in a styrene-butadiene rubber (SBR) matrix. Composite specimens of PBI nanofibers reinforced epoxy matrix were prepared from several plies of the fabric sheets, cut and folded to fit a compression mold. The nanofiber sheets were then impregnated with the resin and thermally cured. Two kinds of specimens were prepared: in the first one the tensile axis was along the winding direction of the nanofiber sheets and in the second one the tensile axis was perpendicular to the winding direction. It was found that with increasing fiber content the

bending Young modulus and fracture toughness of the epoxy non-woven fabric composites were increased marginally, whereas the fracture energy increased significantly. Moreover, the fracture toughness and the fracture energy of the composites were found to depend on the direction of the crack: when the crack was transverse to the fabric winding direction both fracture toughness and fracture energy were higher with respect to the situation where the crack was along the winding direction. The rubber composites reinforced with PBI nanofiber were prepared by milling 0.5 cm squared nanofiber sheets in order to obtain a homogeneous dispersion of the filler into the matrix, followed by curing through compression molding. Also in this case, the reinforcing effect of PBI chopped nanofibers was proved by an increase of both Young modulus and tear strength respect to those of the pristine rubber.

Nylon nanofibers have been extensively employed as reinforcement of several polymeric matrices. Nylon 6 nanofibers (fiber diameter 250 nm) were used by Romo-Uribe et al. [2] as effective mechanical reinforcement of thin films of polyaniline (PANI). Composite membranes were prepared through a solvent-casting procedure: a PANI solution was poured onto either aluminium plates or previously prepared nylon 6 nanofiber coated aluminium plates and dried at 80°C under a stream of air. Subsequently, the as-cast PANI films and PANI-nylon 6 nanofiber composite films were detached from the plates by soaking in distilled water. The asymmetrical reinforced membrane obtained, composed of a dense PANI layer and a 6 mm thick PANI-nylon 6 nanofiber layer, showed good adhesion at the interface attributed to the presence of hydrogen bonding between the amine and the carbonyl moieties of PANI and nylon 6 respectively. Thermal and dynamic mechanical analyses revealed that the composite membrane had a significantly higher tensile modulus than the plain PANI film at room temperature, and that introduction of the nylon 6 nanofiber layer extended the composite working temperature from around 100 °C up to over 200 °C.

Nanocomposites made of a DGEBA epoxy resin reinforced with poly(ethylene oxide) (PEO) electrospun nanofibers were fabricated by Lee et al. [3]. The epoxy resin was mixed with 5wt% of PEO nanofibers and the mixture was subjected to high-energy ultrasonication at 60 °C followed by the addition of the curing agent. The obtained mixture was then degassed to remove bubbles, casted into a mould and thermally cured at 120, 150 and 200 °C. The fracture toughness parameters, critical stress intensity factor and specific fracture energy, were evaluated by single edge-notched specimens tested under three-point flexural loading. All the parameters were found to increase in composites containing PEO nanofibers with respect to the unfilled epoxy resin, resulting in an improvement of the nanocomposites toughness.

The attention toward the chemical properties of electrospun nanofibers in order to improve fiber–matrix interface adhesion is the main focus of the paper by Ozden et al. [4], who prepared poly(styrene-co-glycidyl methacrylate), P(S-co-GMA), electrospun fibrous mats that were crosslinked and embedded into an Araldite epoxy resin matrix containing a polyamine hardener. Electrospun fiber cross-linking was achieved by spraying ethylenediammine (EDA) on the fibrous mat before embedding it into epoxy resin, layer-by-layer, and curing at 50 °C for 15 h. The epoxy matrix composites reinforced by 10 layers of fiber mats (2 wt%) were mechanical characterized by dynamic mechanical analysis (DMA) measurements (three-point bending mode) and by three-point flexural test. It was found that the storage modulus of P(S-co-GMA)/EDA fiber-reinforced epoxy was 10 and 2.5 times higher than that of neat and P(S-co-GMA) fiber-reinforced epoxy respectively. Three-point bending flexural tests performed on a composite containing a single layer of fibrous mat, indicated that incorporation of low-weight-fraction (0.2 wt%) of P(S-co-GMA)/ EDA fibers in the epoxy matrix increased the composite flexural modulus by 30% with respect to that of the neat epoxy. The improvement of mechanical performances was attributed to the combination of two main factors: (i) the

fiber cross-linking, which leads to an increase in inherent stiffness of the fibrous mat and (ii) surface modification, i.e. chemistry, of the electrospun fibers, resulting in a better fiber-matrix interfacial bonding.

4.2.2 Electrospun nanofibers as interface reinforcement of composite laminates

With respect to the employment of electrospun nanofibers as nano-reinforcing agents of bulk polymer composite, the literature review concerning the nanofiber reinforcement of composite laminates is probably more structured. It takes inspiration from the pioneer idea proposed by Dzenis and Reneker [5] in their patent issued in 1999. Their invention regards a novel generation of microfiber reinforced composite laminated materials containing a secondary reinforcement made of nanofibers located at one or more ply interfaces. Here, the main role of nanofibers is to reduce the stress concentration due to mismatch of ply properties, typical of multidirectional laminates, as well as to bond the adjacent plies without increasing either the composite weight and the laminate thickness. Therefore such innovative composites are expected to display an improved interlaminar fracture toughness, strength, and delamination resistance with respect to static, fatigue, and impact loadings. As examples of their invention the authors manufactured laminate composites from a unidirectional graphite/epoxy prepreg with and without non-woven electrospun fabrics of polybenzimidazole (PBI, fiber diameter range 300–500 nm) by using a specialized press-clave. The use of PBI sheets increased the total laminate thickness and the laminate weight by less of 12% and of 2.5%, respectively. The Arcan test method and the mixed-mode interlaminar fracture testing were performed in order to investigate the effect of nanofiber interleaving membranes on both the peel mode (Mode I) and the sliding shear mode (Mode II). Results showed that the use of nanofibrous sheets increased the critical energy release rate by 130% and by 15% in the Mode II and in the Mode I, respectively. Specimens tested under Mode I were also investigated by optical microscopy and SEM observations. This analysis highlighted a variety of fracture modes

including rather extensive intralaminar delamination. Indeed, due to the high toughening effect of the nano-interface, cracks were in some cases induced to propagate inside the ply. Shivakumar et al. [6] prepared composite laminates of a commercial carbon fiber reinforced epoxy resin by using nylon 6,6 nanofibers (fiber diameter range 75–250 nm) and they investigated the effect of nanofiber interleaving on damping factor, interlaminar fracture toughness under static and fatigue loading and low velocity impact behavior. Results were compared with a commercial thermoplastic particulate interleaved composite. DMA tests performed both on plain and interleaved laminates revealed the presence of a single glass transition temperature (Tg). Moreover DMA tests showed that the addition of about 1.4% thick nanofabric interleave in composite laminates determined the increment of damping factors of about 13%. Differently, the Torayca composite showed two values of Tg, the lower one attributed to the thermoplastic particles and the higher one to the matrix. Mode I delamination was evaluated both under static and under fatigue loading conditions and results showed that the average critical strain energy release rate, Gic, was about 150% greater than the pristine laminate. In plane laminate, the fracture resistance increased with the delamination propagation till reaching a constant value, on the contrary, in interleaved laminates the fracture resistance decreased with delamination growth and it reached a plateau after a certain value of the crack extension. The SEM analysis of the fractured surfaces showed the presence of stretching, separation, and breakage of nylon-6,6 nanofibers that could explain the toughness enhancement due to the presence of the nanofibrous membrane at the plies interface. Results of the fatigue delamination tests showed that the onset threshold values, Gic,threshold, of nanofabric interleaved laminates is 67% greater than the plain one. It's possible to conclude that, in the case of impact, electrospun nylon-6,6 nanofiber interleaving increased the impact damage resistance three times with minimal increase in the thickness or weight.

A very recent paper by Zhang et al. [7] investigated the effect of fiber diameter and mat thickness in carbon/epoxy composite laminates interleaved with polyetherketone cardo (PEK-C) nanofibres (average fiber diameters: 450, 750, and 950 nm). They evaluated the Mode I delamination fracture toughness and the flexural properties of the composites. The flexural strength of the interleaved laminates remarkably decreased when thick fibers (diameter 950 nm) were used with a concomitant reduction of the elastic modulus. The critical strain energy release rate, Gic, was found to be rather independent from the fiber diameter. Mechanical tests performed on samples interleaved with electrospun mats of different thickness (40, 70, or 105μm) revealed a constant elastic modulus, a decrease of flexural strength and an increase of Gic with the increase of membrane thickness. The authors concluded that composites interleaved with thinner nanofibers had better improvement in the interlaminar property without compromising the in-plane performance of the toughened composites.

Li et al.[8] manufactured laminates made of a carbon fiber/ epoxy prepreg by interleaving prepreg plies with polysulfone electrospun nanofibers (average fiber diameter 230 nm). Upon curing treatment at high temperature, the polysulfone melted and fiber morphology was lost. Since polysulfone was not miscible with the matrix a phase segregation phenomena occurred and well-dispersed microparticles of polysulfone were visualized by SEM analysis at the interfaces between the laminate plies. Therefore, in these papers electrospun fibers were not directly used as nanoreinforcing agents and the electrospinning technique was employed to obtain a more homogeneous distribution of polysulfone microparticles at the interfaces with respect to conventional approaches. Authors recognized a significant increase of composite strength in the case of polysulfone microparticles obtained by electrospun nanofibers with respect to the polysulfone microparticles obtained by interleaving polysulfone thin sheets at plies interfaces.

4.3 References Chapter 4

[1] J-S. Kim et al., Polym. Compos. 1999, 20, 124.

[2] A. Romo-Uribe et al., ACS Appl. Mater. Interfaces (2009), 1, 2502

[3] J-R. Lee et al., Proc. Mater. Res. Soc. Symp. 2005, 851, 217.

[4] E. Ozden et al., ACS Appl. Mater. Interfaces 2010, 2, 1788.

[5] Y. A. Dzenis, D. H. Reneker, PCT/US99/11755, 1999.

[6] K. Shivakumar et al., AIAA J. 2009, 47, 1723

[7] J. Zhang et al., Compos. Sci. Technol. 2010, 70, 1660.

[8] G. Li et al., Compos. Sci. Technol. 2008, 68, 987

5. Electrospun nanofibers as Filtration Membranes

5.1 Water Membrane classification

A membrane is a selective barrier between two phases [1]. Depending on the application, different membrane morphologies will be used. Several types of membrane separation mechanisms exist. In membrane applications where the solution diffusion mechanism plays the major role, the membrane material is chosen based on the selective sorption and diffusion properties, membrane morphology will be not the main factor to affect the selectivity but it is still important as regarding to total flux. A schematic representation of various morphologies is given in Figure 5.1.

Dense, homogeneous

Latex structure

Cylindrical pores

Cellular, symmetric

Co-continuous

Cellular, assymmetric

Porous with dense layer
of same material

Porous with dense layer
of different material
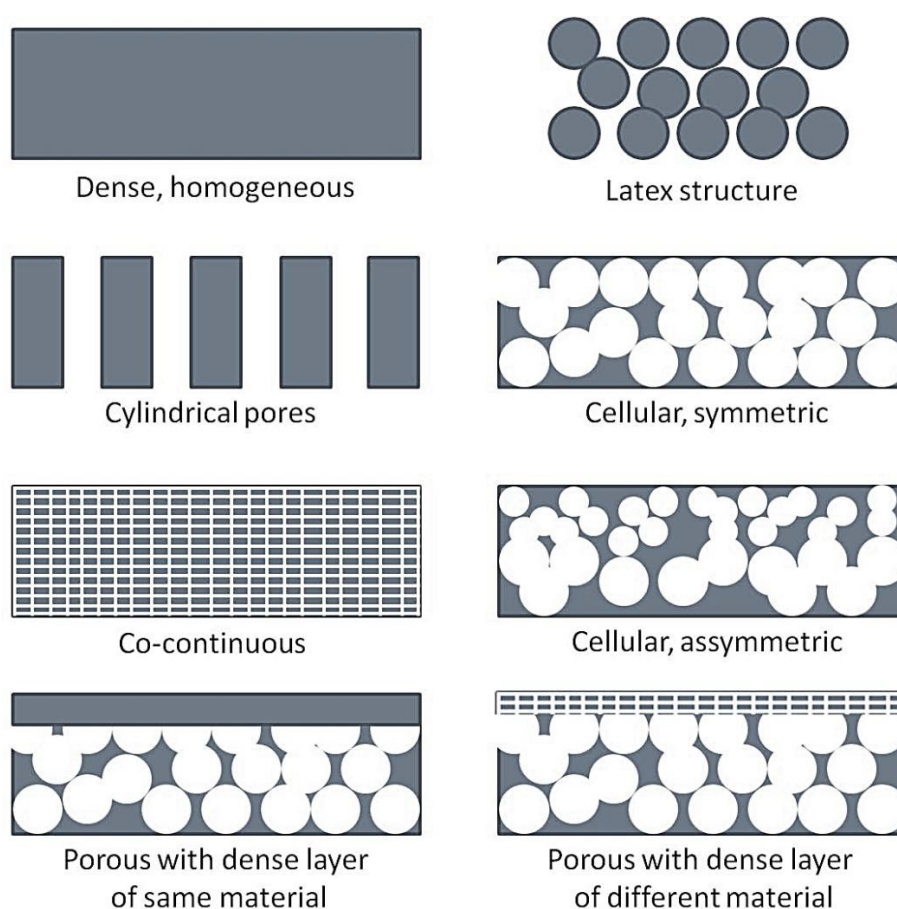
Figure 5.5 *Schematic representation of different membrane morphologies [11].*

86

In all the membrane processes, driving force is essential to deliver the energy to separate the feed molecules or particles; commonly applied driving force differences in pressure, concentration, partial pressure, temperature or electrical potential. The most widely used pressure driven processes are generally classified as microfiltration (MF), ultrafiltration (UF) and hyperfiltration, which is normally subdivided in reverse osmosis (RO) and nanofiltration (NF). Nevertheless, the difference between the processes is not always so sharp, as presents in Table 5.1, summarizing the main characteristics of various membrane processes, in which, typical permeability is for a typical permeate stream, i.e., with rejected species on the retentate side of the membrane.

Membrane process	Typical pressure (bar)	Typical permeability $(l/(m^2 \cdot h \cdot bar))$	Morphology of the selective layer
Microfiltration	0.1-2	>50	Porous
Ultrafiltration	1-5	10-50	Porous
Nanofiltration	5-20	1.4-12	Porous/Dense
Reverse Osmosis	10-100	0.05-1.4	Dense

Table 5.1 *Pressure driven membrane processes [11].*

5.2 Electrospun water filtartion membranes: Literature review

5.2.1 Microfiltration

According to the Baker's definition: "Microfiltration refers to filtration process that use porous membranes to separate suspended particles with diameter between 0.1 and 10 μm" [2]. The electrospun nanofibers membranes could be good candidate for water microfiltration membrane due to these nanofibers membranes have a pore size distribution from sub-micron

to micrometers. The viability of developing high surface area pre-filter through electrospinning has been explored by Gopal et al. [3]. Polysulfone nanofibers were electrospun into membranes and their ability to remove micro-particles from solution was investigated. The nanofiber membranes possess high porosity together with high surface area to produce high flux pre-filters with high loading capacity. The membranes had a bubble-point of 4.6 μm and were able to remove above 99% of 10, 8, and 7 μm particles without any permanent fouling. However, the membranes were observed to foul irreversibly by 2 and 1 μm particles with a cake layer forming on the outer membrane surface. Below 1 μm, the membrane behaved as a depth filter with 0.5 and 0.1 μm particles being attracted onto the nanofiber surface (Fig.5.2). Such nanofiber pre-filters could be used in various applications such as removal of microparticles from waste-water, prior to Ultrafiltration (UF) or Nanofiltration (NF).
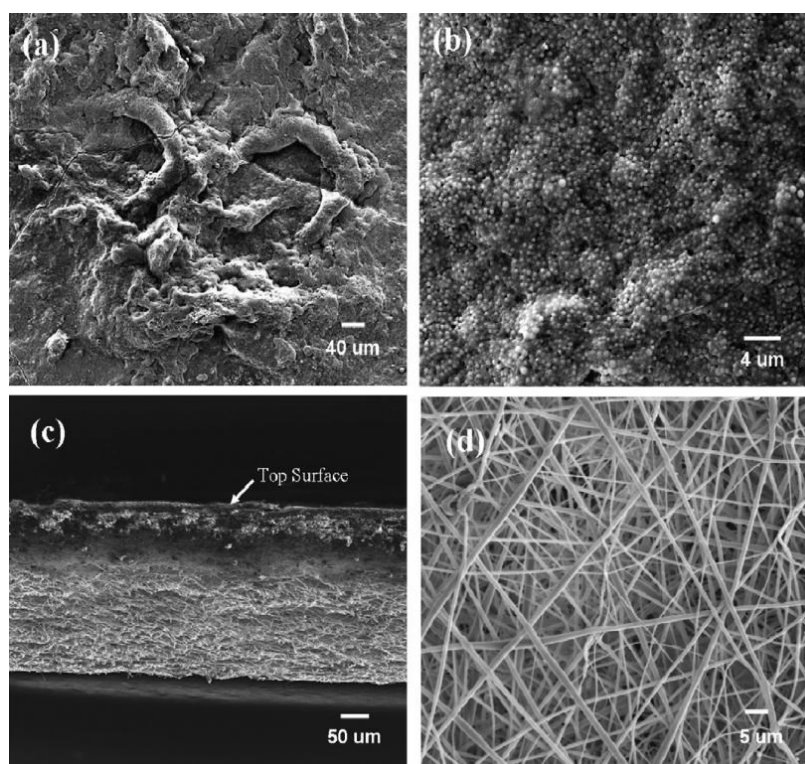
Figure 5.2*PSU electrospun membrane after particle–challenge (polystyre with paticle size ranging between 0.1 – 10 μm) test, a) & b) top surface, c) cross-section and d) bottom surface [3].*

The filtration of PVDF electrospun nanofiber membranes were investigated by Gopal et al. [4] and Kaur et al. [5], their performances were compared with commercial microfiltration membrane. The results indicated an up two times higher flux for the PVDF electrospun membrane than commercial microfiltration membrane at the same pore size distribution and applied pressure and the rejection of PVDF electrospun membrane resulted more than 90% of the micro-particles from solution. The higher flux for PVDF electrospun membrane confirms the better performance and efficiency of the electrospun microfiltration membranes leading to lower energy consumption. Recently, Zhuang et al. [6] fabricated the PVDF nanofibers membrane by a new process so-called "solution blowing". The nanofibers membranes were electrospun by this process exhibited the fiber diameter mostly of 60 - 280 nm and the porosity of membrane of 95.8%. The microfiltration performance of the hot-pressed membrane showed retention ratio more than 90% against 1.0, 5.0 and 10 μm particles and presented high pure water flux at low pressure.

Meanwhile, a heat treated electrospun PAN nanofiber membrane for particle separation from water with average fiber diameter of 165 ± 16 nm, the porosity of 91.7%, pore size in the diameter range of less than 2 μm and specific surface area near 40 m2g-1was obtained by Bazargan et al. [7]. The PAN nanofiber membranes were post-heated treatment exhibited high performance such as the mechanical strength was 4.87 MPa with 23% elongation, the water permeability was 225.6 kg/m2h and the contact angles were equal to zero. It can be concluded that the heat treated electrospun PAN nanofiber membrane was completely hydrophilic. For filtration efficiency, the membrane has high ability to remove more than 90% of microparticles in the range of 1-20 μm from water.

In additions, microfiltration membrane is also used for antibacterial filter application. Cooper et al. [8] reported the development of chitosan - polycaprolactone (PCL) nanofibers membranes. These membranes were prepared from PCL and chitosan content of 25, 50 and

75% and utilized the natural antibacterial property of chitosan for antibacterial water filtration. The performance of chitosan-PCL resulted the fiber diameter of 200 – 400 nm and 25% chitosan-PCL nanofiber membrane showed highest water flux of 6926 L/h/m2 with 100% removal of 300 nm particles, while the 25% chitosan-PCL nanofiber membrane exhibited a similar water flux to that of the PCL membrane (≈ 2756 L/h/m2). In a series of bacterial test, electrospun chitosan-PCL nanofibers membrane can be reduced *Staphylococcus aureus* adhesion compared to PCL nanofiber membranes.

Since PES can be considered as a model membrane material as it is widely use for commercial MF and UF as well as its high chemical, thermal resistance and also its appropriate mechanical properties. The preparation polyethersulfone (PES) electrospun nanofiber membrane for MF applications had been reported by Homaeeigohar et al. [9,10]. The membrane properties exhibited the thickness of 200 μm, areal density of 0.2 -0.3 g/cm2, mean flow pore diameter of 2 μm. Moreover, in term of membrane performance, the water flux measurement indicated that the membrane possess a high initial flux while retention test with polystyrene suspension showed that the filtration efficiency of PES electrospun membrane was highly dependent on size distribution of the suspended particles. When in feed was the particle over 1 μm in size, the rejection of the particles was performed within the first hour of the measurement with highly flux.

In Table 5.2 are summaried the properties and performance of electrospun microfiltration membranes.

Polymer	Fiber diameter (nm)	Pore size (µm)	Thickness (µm)	Permeability (l/m^2.h.bar)	Filtration performance (%)	Particle size (µm)	Ref.
Nylon 6	30-110	6.0	150	9500	90	1.0	[100]
PAN-PET	100	0.22	200	2189	97	0.5	[58]
PCL-Chitosan	300	2.8	N.A.	17536	99	0.3	[90]
PES	280	2.0	200	2080	98	1.0	[92]
PET	420	2.5	N.A.	N.A.	96	N.A. (apple juice)	[89]
PSU	470 ± 150	2.1	135	13333	94	1.0	[6]
PVA	100 ± 19	0.21	100	23529	98	0.2	[103]
PVDF	380 ± 106	4.1	300	4000	91	5.0	[7]

Table 5.2 *Properties and filtration performance of electrospun microfiltration membranes.*

5.2.2 Ultrafiltration

Ultrafiltration is a filtration process discriminating a diverse range of particulates, such proteins, colloids, emulsions and viruses, as big as approximately 1 to 100 nm in the liquid environment [11]. This implies that, in order to use electrospun nanofibers web directly for ultrafiltration, the pore size of the electrospun nanofibers web needs to be less than 0.1 µm.

Yoon et al. [12] proposed a new concept to fabricated high flux UF membranes, involving to use of electrospun nanofiber membrane to replace the asymmetric porous membrane. Their demonstration system consists of a three-tier composite structure: (i) a non-porous hydrophilic top-layer by coating chitosan, (ii) an PAN electrospun nanofiber membrane as mid layer and (iii) a conventional polyester nonwoven microfiber as substrate support, the schematic structure of three-tier approach to fabricate high flux and low-fouling ultrafiltration membranes as presents in Figure 5.3. The membranes, which assembled of electrospun PAN nanofiber membrane with average fiber diameter from 124 to 720 nm and porosity of 70%, was coated a chitosan top layer with a thickness of 1 µm. The results showed that these membranes had higher flux than commercial nanofiltration membranes in 24 h of operation,

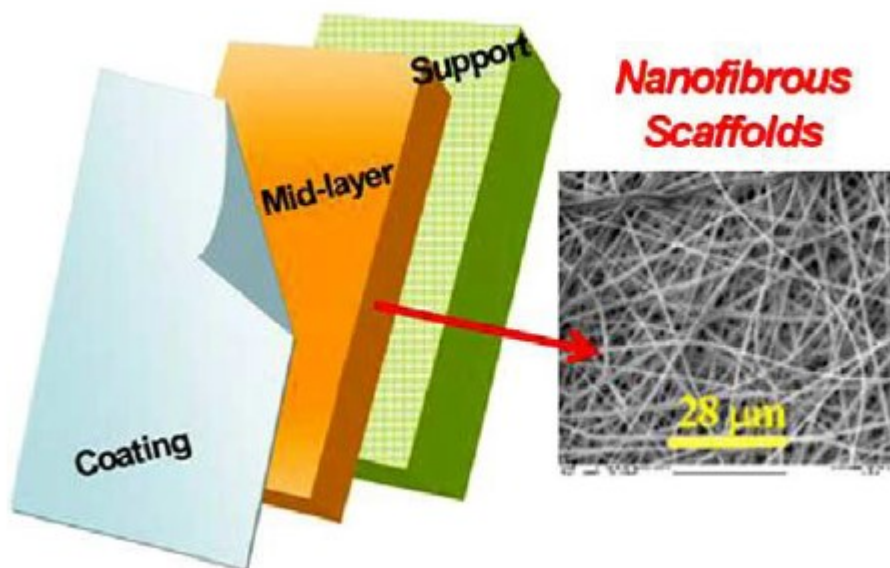while maintaining the same rejection efficiency, more than 99% for oily waste-water filtration.

Figure 5.3 *Schematic structure of three-layer approach to fabricate high flux and low-fouling for ultrafiltration membranes [12].*

Wang et al. [13] prepared the hydrogel PVA in order to coat on top of nanofiber PVA scaffold. Results indicated that hydrogel PVA-PVA TFNC membrane exhibited a flux rate, more than 130 L/m2 h, significantly higher than commercial UF membranes but with similar filtration efficiency of 99% for oily waste-water filtration. In addition, the mechanical property before and after cross linking of hydrogel PVA of the electrospun scaffold fabricated by 96% hydrolyzed PVA with relatively high molecular weight in range of 85,000-124,000 g/mol exhibited the similar performance.

5.3 Why Active Electrospun membranes?

5.3.1 Fouling of membranes

Membrane fouling describes the deposition and accumulation of rejected contaminants from the feed stream on the membrane. The severity of membrane fouling is determined by the combined effect of various physical, chemical, and biological operating factors and can be impacted by the operating flux.

Flux is one of the main parameters determining the economic viability of the membrane process and is the single factor that dictates the size of the membrane plant. Flux is a measure of the rate at which permeate passes through the membrane per unit area. Unit area depends on the membrane configuration. Flux across the membrane varies as flow varies. Another term often used in membrane performance is permeability. Permeability is a calculated parameter of flux normalized against trans-membrane pressure (TMP), and is expressed in units of gfd/psig (Flux/TMP). Trans-membrane pressure (TMP) is a measure of the differential pressure required to push or pull permeate through the membrane. Membrane systems are normally designed to maintain a constant flux, which dictates that TMP will increase over time due to membrane fouling. As TMP increases due to accumulation of particulate matter on the membrane surface, more energy is required to push or pull permeate through the membrane. When flux rates are increased, fouling rates tend to increase because the increase in velocity causes a greater deposition of particulate matter whereby the shear stress on the membrane surface becomes inhibitive.

Membrane fouling caused by a buildup of constituents can be described by three modes:

- pore narrowing;
- pore plugging;

- gel/cake formation.

The three modes of membrane fouling are shown in Figure 5.4.
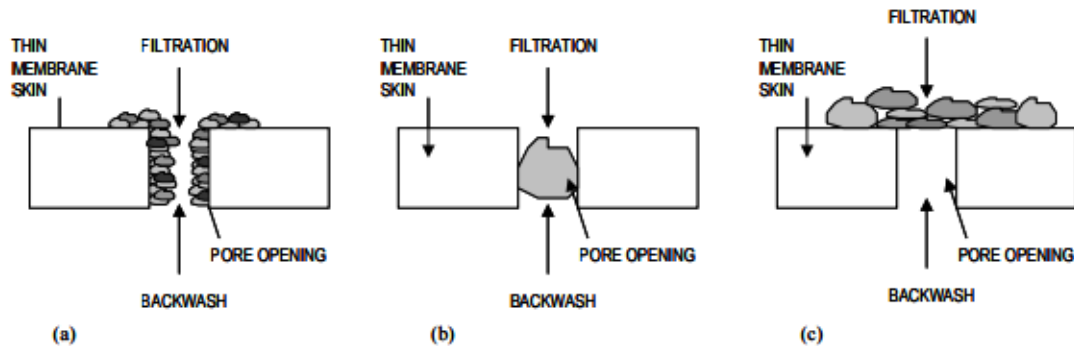
Figure 5.4 Modes for Membrane Fouling (a) Pore Narrowing, (b) Pore Plugging, and (c) gel/cake formation caused by concentration (Adapted from Bourgeous et al, 1999).

Pore narrowing and pore plugging will only occur when the particles in the feed stream are smaller than the pore size. Pore narrowing, also known as pore constriction, is a result of the adsorption of filtered species within the membrane pores. Pore narrowing and plugging are believed to create an increase in concentration polarization and therefore, promote gel/cake formation. Filtration membranes, in general, foul due to the combined effects of pore blockage and cake formation [14].

The type of particulate matter removed by the membrane that can cause membrane fouling can be classified as inorganic (scaling) fouling, particulate/colloidal fouling, biological/microbial fouling, and organic fouling [15]. Metal hydroxides and carbonates which precipitate onto and inside the membrane pores cause inorganic fouling, which results in pore narrowing. Inorganic fouling is less predominant in MF membranes but is most likely caused by the interaction of ions and other fouling material via chemical bonding. Suspended solids or colloids in the feedwater cause particulate fouling, which can cause pore narrowing, pore plugging or even cake formation. Irreversible fouling has happened in rare cases with

particulate fouling when the particle size is smaller than that of the pore size, resulting in particles becoming trapped within the membrane structure matrix. Fouling resulting from the formation of a biofilm is termed biological/microbial fouling, which typically causes a gel/cake formation on the membrane surface. Organic fouling is caused by feedwaters containing natural organic matter (NOM), which also causes a gel/cake formation on the membrane surface.

The following Table 5.3 summarizes the type of fouling potential that different constituents cause and their fouling mechanism.

Fouling Category	Responsible Constituent	Fouling Mechanism
Inorganic/Scaling	Metal Oxides Inorganic colloids Calcium Sulfate, Carbonate and Fluoride Barium Sulfate Silica	Pore narrowing Gel/Cake Formation
Particulate Fouling	Suspended Solids Colloids Biologically Inert Particles	Pore Narrowing Pore Plugging
Biological/Microbial Fouling	Bacteria Microorganisms Concentration Polarization	Pore Narrowing Pore Plugging Gel/Cake Formation – most prominent
Organic Fouling	NOM	Pore Narrowing Gel/Cake Formation

Table 5.3 Fouling Wastewater Constituents that Impact Fouling.

5.3.2 Active mebranes: structures with photocatalytic properties

As seen before, the broad application of membrane technologies is dictated to certain extent by the membrane fouling issues which results in low water quality, high operation cost, and short lifespan of membrane. In order to overcome these limitations, introduction of heterogeneous photo-catalysis with semi-conductors has been rapidly accepted in the field of water treatment to remove organic and inorganic pollutants from influents [16-18]. This

technique gradually breaks down the molecules of the pollutants and generates no residual by-products thus zero sludge disposal complication [19].

TiO₂ and ZnO are two of the widely used semiconductor photocatalysts. They must be irradiated with UV light to be excited and capable of photo-oxidation.

As illustrated in Figure 5.5 and Eqs. (1)–(4), when TiO₂ absorbs UV light (<380 nm), electrons are promoted from valence band (VB) to the conduction band (CB) to generate electron–hole pairs (e–/h+). Positive holes typically oxidize organic compounds, inducing their oxidative degradation, while electrons mainly reduce molecular oxygen to superoxide radical anions, which can lead to a number of reactive oxygen species (.OH, O_2^-, H_2O^- etc.). These radicals oxidize a wide variety of organic pollutants to harmless inorganics such as CO_2, H_2O and other minerals

$$TiO_2 + h\upsilon \ (E_G \geq 3.2 \ eV) \rightarrow TiO_2 + (e_{CB} + h_{VB}) \qquad (1)$$

$$TiO_2 + h_{VB} + HO^- \rightarrow TiO_2 + OH \qquad (2)$$

$$TiO_2 + e_{CB} + O_2 \rightarrow TiO_2 + O_2^- \qquad (3)$$

$$R + HO^. \rightarrow R(HO^.) \rightarrow R_1 + R_2 \rightarrow Inorganic \ pollutant \qquad (4)$$
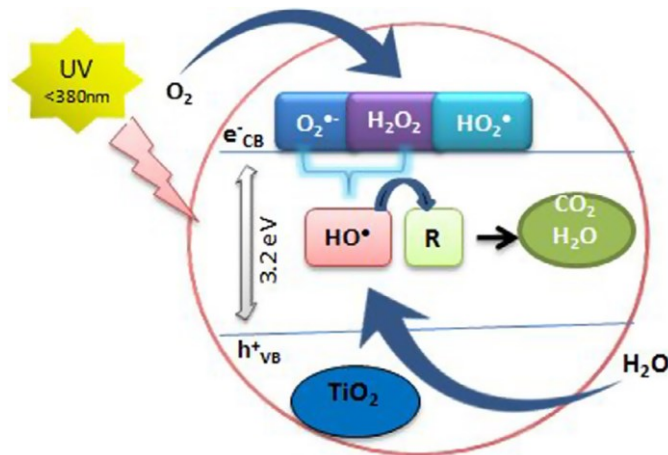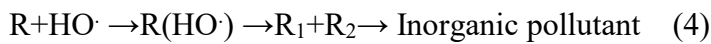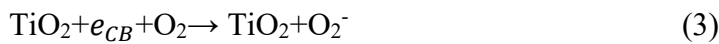
Figure 5.5 Mechanism of TiO₂ photocatalytic oxidation [20]

TiO$_2$ photocatalytic degradation has revealed a great potential as a low-cost, non-toxic, chemically stable, high photoactivity, environmental friendly and sustainable treatment technique to fulfill the zero waste scheme in water and wastewater industry. and chemically inert, photostable, inexpensive. Among the group of metal oxides ZnO is growing in interest as a potential photocatalyst to compete with TiO2. ZnO is one of many naturally oxygen deficient metal oxides that will photocatalytically decomposes complex organic molecules in the presence of UV illumination.

5.3.3 Active membranes: AgNps with antimicrobial properties

Silver nanoparticles (AgNPs) have attracted much attention in the scientific field [21–23]. AgNPs were considered, in recent years, particularly attractive for the production of a new class of antimicrobials [24] opening up a completely new way to combat a wide range of bacterial pathogens. The potent antibacterial and broad-spectrum activity against morphologically and metabolically different microorganisms seems to be correlated with a multifaceted mechanism by which nanoparticles interact with microbes. Moreover, their particular structure and the different modes of establishing an interaction with bacterial surfaces may offer a unique and under probed antibacterial mechanism to exploit. From a structural point of view, AgNPs have at least one dimension in the range from 1 to 100 nm and more importantly, as particle size decreases, the surface area-to-volume ratio greatly increases. As a consequence, the physical, chemical and biological properties are markedly different from those of the bulk material of origin.

AgNPs are able to physically interact with the cell surface of various bacteria. Many studies have reported that AgNPs can damage cell membranes leading to structural changes, which render bacteria more permeable [25,26]. This effect is highly influenced by the nanoparticles' size, shape and concentration [26–28]. Smaller nanoparticles seem to have a superior ability

to penetrate into bacteria. In fact, the interactions with the membranes and any resulting damage, which may lead to cell death, are certainly more evident in the case of nanoparticles with smaller diameter.

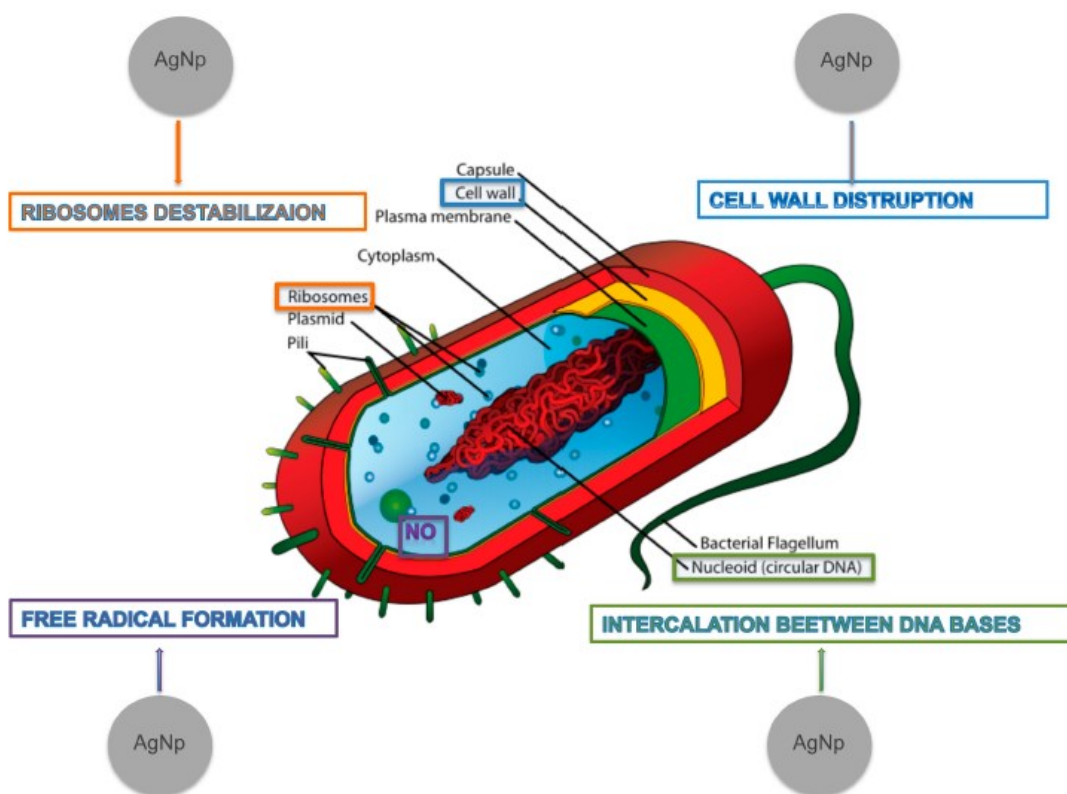In Figure 5.6 are summarized the possible toxicity mechanisms of AgNPs.

Figure 5.6 Mechanisms of AgNPs' toxic action [29]

It should be consider that a certain amount of cationic silver is released from the nanoparticles when these are dissolved in water or when they penetrate into the cells. It is likely that a combined effect between the activity of the nanoparticles and free ions contributes in different ways to produce a strong antibacterial activity of broad spectrum. Furthermore, The silver ions bind to the protein and nucleic acid negatively charged, causing structural changes and deformations in the wall, in the membranes and in the nucleic acids of the bacterial cell. In fact, silver ions interact with a number of electron donor functional groups such as thiols,

phosphates, hydroxyls, imidazoles and indoles. The AgNPs also damage membranes and induce the release of reactive oxygen species (ROS), forming free radicals with a powerful bactericidal action [30]. Silver ions or small AgNPs can easily enter the microbial body causing the damage of its intracellular structures. Protein synthesis has been shown to be altered by treatment with AgNPs and proteomic data have shown an accumulation of immature precursors of membrane proteins resulting in destabilization of the composition of the outer membrane [31].

For all the reasons explained before, since AgNPs possess a strong antibacterial and antiviral activity, they may be used as active part in ultrafiltration membranes in order to reduce the biofouling problem.

5.4 Chapter 5 References

[1] M. H. V. Mulder, Basic Principles of Membrane Technology, 2nd ed., Kluwer Academic Publishers, 1996.

[2] R. W. Baker, Membrane Technology and Applications, 2nd ed., Wiley, 2004.

[3] R. Gopal et al., J. Membr. Sci., 289 (2007) 210-219.

[4] R. Gopal et al., J. Membr. Sci., 281 (2006) 581-586.

[5] S. Kaur et al., Langmuir, 23 (2007) 13085-13092.

[6] X. Zhuang et al., J. Membr. Sci., 429 (2013) 66-70.

[7] A. M. Bazargan et al., Desalination, 265 (2011) 148-152.

[8] A. Cooper et al., Carbohydrate Polymer, 92 (2013) 254-259.

[9] S. Sh. Homaeiogohar et al., J. Membr. Sci., 365 (2010) 68-77.

[10] S. Sh. Homaeiogohar et al., J. Membr. Sci., 98 (2012) 456-463.

[11] R.W. Baker, Membrane technology and applications, 2nd ed., John Wiley & Sons, Ltd., Chichester, 2004.

[12] K. Yoon et al., Polymer, 47 (2006) 2434-2441.

[13] B. Wang et al., J. Appl. Polym. Sci., 115 (2010) 1781-1786.

[14] Katsoufidou et al., J. Mem. Sci. 266, 40-50.

[15]Liu et al., Proceedings of Membrane Technology Conference, March 4-7, San Antonio, TX.

[16]A. Fujishima et al.,Int. J. Hydrogen Energy 32 (2007) 2664–2672.

[17] M.A. Fox, M.T. Dulay, Chem. Rev. 93 (1993) 341–357.

[18] S. Leong, et al., J. Membr. Sci. 472 (2014) 167–184.

[19] H. Bai, D.D. Sun, Water Sci. Technol.: Water Supply (2011) 324–332.

[20] M. Hassan et al., Chemical Engineering Journal 285 (2016) 264–275.

[21]. Jana, S.; Pal, T., J. Nanosci. Nanotechnol. 2007, 7, 2151–2156.

[22]. Stiufiuc, R.et al., Nanoscale Res. Lett. 2013, 8.

[23]. Szmacinski, H. et al., Appl. Spectrosc. 2008, 62, 733–738.

[24]. Dos Santos, C.A. et al., J. Pharm. Sci. 2014, 103,1931–1944.

[25] Lazar, V., Anaerobe 2011, 17, 280–285.

[26] Periasamy, S. et al., Proc. Natl.Acad. Sci. USA 2012, 109, 1281–1286.

[27]Rolim, J.P. et al., J. Photochem. Photobiol. B 2012, 106, 40–46.

[28]Hashimoto, M.C. et al., Photochem. Photobiol. 2012, 88, 590–595.

[29]G.Franci et al., Molecules 2015, 20, 8856-8874

[30]Wu, D. et al., J. Endod. 2014, 40, 285–290.

[31]Mirzajani, F. et al., Microbiol. 2011, 162, 542–549.

6. Aim of the project

The aim of this project was focused on the development of novel multifunctional composites based on the use of hierarchical structuring. The obtained multifunctional systems have been used for two different applications. In the first one, hybrid thermoplastic/carbon fabrics (Fig.6.1) by means of electrospinning, was used in order to manufacture toughened and nanorinforced (by using MWCNT) composite laminates by Resin Transfer Molding (RTM) and other infusion techniques. While in the second application, hybrid inorganic/organic membranes have been used as active membranes for water filtration. (Fig.6.2).
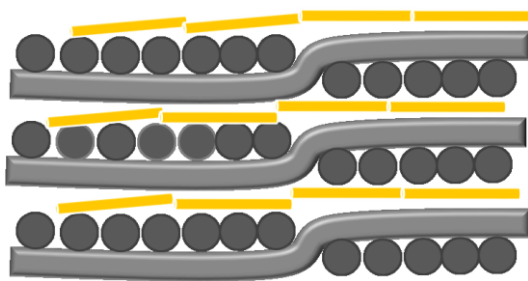
Figure 6.1 Scheme of the hybrid electrospun thermoplastic/carbon fabric
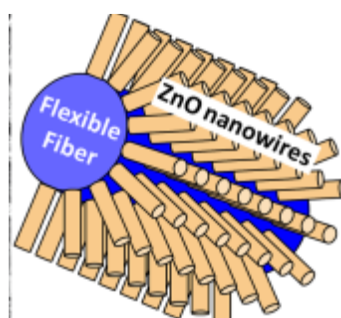
Figure 6.2 Scheme of the hybrid organic/inorganic active membrane. Journal of the American Ceramic Society—Sugunan et al. Vol. 93, No. 11

Figure 6.3 show the concept for the first application: using the hybrid fabrics in order to take the toughener out of the epoxy resin which can be injected into the mould without any viscosity issue. Furthermore, the electrospun thermoplastic veils can act as nanofiller carriers as well, if multifunctionality is desidered.
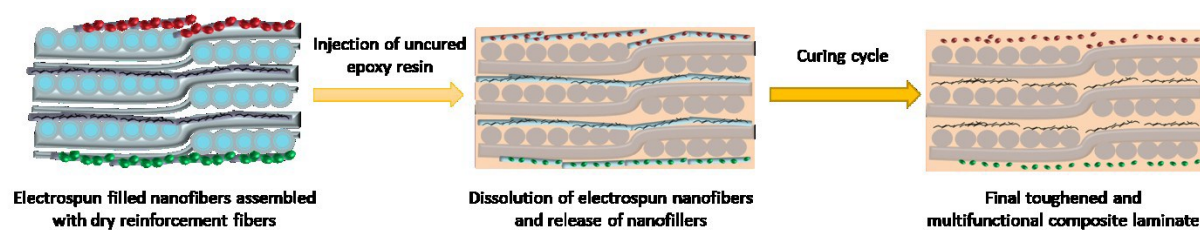
Figure 6.3 Concept of the manufacturing of multifunctional toughened composite laminates by the use of hybrid electrospun thermoplastic/carbon fabrics

Although composite materials provide many advantages compared to traditional materials, there are also some disadvantages connected with their use. The main problem is represented by delamination along interlaminar planes due to the ply-by-ply nature of such materials. Delamination is often the dominating failure mode in laminates subjected to impact and fatigue loadings. For this reasons, in the first year, studies have been directed to the resolution or the mitigation of this problem using nanofibers that can be small enough to reinforce regions of the matrix located in between adjacent plies of the laminate. Furthermore, in order to impart other functionality to the composite, systems of epoxy resins with nanofillers have been studied. These systems show very high performance but they cannot used in the Resin Transfer Moulding (RTM) process due to their increased viscosity caused by nanofillers. However, some of these nanofillers, like carbon nanotubes, have been shown to be promising as functional fillers in order to either reinforce and give multifunctionalities to composites such as fire resistance, lightining-strike, self-sensing, etc.

The first PhD year aims at overcoming the limitation of the already-available resin systems to be used in RTM process, combining the use of soluble thermoplastic nanofibres with the addition of nanofillers as well. In order to achieve this goal, the use of electrospun thermoplastic nanofibres that can be dissolved into the resin without any increase in thickness and weight, will be studied. Furthermore the dispersion of the nanofillers into the electrospun nanofibres will be analyze so that, after the fiber dissolution, they can be diffused where they

are necessary. This approach seems to be more efficient than direct mixing of the nanofiller into the resin since the viscosity in the injection phase will not influenced from the presence of the nanofillers into the thermoplastic fibres. Using the thermoplastic toughener as electrospun veils placed inside the mold allows to inject the resin avoiding the wash-out effect that can occur if placing the modifier as powder.

The main goal of the others two PhD years was the development of hybrid structures for water filtration. Currently, polymeric membranes are mostly used for filtering applications due to their straightforward pore forming mechanism, higher flexibility, smaller footprints required for installation and relatively low costs if compared to inorganic membranes. Accordingly, filtration mechanisms of these membranes are mostly based on mechanical driven sieving effects, thus no chemical removal of toxic substances can be achieved resulting also in fouling effects limiting membrane performances.

The idea was to develop advanced membranes for active water filtering, characterised by combined sieving, photo-catalytic and antibacterial properties. For this purpose ZnO nanowires was grown by a Chemical Bath Deposition process, on the surface of undoped and ZnO doped Polyethersulfone (PES) electrospunfibres. In fact, most of the commercial ultrafiltration membranes are made using polyethersulfone (PES) because of the excellent chemical and physical stabilities of these polymers . Furthermore, antibacterial PES membranes was produced by a one-step procedure starting from a polimeric solution with silver nanoparticles precursors.

7.Experimental section

In this section, all the experimental phases will be following. Firstly, the production and the electrospun veils will be described in details, including the upscale of the process at Elmarco facilities (Liberec, Czech Republic). Then, since these fibers has been used for two different applications, this section will be divided in two parts. In each of these parts, the processes used in order to obtain thoughened composites and active membranes will be described.

7.1 Materials

7.1.1 Tougheners for composite laminates

coPES9k

This thermoplastics is a copolyetherether sulfones that have been synthesized in laboratory [1]. It is a random copolymer, which has been functionalised with amine end-groups so that can react and chemically link to the epoxy network. It's average molecular weight is around 9000 Da. It has been used after drying at 45°C. The structure is shown in Figure 7.1
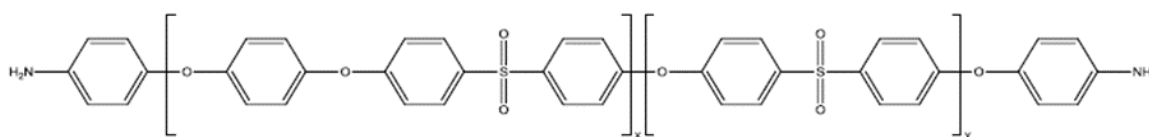
Figure 7.1 Structural formula of coPES9k

Virantage 30500 RP and 10200 RP

Two polyethersulfones sold by Solvay were selected for the scale-up of the electrospinning process: Virantage® 30500 RP and Viratange® 10200 RP. Both of them are PESs but differ

for the average molecular weight and for chemistry of the reactive end-groups. Main properties are reported in Table 7.1.

Virantage Grade	M_{GPC}[g/mol*1000]	End groups
30500RP	45	-NH_2
10200RP	14	-OH

Table 7.1 Main properties of Viratange® polymers

OpteSTAT™ NC PES 6010

OpteSTAT™ master batches are Ovation Polymers' line of nano-compounds based on carbon nanotubes (Fig.7.2). The proprietary dispersion technology debundles and disentangles carbon nanotubes without compromising their integrity. OpteSTAT™ compounds exhibit good conductivity at minimal nanotube loadings, achieving exceptional cleanliness and physical property retention. OpteSTAT™ NC PES 6010 is Polyether Sulfone-based carbon nanotube compound. The material resistivity can be tailored to the application, while retaining the physical and thermal properties of the base polymer. Target applications include components of disk drives, business machines or other electronic assemblies where ESD control is required.
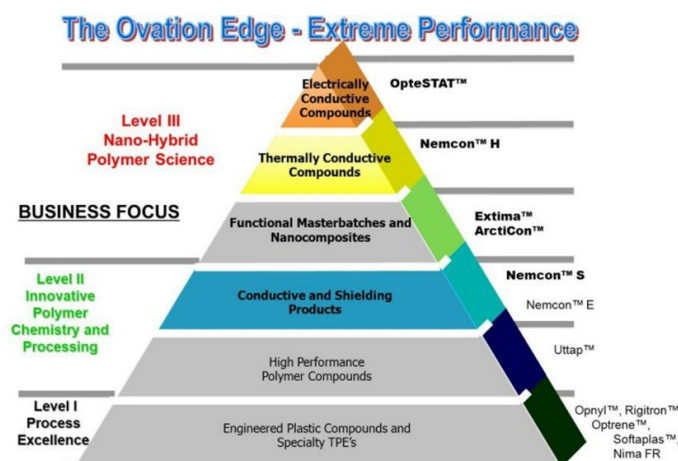
Figure 7.2 Ovation Polymers' compounds, OpteSTAT at the top of technology

7.1.2 Epoxy resin

DGEBA

The epoxy resin DGEBA is a diglycidly ether of Bisphenol A. It is a difunctional epoxy resin provided by Hunstman (Araldite GY 240) and it has been used as received. In Figure 7.3 the DGEBA structure is shown.The molecular weight is 330 g/mol and the epoxy equivalent weight is 165 g/mol. It has a low viscosity and is liquid at ambient temperature but tends to crystallize after some time, becoming a white solid. If heated at 50°C it returns to its viscous state.
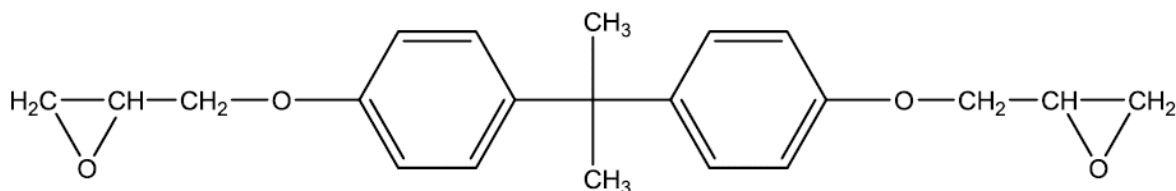
Figure 7.3 DGEBA structure formula

7.1.3 Crosslinker

MDEA

The crosslinker used in this work is the 4-4'-metilenebis(2,6-dietil)-aniline. It is an aromatic diamine available by Lonza Chemical. It is a white cristallin solid at ambient temperature. Its meltin point is about 88-90°C and its structure is reported in Figure 7.4. MDEA molecular weight is 310.5 g/mol while its amine equivalent weight is 76.625 g/mol. At room temperature it is partially soluble in the epoxy resins, at 80°C it is totally soluble and allows to achieve homogenous solutions.
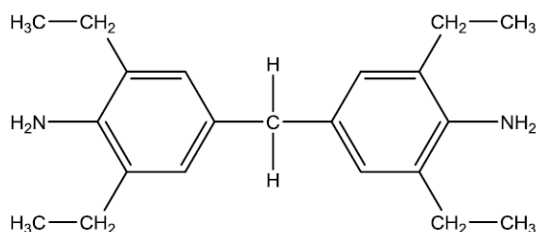
Figure 7.4 MDEA structure formula

7.1.4 Polymer for UF membranes

Veradel®3000P

Veradel®3000P sold by Solvay was selected for the production of the fibers to use for UF membranes. It is also a Polyethersulfone with high molecular weight and was used after drying al 45°C.

7.1.5 Nanofillers

Multi-Wall Carbon Nanotube

Multi-wall carbon nanotubes Graphistrenght TM C100 (provided by Arkema) have been used. Their properties are reported in Table 7.2.

Description		CCVD multi-wall carbon nanotubes
Appearance		Black powder
Powder characteristics	Apparent density	50-150 kg/m^3
	Mean agglomerate size	200-500 μm
	Weight loss at 105°C	<1%
MWCNT characteristics	C content	>90wt%
	Free amorphous carbon	Not detectable (SEM/TEM)
	Mean number of walls	5-15
	Outer mean diameter	10-15 nm
	Length	0.1-10 μm

Table 7.2 Graphistrenght TM C100

As a consequence of their outstanding mechanical properties, and electrical and thermal conductivities, high-quality Graphistrengt TM C100 multi-wall carbon nanotubes can be used in a variety of applications, such as: high-performance electrostatic dissipative plastic parts and coatings, high-strength thermosetting composites, high-strength rubbery materials, and electrode materials for batteries, super-capacitors, and fuel cells. GraphistrengtTM C100 can also be used as catalyst support in different industrial chemical processes.

Nanosilica

CAB-O-SIL® M-5, an untreated fumed silica provided by Cabot, was used. It is a synthetic, amorphous, colloidal silicon dioxide that is generally regarded as unique in industry because of its unusual particle characteristics (Table 7.3). CAB-O-SIL fumed silica's extremely small particle size, its enormous surface area, its high purity, and its chain-forming tendencies set it apart in a class of its own. CAB-O-SIL fumed silica is a light, fluffy powder that is white in appearance and is used in many applications and a variety of industries.

BET Surface Area	200m^2/g
pH (4% aqueous slurry)	3,7-4,3
Loss on heating	<1,5% max
Loss on ignition (@1000°C)	<2wt%
Specific gravity	2,2g/cm^3
X-ray form	Amorphous
Average particle lenght	0,2-0,3 µm

Table 7.3 Properties of CAB-O-SIL® M-5

POSS

Polyhedral oligomeric silsesquioxanes (POSSs) were laboratory synthetized [2]. POSSs are hybrid inorganic/organic compounds of general formula (RSiO1.5)n, where R = H or organic substituents directly linked to silicon cage and n = 6, 8, 10 or 12 (Fig.7.5).
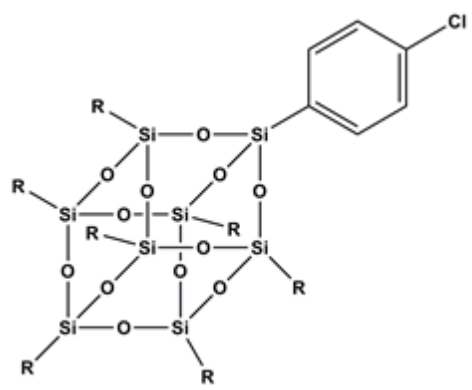
Figure 7.5 Molecular structure of ph,hib-POSS

POSSs can be well used as drug materials and imaging agents, since these materials have potential advantages such as their biodegradation, thermodynamic stability and biocompatibility [3]. The increasing importance of POSSs is also due to their employment as fillers or end-linking agents in the production of polymer and shape memory polymers nanocomposites, materials that have acquired application relevance in a variety of technological fields ranging from medical to aeronautics [4].

Zinc Oxide

The zinc oxide used in this work was purchased from Sigma Aldrich, with a specific density of 5.61 g/cm3. Nanostructured ZnO materials have received broad attention due to their distinguished performance in electronics, optics and photonics. From the 1960s, synthesis of ZnO thin films has been an active field because of their applications as sensors, transducers and catalysts. ZnO is a key technological material.

In addition, ZnO is a wide band-gap (3.37 eV) compound semiconductor that is suitable for short wavelength optoelectronic applications.

Carbon Black

Carbon black is a material that has been known and produced since olden days but only found its widespread manufacture and use in the last century when it was discovered that when mixed into rubber it improves its mechanical properties. Carbon black is virtually pure elemental carbon in the form of colloidal particles that are produced by incomplete combustion or thermal decomposition of gaseous or liquid hydrocarbons under controlled conditions. Its physical appearance is that of a black, finely divided powder. Its use in tires, rubber and plastic products, printing inks and coatings is related to properties of specific surface area, particle size and structure, conductivity and color.

7.1.6 Precursors

Zinc Acetate dihydrate

Zinc Acetate dihydrate was purchased by Carlo Erba. It's a colorless and solid salt and it was used as precursor for ZnO nanowire.

Silver Nitrate

Silver nitrate was purchased by Sigma Aldrich and it was used as precursor for silver nanoparticles.

Silver Hexafluoroacetylacetonate Ag(hfa)

Ag(hfa) was also used as silver nanoparticles precursor. It was synthesized in laboratory using a single step reaction of silver oxide with hexafluoroacetylacetone and polyether in dichloromethane [5]. The structure of this precursor is shown in Figure 7.6.
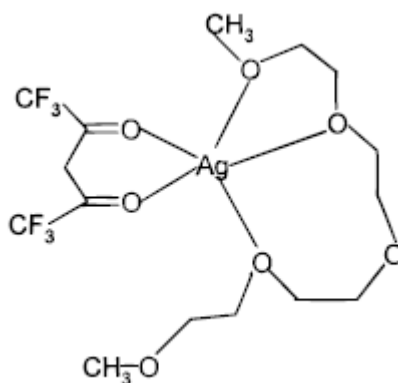
Figure 7.6 Structure of Ag(hfa)

7.2 Samples preparation

7.2.1 Electrospinning of thermoplastic nanofibers

All the thermoplastics used were solubilized in a mix of N,N-dimethylformamide (DMF) and tholuen as electropinning solvent, with a 1:1 volume ratio.

The choice of tholuen together with DMF relies on the necessity of having an enough volatile solvent during the electrospinning process. The thermoplastics with high molecular weight

with a concentration of 0.25 g/ml, while that ones with low molecular weight with a concentration of 0.5 g/ml, in order to obtain as similar as possible viscosities. The solutions have been magnetically stirred while heating until polymers were completely solubilized.

In the systems used as laminates tougheners, after obtaining homogenous solutions, nanofillers were added into the solution and dispersed by using an ultrasound probe (UP 200 Ht by Hielscher).

In the solutions used for membrane filtration, the precursors of ZnO and AgNps, were added and solubilized.

Two different electrospinning machines, one by IME Technologies and the other one by Nanon (Fig.7.7 and 7.8) were used. All these two consists of a syringe that is filled with the polymer solution, a high voltage source and a grounded conductive collector. In addition, a metering syringe pump is used to control the flow rate of the polymer solution. The difference between the two machines is the dimension of the collector, so, by using that one by IME Technology is possible to obtain a A4 paper of membrane, while using that one by NANON a A3 paper.

Figure 7.7 Electrospinning apparatus by IME Technology

Figure 7.8 Electrospinning apparatus by IME Technology

7.2.2 Composite laminates preparation

Six layers of dry carbon fabrics with veils electrospun onto were stacked on a steel plate. An adhesive silicone tape was placed around the perimeter of the layered stack to provide a proper seal and a flexible vacuum bag was placed on top. An inlet tube and an outlet tube were placed inside the vacuum bag. The inlet tube was connected by a valve to a pot filled with unmodified epoxy resin while the outlet tube was connected to a vacuum pump. The vacuum was applied while the inlet valve was closed in order to compact the layers and to remove excess air. All the stacked layers were placed in an oven preheated to 130°C. The epoxy resin was vacuum infused into the stacked layers, which was maintained at 130 °C under a constant vacuum (75 cmHg). The temperature was kept at 130°C for 30 min and then increased by 2°C/min up to 180 °C and held at that value for 3 h.

A similar cure cycle was used for the prepreg composites. However, in this case the epoxy/coPES blends were used to impregnate the carbon fabrics which were then laid on the steel plate. The obtained stack was compacted using a vacuum bag at room temperature for

15min. The stack was placed in an oven preheated to 130°C for 30 min. The temperature was then increased to 180°C and held at that value for 3 h.

7.2.3 Active membrane preparation: ZnO nanorods growth

ZnO nanorods were grown onto the surface of electrospun PES fibres by a Chemical Bath Deposition (CBD) process. First of all a seeding procedure consisting of pre-treatment of PES based mats in $Zn(Ac)_2/H_2O$ solution (0.5M) was done using a proper support in order to allow a repeatable sample positioning inside the seeding solution inside which it remains dipped for a variable time, ranging from 30 minutes to 1hours. After dipping, fibres were dried in a oven at 110°C overnight. Zinc acetate hydrolysis is responsible for the formation of an insoluble zinc hydroxide precipitate which seeds the substrate surface.

After that seeded fibres were immersed, using the same support employed for seeding, in a 1:1 $Zn(Ac)/H_2O$ and EDA solution (0,025 M), and kept magnetically stirredat 80°Cfor 3h. At the end core shell ZnONR/PES fibres were washed with distilled water and dried at 110°C for 1 h.

7.3 Characterization technique

Mechanical, thermos-mechanical and morphological properties of the laminates were carried out. For active membranes a morpholical and thermal analysis was done.

7.3.1 Scanning Electron Microscopy (SEM)

The scanning electron microscopy (SEM) works with a focused beam of high-energy electrons to generate a variety of signals at the surface of solid specimens. The signals that derive from the electron-sample interactions reveal informations on the sample including external morphology (texture), chemical composition, and crystalline structure and orientation

of materials making up the sample. In most applications, data are collected over a selected area of the surface of the sample, and a 2-dimensional image is generated that displays spatial variations in these properties. The resolution of a SEM is about 5 nm but some models exist with a 1nm resolution.

Accelerated electrons in an SEM carry significant amounts of kinetic energy, and this energy is dissipated as a variety of signals produced by electron-sample interactions when the incident electrons are decelerated in the solid sample. These signals include secondary electrons (that produce SEM images), backscattered electrons (BSE), diffracted backscattered electrons (EBSD that are used to determine crystal structures and orientations of minerals), photons (characteristic X-rays that are used for elemental analysis and continuum X-rays), visible light (cathodoluminescence-CL), and heat. Secondary electrons and backscattered electrons are commonly used for imaging samples: secondary electrons are most valuable for showing morphology and topography on samples and backscattered electrons are most valuable for illustrating contrasts in composition in multiphase samples (i.e. for rapid phase discrimination). X-ray generation is produced by inelastic collisions of the incident electrons with electrons in discrete orbitals (shells) of atoms in the sample. As the excited electrons return to lower energy states, they yield X-rays that are of a fixed wavelength (that is related to the difference in energy levels of electrons in different shells for a given element). Thus, characteristic X-rays are produced for each element in a mineral that is "excited" by the electron beam. SEM analysis is considered to be "non-destructive"; that is, x-rays generated by electron interactions do not lead to volume loss of the sample, so it is possible to analyze the same materials repeatedly. inside the fibres.

It has been said that in a SEM different signal are produced due to the electron-sample interaction. In particular, when a high-energy electron beam hits a specimen, X-rays characteristic of the atoms in the specimen are generated within the region illuminated. This

116

allows the possibility of microanalysis, that is, the chemical analysis of a small amount of material, or a small part of a larger specimen. If we can measure the energy of the X-rays (or equivalently their wavelength, since they are related by Planck's constant, $E = hc/\lambda$ or specifically $EkV = 12.4/\lambda Angstroms$), then we can immediately tell qualitatively which elements are present in the part of the specimen under investigation. If we measure X-ray intensities, we also get an immediate rough idea of how much of each element is present (EDX Analysis).

7.3.2 Dynamic Mechanical Analysis (DMA)

Dynamic Mechanical Analysis, otherwise known as DMA, is a technique where a small deformation is applied to a sample in a cyclic manner. This allows the materials response to stress, temperature, frequency and other values to be studied.

At the beginning the DMA tests were developed for structural investigations on metals. Today it is one of the most efficient technique used in order to study polymeric materials since the value of a DMA test is very significant allowing a large number of information on the sample under consideration. The value of the modulus below the Tg depends from molecular orientation and crystallinity. The transition that occurs can be related to the polymer structure and can be very useful studying multicomponent mixtures.

In a dynamic mechanical test it is the sample stiffness and loss that are being measured. The sample stiffness will depend upon its Modulus of Elasticity and its geometry or shape. The modulus measured will depend upon the choice of geometry, Young's (E^*) for tension, compression and bending, Shear (G^*) for torsion. The modulus is defined as the stress per unit area divided by the strain resulting from the applied force. Therefore it is a measure of the material's resistance to deformation, the higher the modulus the more rigid the material is.

The definition given above for modulus does not take time into account. For materials that exhibit time-invariant deformation, for example metals and ceramics at room temperature, any measurement of strain will lead to a constant value of modulus. However for materials that exhibit time-dependent deformation, such as polymers, the quoted modulus must include a time to be valid. This is where dynamic mechanical testing offers a powerful advantage. Dynamic mechanical testers apply a periodic stress or strain to a sample and measure the resulting strain or stress response. Due to the time-dependent properties of polymers the resultant response is out-of-phase with the applied stimulus. The Complex Modulus M* is defined as the instantaneous ratio of the stress/ strain. To understand the deformational mechanisms occurring in the material this is resolved into an in-phase and out-of-phase response. This is equivalent to a complex number (see below), where M' is the in-phase or elastic response this being the recoverable or stored energy.

DMA works by applying a sinusoidal deformation to a sample of known geometry. For an applied stress varying sinusoidally with time, a viscoelastic material will also respond with a sinusoidal strain for low amplitudes of stress. The strain of a viscoelastic body is out of phase with the stress applied, by the phase angle, δ. This phase lag is due to the excess time necessary for molecular motions and relaxations to occur. Dynamic stress, σ, and strain, ε, given as:

$$\sigma = \sigma_0 \sin(\omega t + \delta)$$

$$\varepsilon = \varepsilon_0 \sin(\omega t)$$

where ω is the angular frequency. Using this notation, stress can be divided into an "in-phase" component ($\cos\delta$) and an "out-of-phase" component ($\sin\delta$) and rewritten as,

$$\sigma = \sigma_0 \sin(\omega t) \cos\delta + \sigma_0 \cos(\omega t) \sin\delta$$

Dividing stress by strain to yield a modulus and using the symbols E′ and E′′ for the in-phase

(real) and out-of-phase (imaginary) moduli yields:

$$\sigma = \varepsilon_0 E' \sin(\omega t) + \varepsilon_0 E'' \cos(\omega t)$$

$$E' = \frac{\sigma_0}{\varepsilon_0} cos\delta$$

$$E'' = \frac{\sigma_0}{\varepsilon_0} sin\delta$$

$$\varepsilon = \varepsilon_0 e^{i\omega t}$$

$$\sigma = \sigma_0 e^{i\omega t}$$

$$E^* = \frac{\sigma}{\varepsilon} = \frac{\sigma_0}{\varepsilon_0} e^{i\delta} = \frac{\sigma_0}{\varepsilon_o}(cos\delta + isin\delta) = E' + iE''$$

The last equation shows that the complex modulus obtained from a dynamic mechanical test

consists of "real" and "imaginary" parts.

The real (storage) part, E' describes the ability of the material to store potential energy and

release it upon deformation (fig.7.9). So, for a perfect elastic material , while for a total

viscous material $E^* = E''$

STEEL

$\delta = 0^0$

ELASTIC SAMPLE

$E' = \underline{\text{AMPLITUDE OF STRESS}}$
$\overline{\text{AMPLITUDE OF IN-PHASE STRAIN}}$
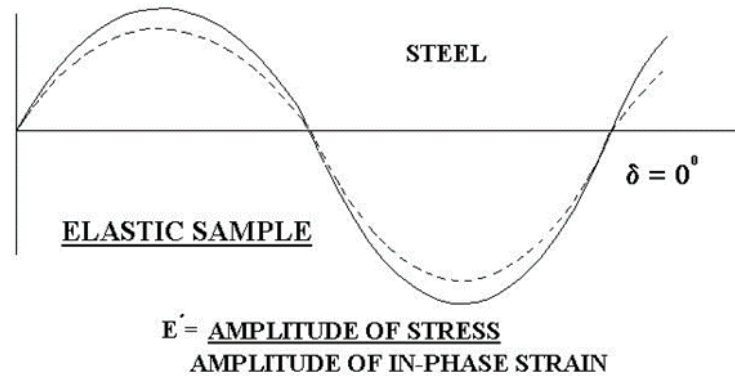
Figure 7.9 Out phase component of a viscous system

The imaginary (loss) portion, E'' is associated with energy dissipation in the form of heat upon deformation (fig.7.10).

NEWTONIAN LIQUID WATER OR GLYCERINE

δ

$\delta = 90^0$

VISCOUS SAMPLE

$E'' = \dfrac{\text{AMPLITUDE OF STRESS}}{\text{AMPLITUDE OF OUT OF PHASE STRAIN}}$
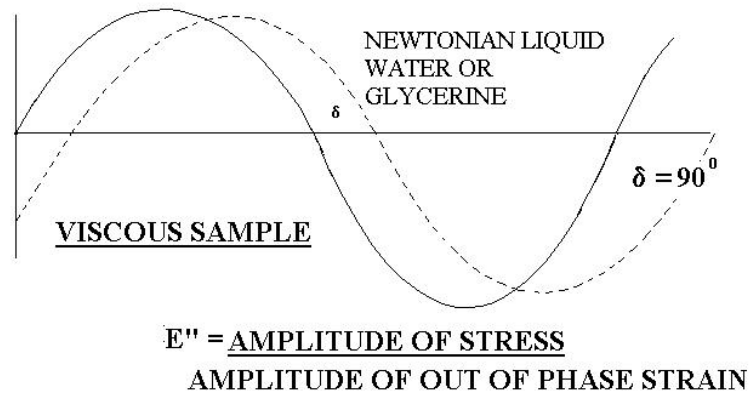
Figure 7.10 Complex component of a viscoelastic system

Figure 7.11 reports the typical behavior of visco-elastic materials like polymers.

POLYMERS

δ

$0^0 > \delta < 90^0$

VISCOELASTIC SAMPLE

$E^* = \dfrac{\text{STRESS}}{\text{STRAIN}}$
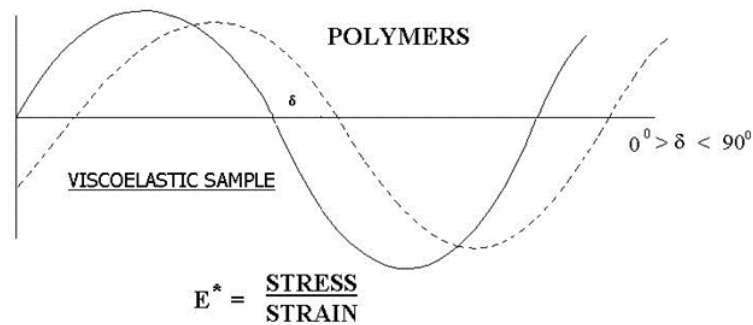
Figure 7.11 Representation of the visco-elastic behavior of polymers

The above equation is rewritten for shear modulus as:

$$G^* = G' + iG''$$

where G' is the storage modulus and G'' is the loss modulus. The phase angle δ (fig.7.13) is given by:

$$tan\delta = \frac{G''}{G'}$$
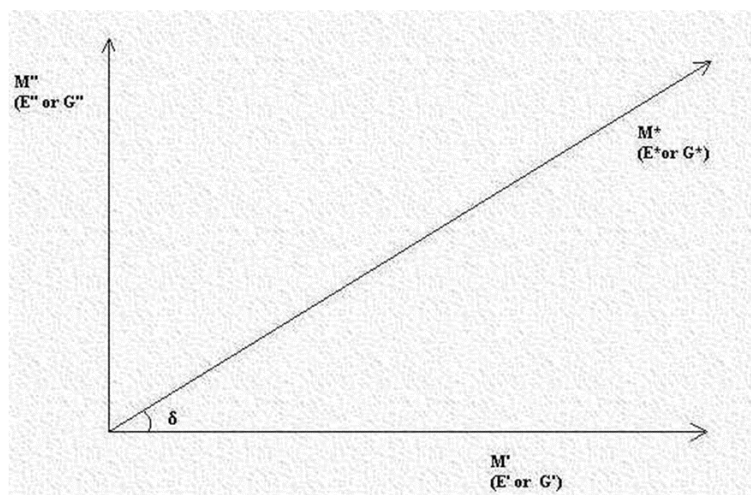
Figure 7.12 Geometric graphic description of phase angle δ.

The storage modulus is often times associated with "stiffness" of a material and is related to the Young's modulus, E. The dynamic loss modulus is often associated with "internal friction" and is sensitive to different kinds of molecular motions, relaxation processes, transitions, morphology and other structural heterogeneities. Thus, the dynamic properties provide information at the molecular level to understanding the polymer mechanical behavior.

The thermal scan method is the one used in this work as it provides more relevant DMA data.

The temperature range scanned changes depending to the sample under consideration with a speed of 2°C/min. The frequencies used are 1 Hz and 10 Hz. Measures were conducted using a TRITECH 2000 from TRITON Technology.

7.3.3 X-ray diffraction (XRD)

The X-ray diffraction (XRD) is a non-destructive technique [6] which provides information about structure and size of crystallites.

Diffraction is a phenomenon that results from the interaction between electromagnetic radiation and periodic structures. The inter-atomic distances in order of 0.15-0.4 nm are

121

crystals and are comparable with the wavelength of the wave of X-rays, having energies between 3 and 8 keV.

When a sample is hit with a beam of X-rays having a wavelength comparable with the distance between the atomic planes of its crystal lattice, the radiation undergoes elastic scattering with consequent variation of the direction and energy conservation. Considering that:

> all the photons of the incident beam have the same wavelength and the same phase;

> each atom has spherical electronic distribution;

the electron clouds of the atoms constituting the sample representing the centers of diffusion. Furthermore, if the sample is crystalline, the electron clouds are arranged in space on a regular basis and the scattered radiation from the atomic planes of the crystal gives rise to constructive interference only when it is verified Bragg's law:

$$2d_{hkl}\,sin\vartheta = n\lambda$$

where d_{hkl} is the distance between the lattice planes, θ is the angle of incidence of the radiation, n is the diffraction order and λ is the wavelength of the incident radiation. The diffractometer is made from an X-ray source, by a door samples and by a detector, arranged in a suitable geometry (Fig. 7.13).
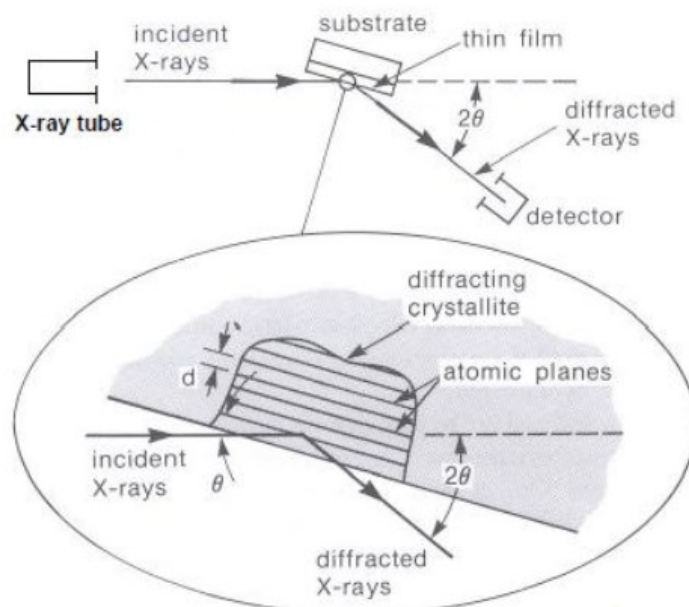
Figure 7.13 Representation of a X-ray diffractometer

7.3.4 Thermogravimetric analysis

Thermal gravimetric analysis (TGA) is a method of thermal analysis in which changes in physical and chemical properties of materials are measured as a function of increasing temperature (with constant heating rate), or as a function of time (with constant temperature and/or constant mass loss.

One of the most frequent uses of TG regards

- evaluation of thermal stability of a compound: if decomposes at a higher temperature means higher stability. However, the identification of the often complex reactions that occur due to the heat, cannot be made only on the basis of weight variation that they determine (complementary use of thermo-analytical techniques, eg. DSC)
- information on the purity of the sample: for example, in the sample, there can be: impurity inert potentiometrically, inorganic impurity, inorganic salt.

7.3.5 Ultraviolet–visible spectroscopy

The UV-visible absorption spectroscopy is based on the study of the interactions between a molecule with electromagnetic radiation of a wavelength between 200 and 380 nm (UV) and between 380 and 780 nm (visible). The interaction of radiation with such a molecule, can results in the transition of an electron from a molecular orbital to bond or not to bond to an empty antibonding orbital, and can therefore result in the clearance of the molecule from the ground electronic state to one of the various electronic excited states possible. The electronic transitions are subject to magnetic selection rules of symmetry and for which a transition can be permitted or prohibited in relation to the probability that it occurs. The term "prohibited" does not indicate the absolute impossibility that the transition takes place, but only a low possibility. The absorption spectrum of a compound in solution is generally presented as a curve in which the extent of absorption shows along the ordinate and the wavelength of the incident radiation on the horizontal axis. The absorption normally is expressed in terms of absorbance or optical density, defined as *A*. The principal laws of absorption of the radiation are summarized as follows:

1. The fraction of light absorbed by a transparent medium is independent of the intensity of the incident radiation, and each layer of equal thickness absorbs the same fraction of radiant energy that passes through it (Lambert Beer Law);

2. The amount of absorbed fraction is proportional to the number of atoms or molecules absorbed.

It follows that:

- The amount of radiation absorbed by the sample depends on the length of the optical path taken by the radiation;

- Fixed the optical path traversed by the solution, the absorption depends on the concentration of the absorbing species.

The mathematical equation that expresses such radiation is known as the law of Lambert-Beer-Bouguer:

$$T = \frac{I}{I_0} = e^{-\varepsilon lc}$$

where s is the coefficient of molar extinction (molar absorptivity expressed in $mol^{-1}L\ cm^{-1}$), l is the length of the optical path traversed by the radiation and c is the molar concentration of the absorbing species. By rewriting the equation in terms of absorbance you will have:

$$A = \varepsilon lc$$

7.4 Results and discussion

This section is divided in two parts, in the first one results relative to laminates characterization will be shown, while in the second one tests relative to UF membranes will be presented.

7.4.1 Characterization of Electrospun nanofibers for composite laminates

SEM Analysis

SEM images reported in Figure 7.14 show the morphology of the coPES9k electrospun nanofibers. The fibers show smooth surfaces and no sign of significant defects is observable.
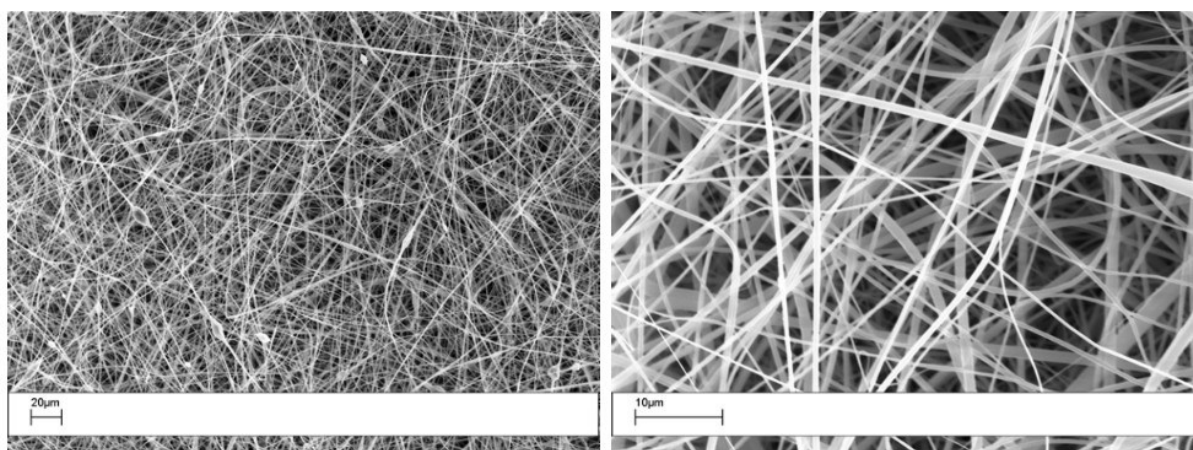
Figure 7.14 SEM images of coPES9k

Figure 7.15 shows the SEM analysis of the electrospun coPES9k nanofibres with respectively 1wt% (a) and 10wt% (b) of MWCNTs. The coPES9k with MWCNTs shows bead-on string morphology, whereas fibers without MWCNTs are bead-free. This can be caused by an incomplete dispersion of MWCNTs in the solution during sonication or, by the agglomeration of carbon nanotubes during the electropinning process. Furthermore, it is clear that, by increasing the percentage of MWCNTs, the amount and dimension of beads increase.
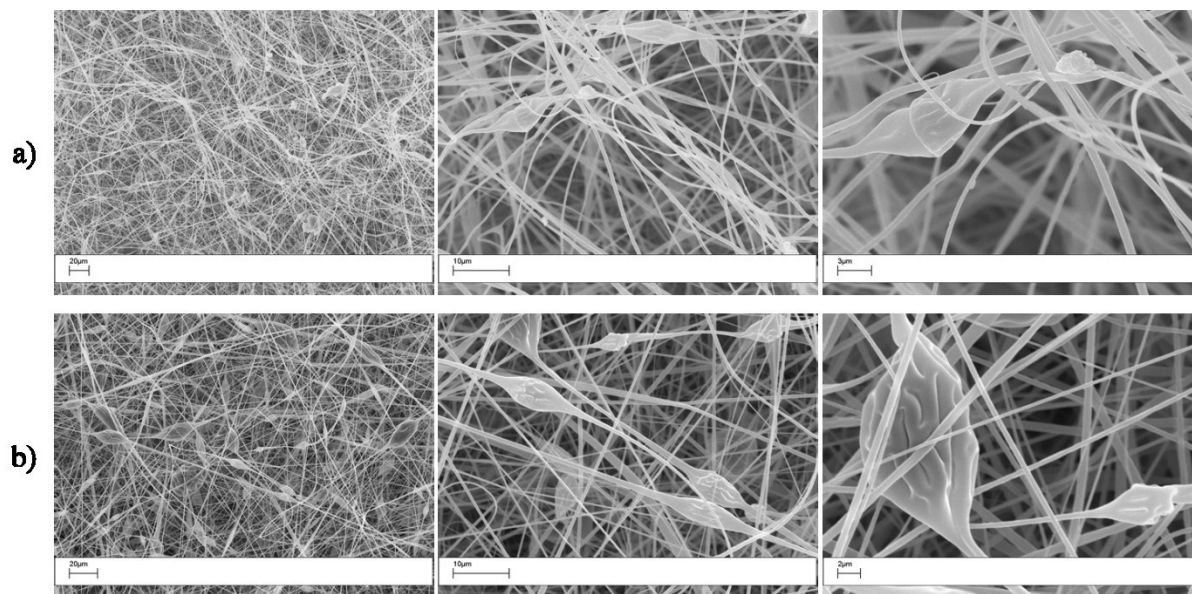
Figure 7.15 SEM images of coPES9k nanofibers filled with 1wt% (a) and 10wt% (b) of MWCNT

In figure 7.16 the comparison of the different MWCNTs content is shown with the final average diameters of the nanofibres.
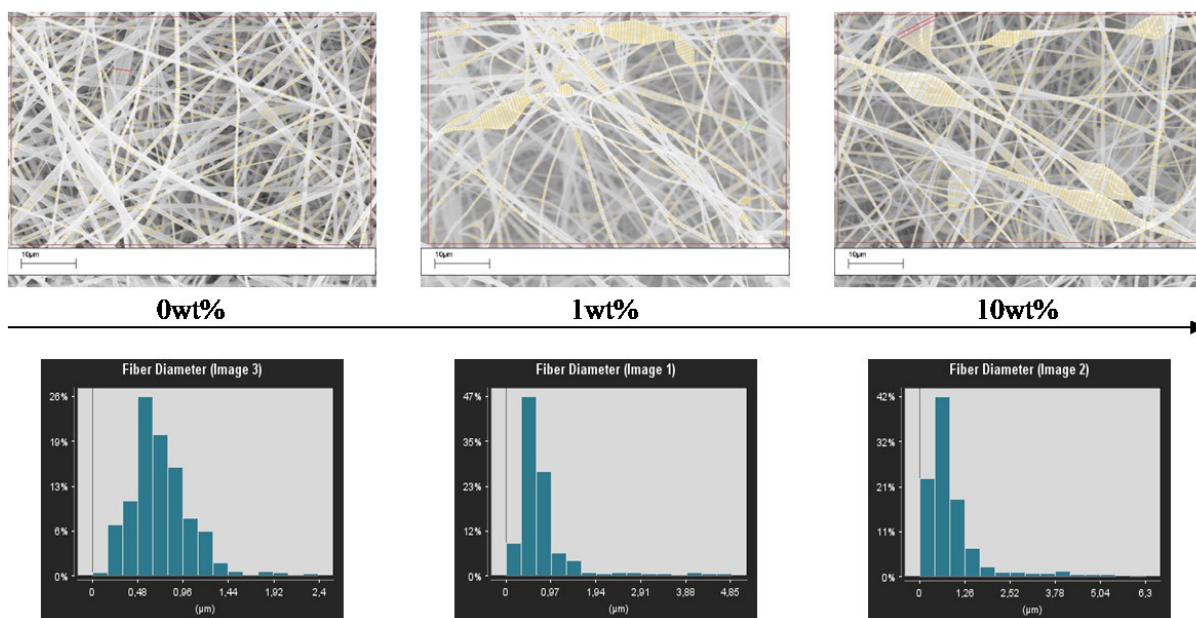
Figure 7.16 Comparison of electrospun coPES9k nanofibers with different amount of MWCNTs with average fiber diameters.

In figure 7.17 sections of coPES9k nanofibres are shown. It is possible to note that fibres without nanofillers are more compact than the ones filled with MWCNT. Furthermore, as the percentage of MWCNTs increases the nanofibres become larger and it is possible to imagine MWCNTs wrapped by thermoplastic inside the nanofibres.

In order to better confirm the presence of MWCNTs inside the fibres, TEM analysis was carried out as well (figure 7.18). Nanofibers were electrospun directly onto the TEM grid. Both agglomerates (figure 7.18a) and dispersed nanotubes (figures 7.19 b, c, d) aligned in the fiber-direction were observed.
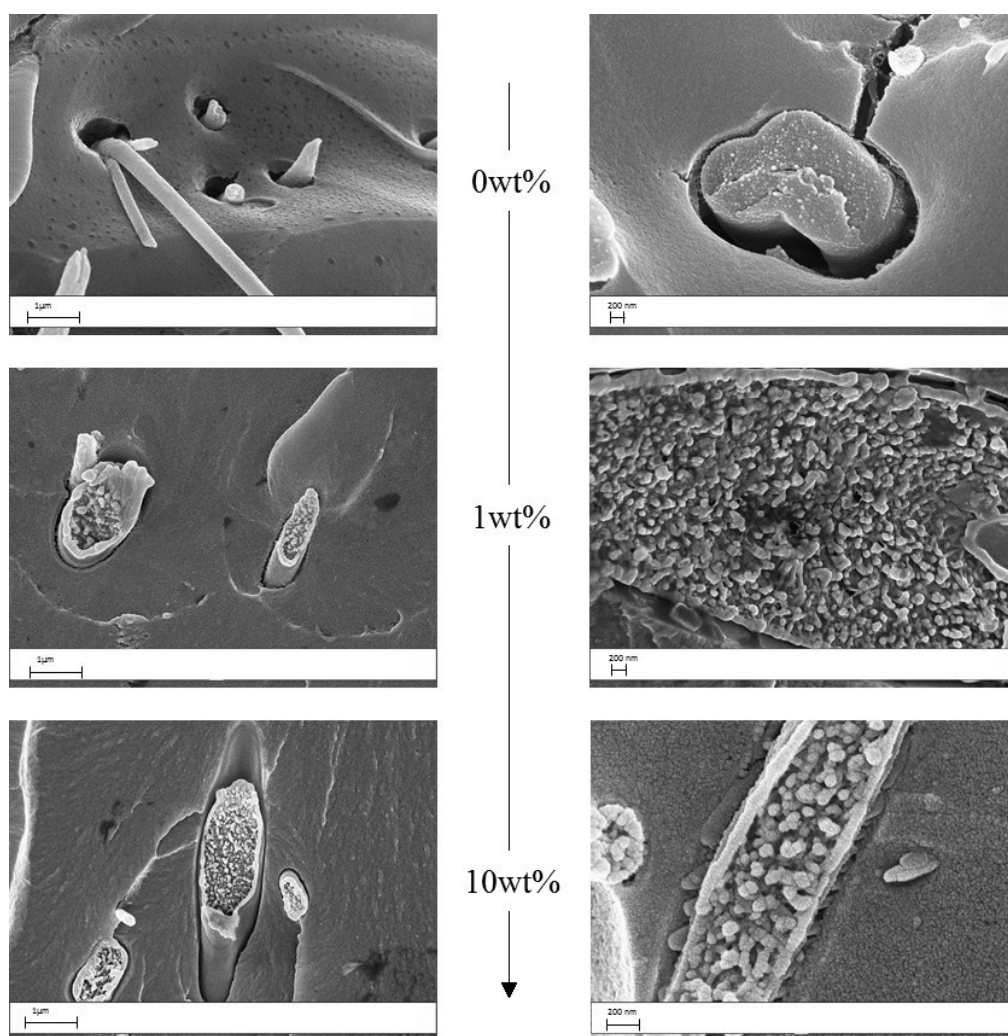
Figure 7.17 Sections of coPES9k nanofibres filled with MWCNTs
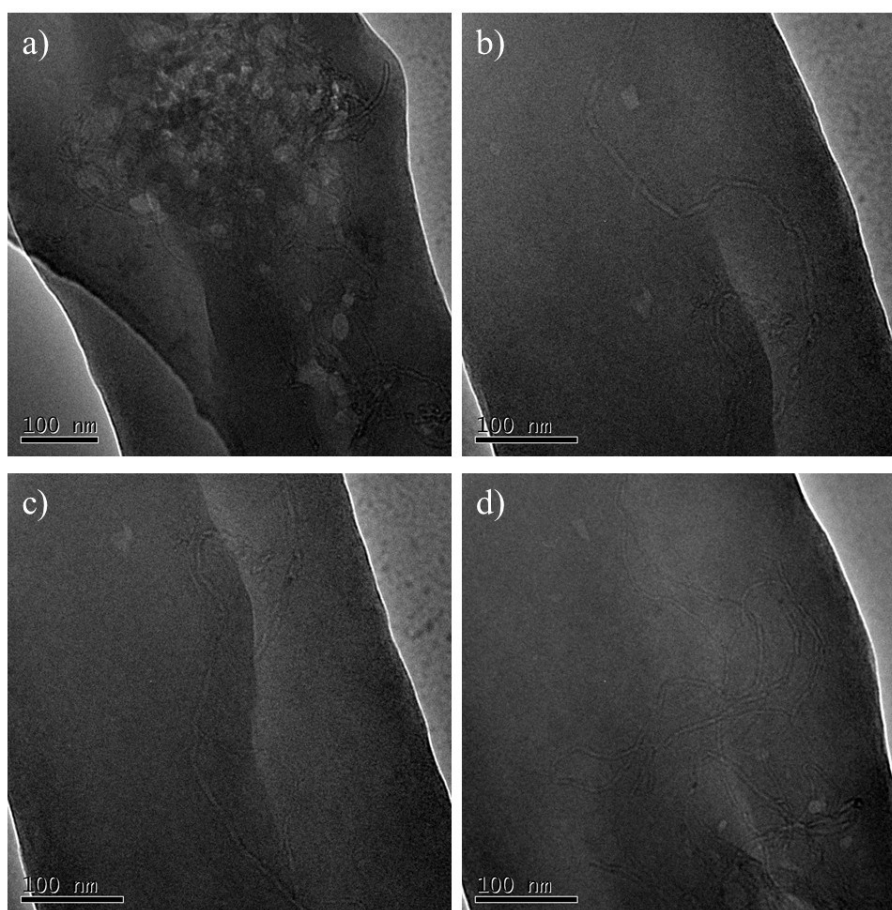
Figure 7.18 TEM images of coPES9k nanofibres filled with MWCNTs

It is also possible to see that MWCNTs are not well dispersed and kind of aligned along the fibres' direction. MWCNT distribution inside the nanofibres may be the one shown in Figure 7.19.
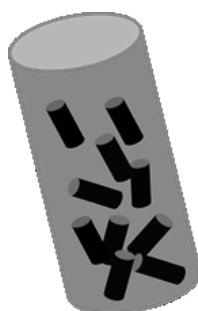
Figure 7.19 Scheme of MWCNTs inside the fibre

Figure 7.20 and 7.21 show the SEM analysis of the coPES9k nanofibres electrospun respectively with 1wt% of SiO_2 and 1wt% of carbon black.
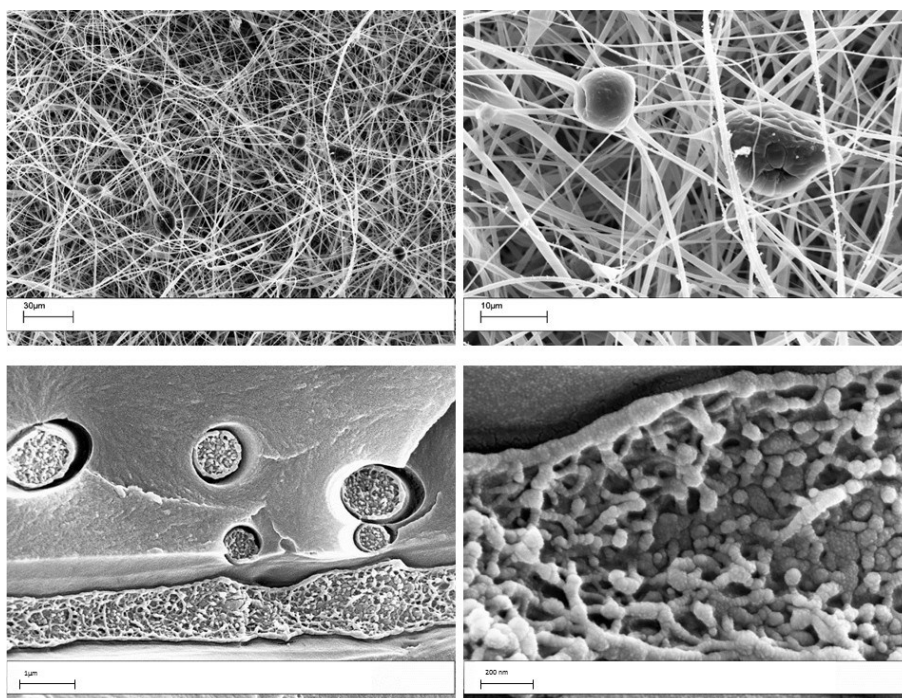
Figure 7.20 Sections of coPES9k nanofibres filled with 1wt%SiO_2
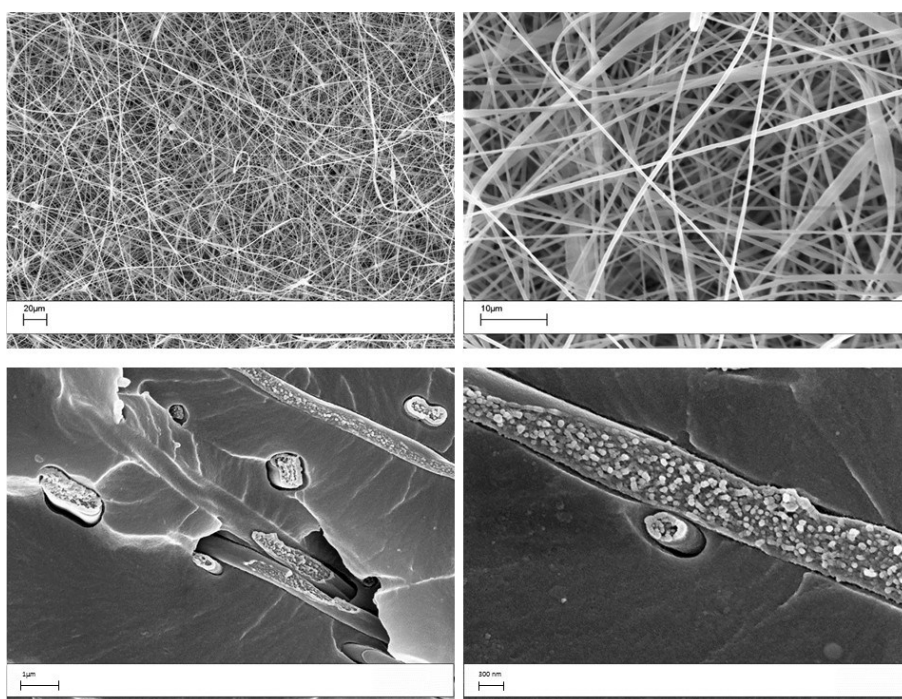
Figure 7.21 Sections of coPES9k nanofibres filled with 1wt%carbon black

It is possible to see that fibres with nanosilica show bead-on string morphology, as seen with MWCNTs, whereas fibres with CB are bead-free. This is an evidence of a better dispersion and stability of CB compared to MWCNTs and SiO_2. For both SiO_2 and carbon black nanofillers, an irregular inner morphology similar to that one of MWCNTs is observable.

It was seen that with SEM analysis it is not possible to effectively see the nanofillers inside the fibres. In oreder to overcome this issue, EDX analysis was performed proving the actual presence of such nanofillers inside the fibres.

EDX analysis was conducted on ZnO filled nanofibers. ZnO was used in order to have Zn as a distinctive element to follow. In fact, MWCNT and CB have not any specific peak that distinguish from coPES chains, while SiO_2 has the Si peak overlapped to that ones of the resin or of the polymer. On the contrary, in the case of ZnO is possible to distinguish the Zn peak (Fig.7.22).
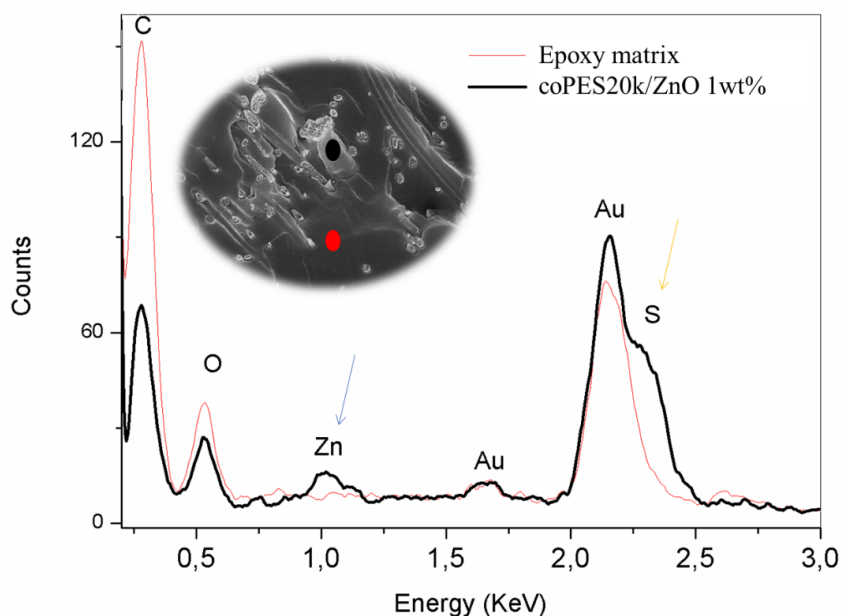
Figure 7.22 EDX Analysis of ZnO-filled nanofibers

SEM images of OpteSTAT electrospun fibers are reported in Figure 7.23. It is very clear the larger amount of CNTs achievable with technology polymer, since a lot of defects due to CNT-agglomerates are present.
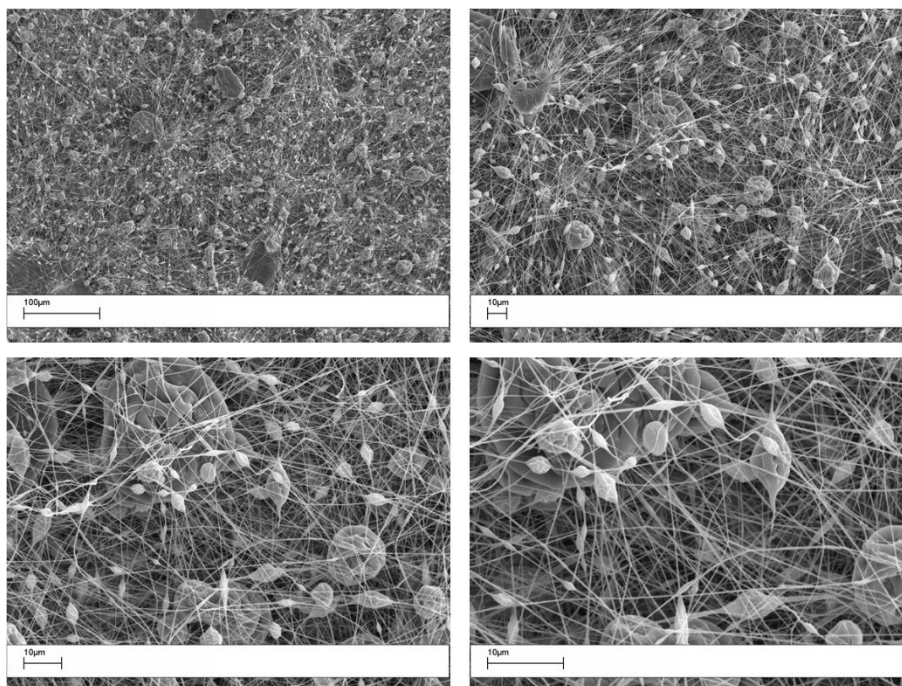
Figure 7.23 SEM images of OpteSTAT electrospun fibers

Scale- up of the electrospinning process

In order to scale up the project, it was necessary to move to commercially available thermoplastics. Two polyethersulfones sold by Solvay were the choice: Virantage® 30500 RP and Viratange® 10200 RP. Both of them are PESs but differ for the average molecular weight and for chemistry of the reactive end-groups.

The scale up of the electrospinning process was performed at Elmarco facilitiy placed in Liberec, Czech Republic. Elmarco machines work with the needle-less technology. In this specific electrospinning process, the needle is not expected to be used. Instead, there is a wire which act as positive electrode which is constantly wet with the polymer solution by a basket

that moves back and forward (Fig.7.24). This kind of machine electrospins with higher voltages applied, and allow continuous and, as a consequence, bigger production volumes.
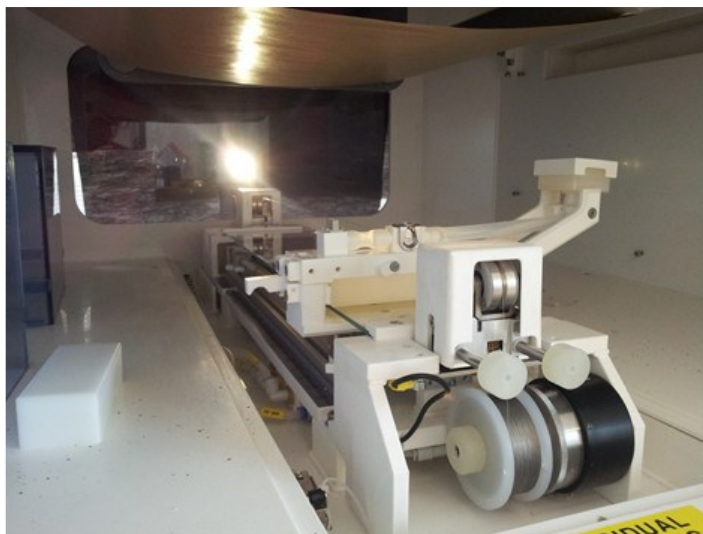
Figure 7.24 Needle-less technology of Elmarco machines

A first set-up was done with a laboratory machine in order optimize the process because of the needle-less technology (Fig.7.25). The polymers were electrospun on both antistatic PP and silicon paper in order to facilitate the subsequent peel of the veils.

Figure 7.25 NanoSpider NS 1WS500U by Elmarco

Figure 7.26 reports the SEMs of the electropun Virantage 30500. SEM analysis showed fibers with more defects with respect to needle machine, with a bead-on-string morphology. Instead, the fibers diameter analysis revealed a lower value, with an average of 380 nm.
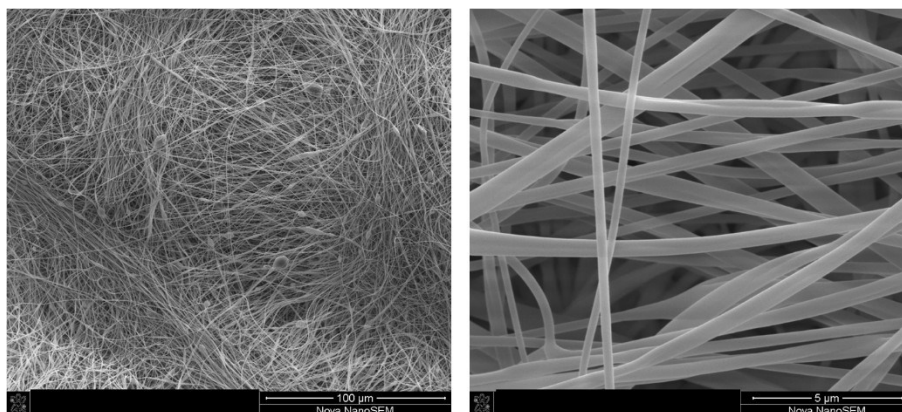
Figure 7.26 SEM images of electrospun Virantage 30500 by NanoSpider NS 1WS500U

Once all the conditions were set up, the process was transferred to the industrial production machine shown in Figure 7.27. This machine works with four wire at the same time.

Figure 7.27 NanoSpider NS 4S1000U by Elmarco

Figure 7.28 reports the SEMs of the electropun Virantage 30500 with the NS 4S1000U machine. SEM analysis showed fibers with less defects with respect to the lab machine, with

reduced bead-on-string morphology. Instead, the fibers diameter analysis revealed a bigger value, with an average of 504 nm.

7.4.2 Composite laminates characterization

Hybrid carbon fabrics with electrospun veils deposited onto were prepared to produce by infusion technique composite laminates as detailed in the experimental section. In this case unmodified epoxy resin was used for the infusion trials. The areal weight of the veil was balanced against the areal weight of the carbon fabric to obtain the desired amount of thermoplastic in the interlaminar region. The thermoplastic content varied between 10wt% and 20wt% for coPES9k veils. For comparison purposes, prepreg resins with predissolved coPES were used to impregnate carbon fabrics which were then cured.

Figure 7.29 reports the Tan δ-versus-temperature curves for the composite laminates prepared with veils and prepreg route at 10wt% of coPES9k in comparison to the unmodified epoxy resin. The tan δ curves for the sample of coPES9k veil is also reported as well. The samples containing the thermoplastic showed two peaks in the tan δ curves. The lower tan δ peaks of modified blends (166°C and 164°C for prepreg and veil, respectively) were at higher temperatures than the single peak of the unmodified epoxy resin (158°C). The higher tan δ

peaks (197°C and 194°C for prepreg and veil, respectively) were at lower temperatures than the tan δ peak shown by coPES9k veil (209°C). These tan δ peaks were due to the glass transition relaxations of epoxy-rich and thermoplastic-rich phase domains at low and high temperatures, respectively.
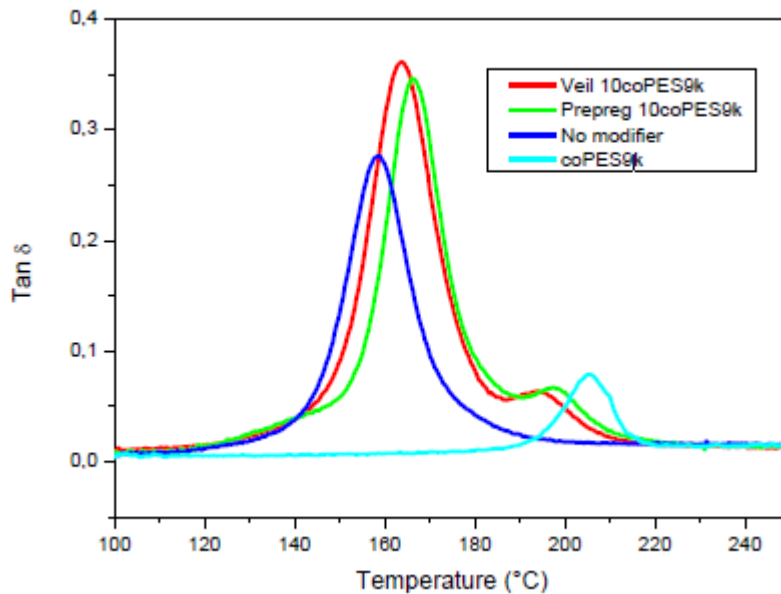
Figure 7.29 Comparison of Tan δ curves for three cured DGEBA composite laminates: prepreg, veil-modifier and no-modifier. The graph reports the Tan δ for the coPES9k veil analyzed with pocket tool

Figure 7.30 shows the comparison between the Tgs of the prepreg and veil composite laminates with a different modifier's content. Differences between Tgs for prepreg and veil samples were smaller as coPES9k amount increased. The phase-separated domains showed differences compared to the pure blend components (159°C and 205°C for pure epoxy and coPES9k, respectively). This result, again, is in accordance with has been reported in literature [7].
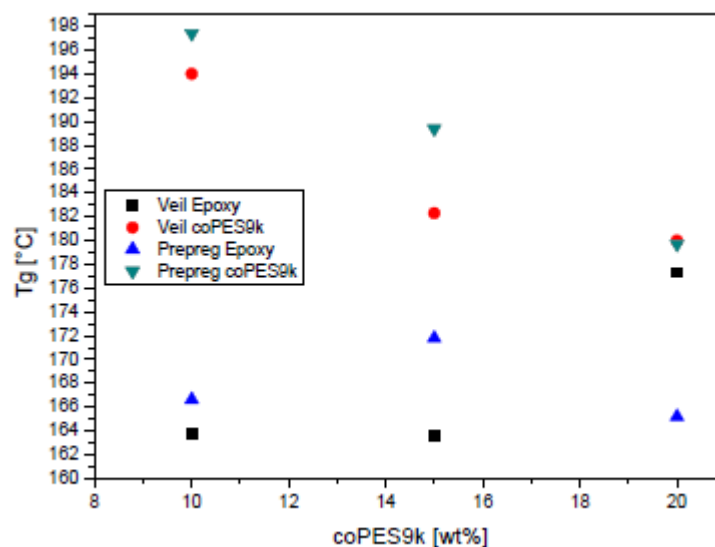
Figure 7.30 Glass transition temperatures (Tgs) versus coPES9k content for DGEBA composite laminates

Figure 7.31 shows the comparison between the interlaminar regions for the samples modified with the coPES9k veils and the predissolved coPES9k (i.e. prepreg). No undissolved veil was observed for all the percentages analyzed for the infused specimens. The morphology of the samples loaded with 10wt% of coPES9k was very similar for the prepreg and the veil samples. When the thermoplastic content raised to 15wt%, the prepreg sample showed smaller thermoplastic particles compared to the veil sample. Finally, the sample at 20wt% of coPES9k showed a morphology that became a combination of particulate and phase inverted for both the prepreg and the veil samples. However, the prepreg sample (at 20wt%) showed a predominant presence of particulate morphology over the veil sample, which showed an even presence of phase-inverted morphology.
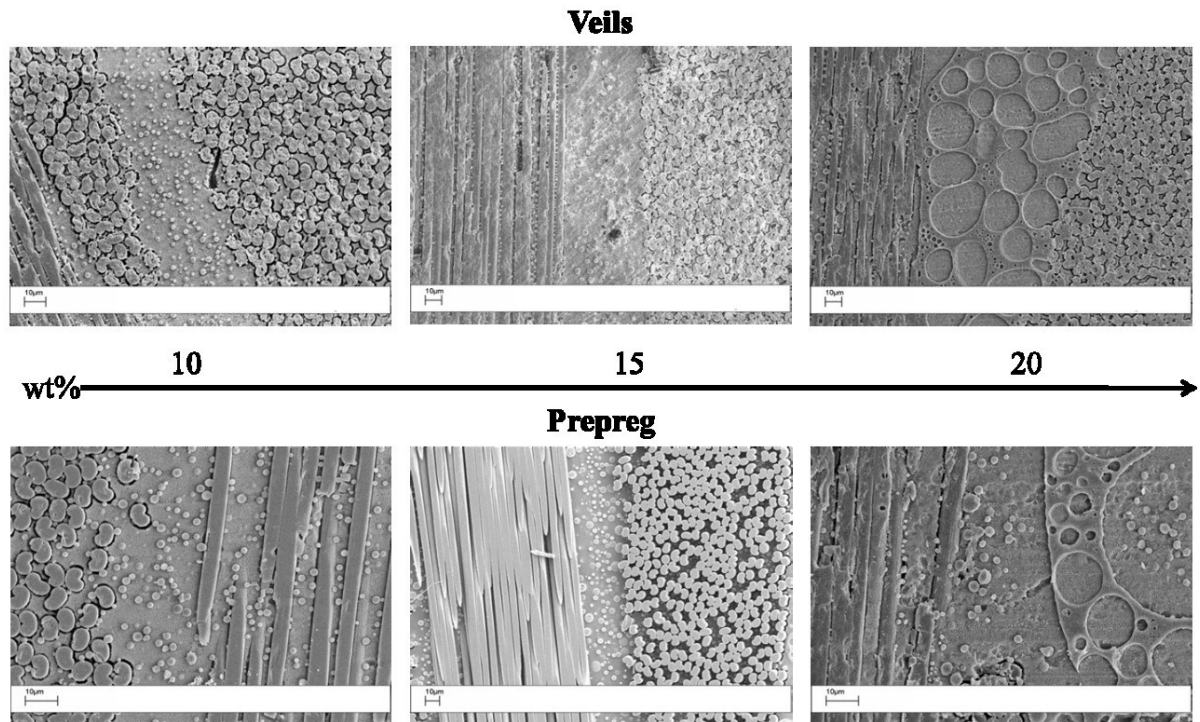
Figure 7.31 Interlaminar regions of coPES9k modified laminates (prepreg down, veil up) for different coPES9k contents

Figure 7.32 reports a SEM analysis for fractured veil samples with 10wt% of coPES9k. These pictures confirm the presence of particulate morphology both in the interlaminar region and between the carbon fibers. These results suggest the complete dissolution of the veil with a diffusion of the dissolved thermoplastic across the laminate during curing.
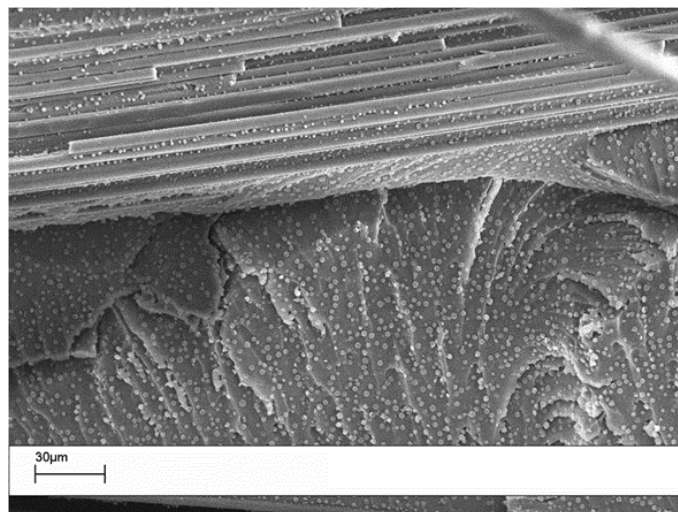
Figure 7.32 SEM images of fractured surfaces obtained from 10%wt coPES9k veil modified laminates

Laminates modified with Solvay's Virantage® PESs were manufactured following the scale-up process. Figure 7.33 shows the comparison of the Tanδ curves of Vir10200 and Vir30500 at 10wt%. Both of them show increases of Tg with respect to the unmodified system: +6°C for Vir 30500, +9°C for Vir10200, due to its higher molecular weight. It has to be noted that for Vir30500 there seems not to be phase separation. SEM analysis was carried out in order to better study these systems. Figure 7.34a show a phase-inverted morphology for the sample with 10wt% of veils of Vir10200, due to its higher molecular weight. Vir30500 showed a very fine particulate morphology (figure 7.34b), with dimensions of the particle less than 1 μm. This can justify the apparent single peak tanδ curve.
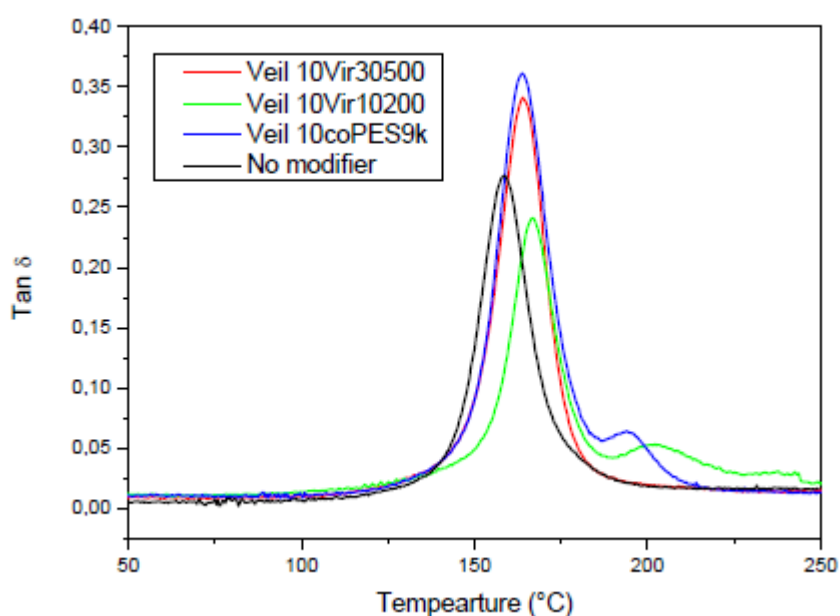
Figure 7.33 Comparison of Tan δ curves for four cured DGEBA composite laminates: Veil 10Vir30500, Veil 10Vir10200prepreg, Veil 10coPES9k and no-modifier.
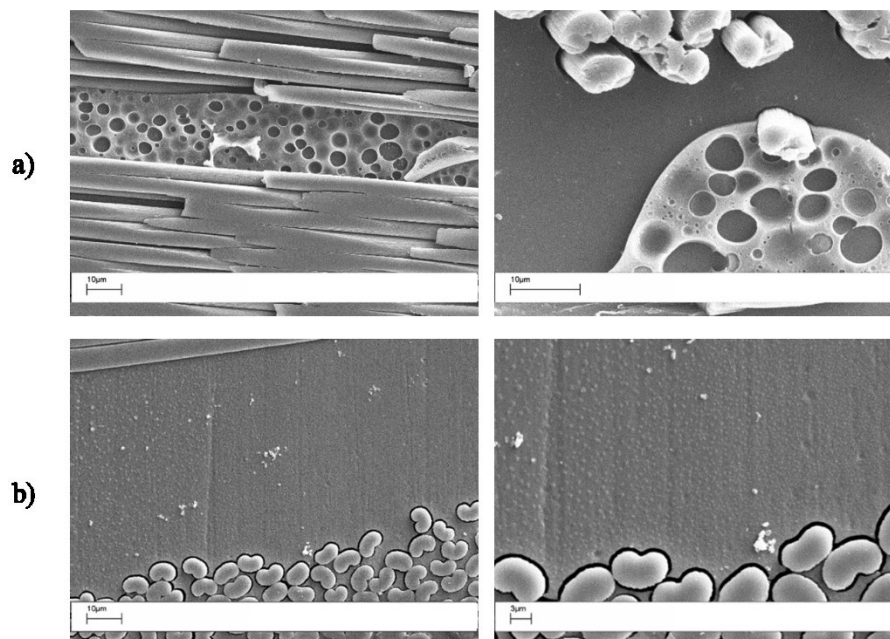
Figure 7.34 SEM images of interlaminar regions of laminates modified with 10wt% of (a) Veil 10Vir10200 and (b)Veil 10Vir30500

7.4.3 Nanofilled composite laminates characterization

Nanofilled composite laminates were manufactured by using MWCNTs and POSS particles. Figure 7.35 reports the Tanδ curves for samples modified with 1wt% of MWCNTs and POSS with respect to the thermoplastic content. A strange behavior was brought in by MWCNTs, since the sample showed a broad peak. This is a consequence of MWCNTs' interaction with both the epoxy-rich phase and the coPES-rich phase, activating the glass transition at an earlier stage. A narrower peak was observed for the POSS-filled veils. On the contrary of the neat resin results, the Tg was lowered by -11°C, this may come from a bad distribution of the particle, like for MWCNTs, in the matrix. Figure 7.36 reports the elastic moduli curves. It can be seen that there is a drop-off of the elastic modulus for the phase-separated coPES9k cured sample with respect to the unmodified one. E' is recovered when coPES9k veils are filled with nanoparticles.

SEM images are reported in figure 7.37 and 7.38 for MWCNT- and POSS-filled samples. MWCNTs tend to stay in the thermoplastic-rich phase, even though there is also some evidence in the epoxy phase. As for POSS, cubic agglomerates are evident in some points of the epoxy-rich phase. Furthermore, it is clear how the interactions of POSS particle with both thermoplastic and epoxy modify the final morphology from particulate to a more complex one, which is particulate plus phase inversion.
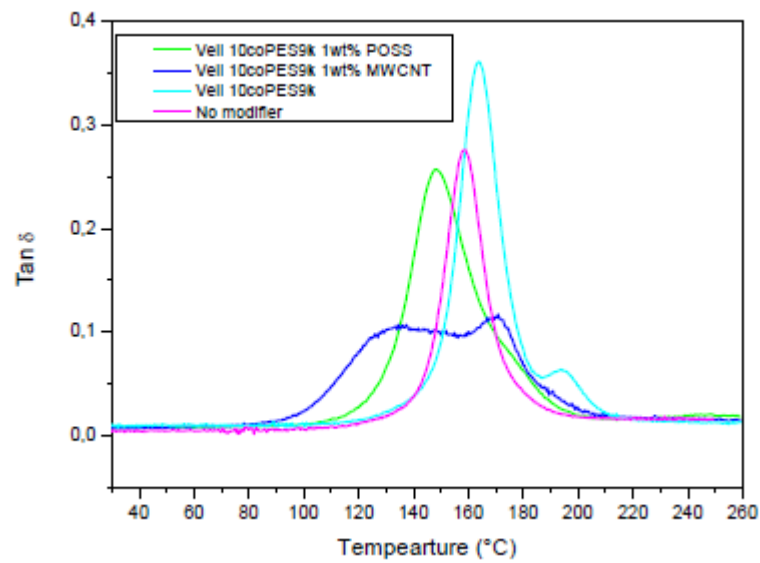

Figure 7.35 Comparison of Tan δ curves for cured DGEBA veil-modified composite laminates: 10wt%coPES9k +1wt%MWCNT, 10wt%coPES9k +1wt%POSS, 10wt%coPES9k no modifier
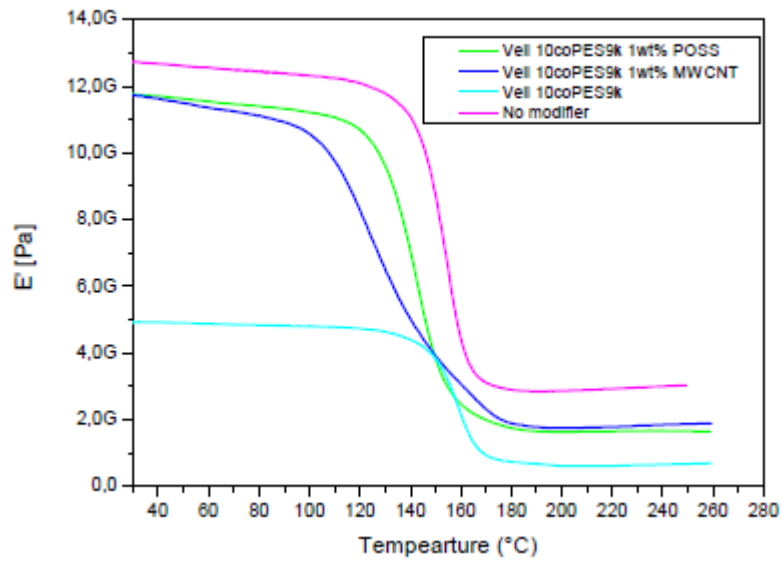
Figure 7.36 Comparison of elastic moduli curves for cured DGEBA veil-modified composite laminates: 10wt%coPES9k +1wt%MWCNT, 10wt%coPES9k +1wt%POSS, 10wt%coPES9k no modifier
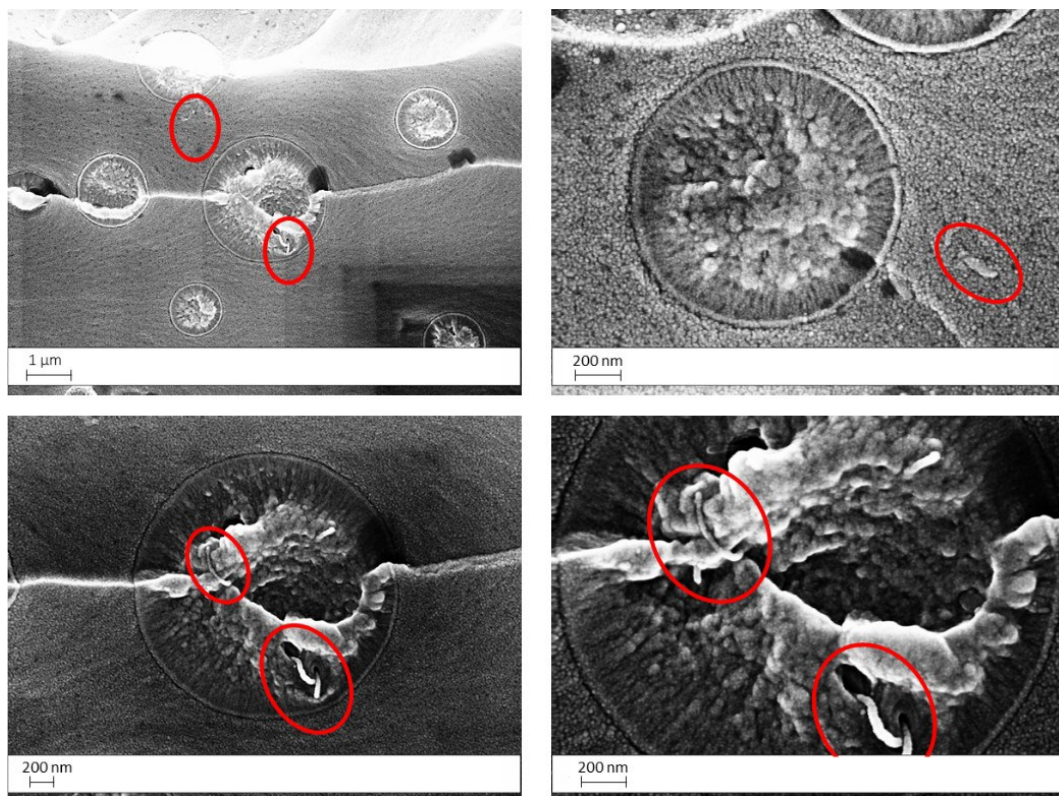
Figure 7.37 SEM images of 1wt% MWCNT-filled sample
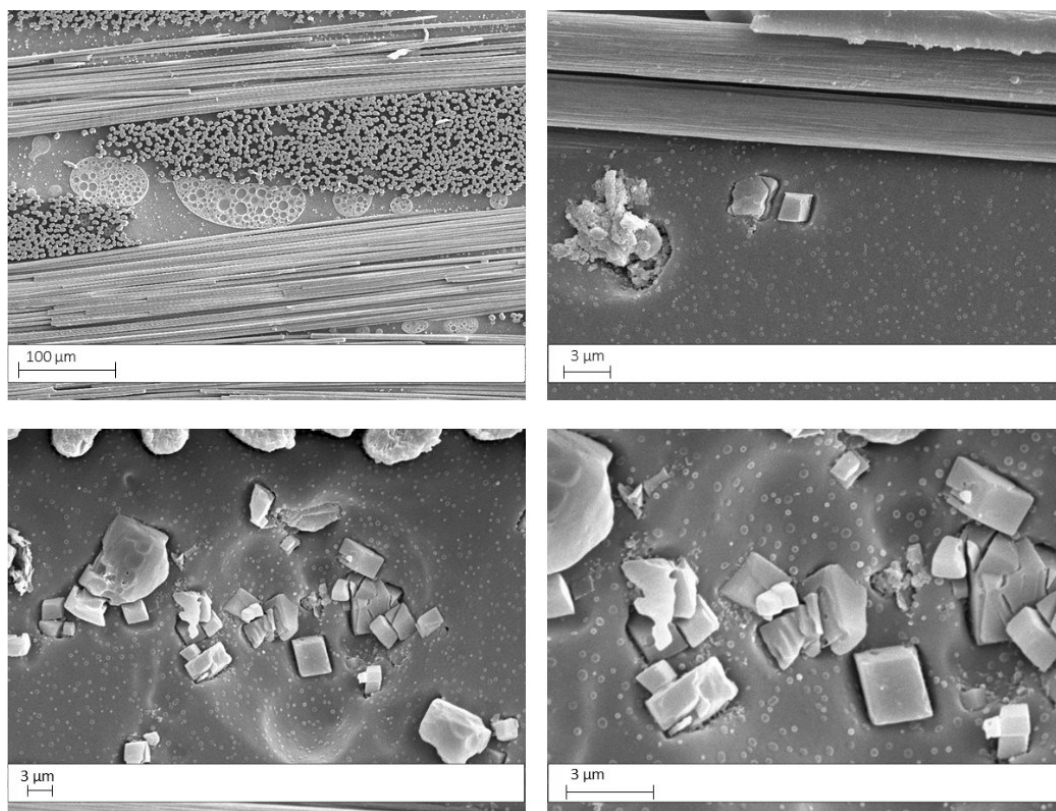
Figure 7.38 SEM images of 1wt% POSS-filled sample

A composite laminate was prepared by following the scheme reported in figure 7.39 with the compound OpteSTAT PES/MWCNT provided by OVATION Polymers. The idea was to put a large excess of thermoplastic/MWCNT on one surface in order to achieve phase separation and percolation for carbon nanotubes. This was confirmed by SEM analysis reported in figure 7.40.

It is evident the phase inversion that occurred in the outer surface due to the large excess of polymer with respect to the resin. In this way, percolation of CNTs was achived, as shown by the greater SEM magnification where it is possible to observe most of CNTs in the thermoplastic-rich phase and a few in the epoxy-rich phase as well. This CNT-percolated morphology was wanted in order to ensure an improved electrical conductivity on the outer surfaces of the composite laminate.
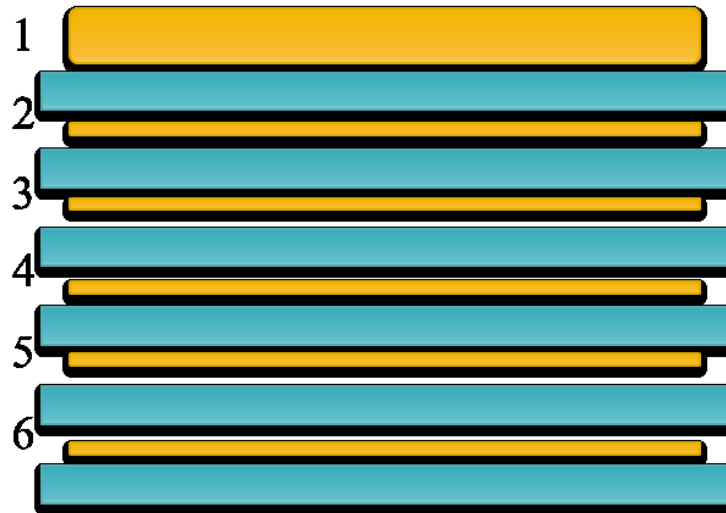
Figure 7.39 Scheme of the composite laminate prepared with OPTEStat elctrospun nanofibers
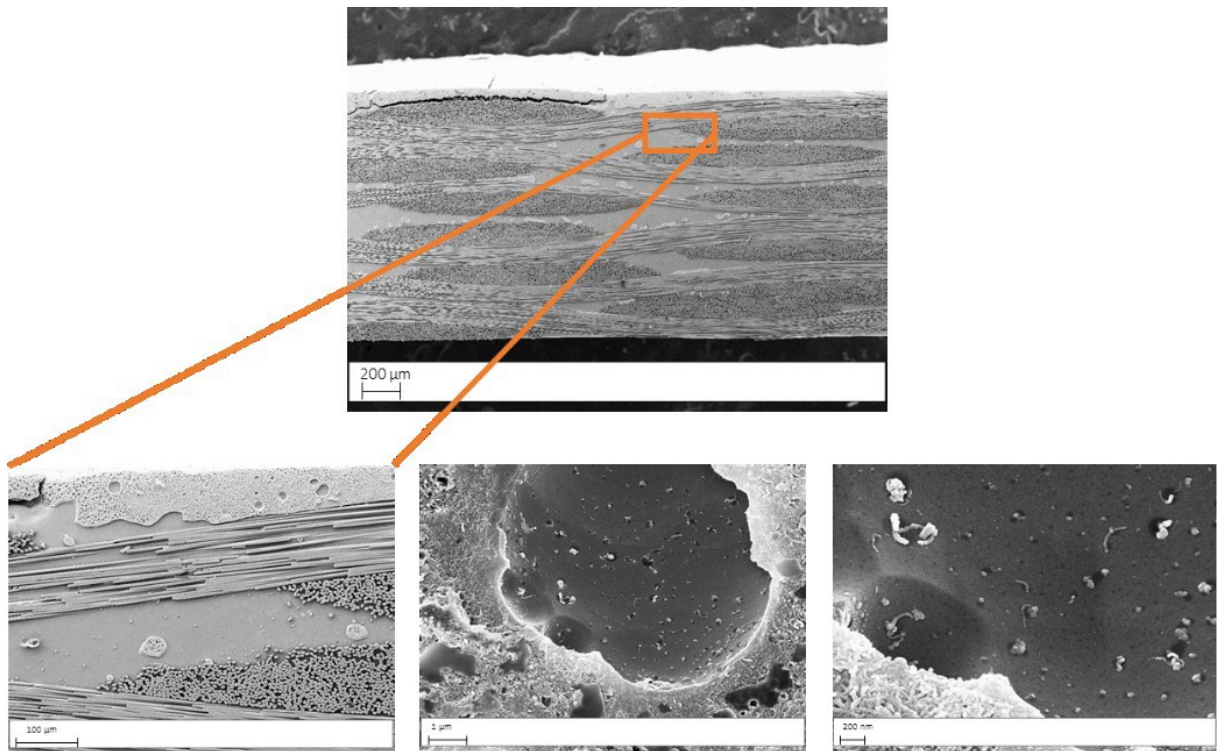

Figure 7.40 SEM images of OPTEStat-veil modified composite laminate reproducing the sheme shown in figure 6:66. MWCNTs coming out from the epoxy-rich phase and percolation in the thermoplastic-rich phase are evident.

7.4.4 Characterization of Electrospun nanofibers for active UF membranes

SEM and EDX Analysis

As seen in samples preparation paragraph, for this part of the work, two different solutions have been prepared and electrospun. In the first one Zinc Acetate (the precursor for ZnO) was added to VERADEL solution, while in the second one no.

Figures 7.41 and 7.42 show the morphologies and diameter distributions of the fibers obtained starting from the two different solutions.
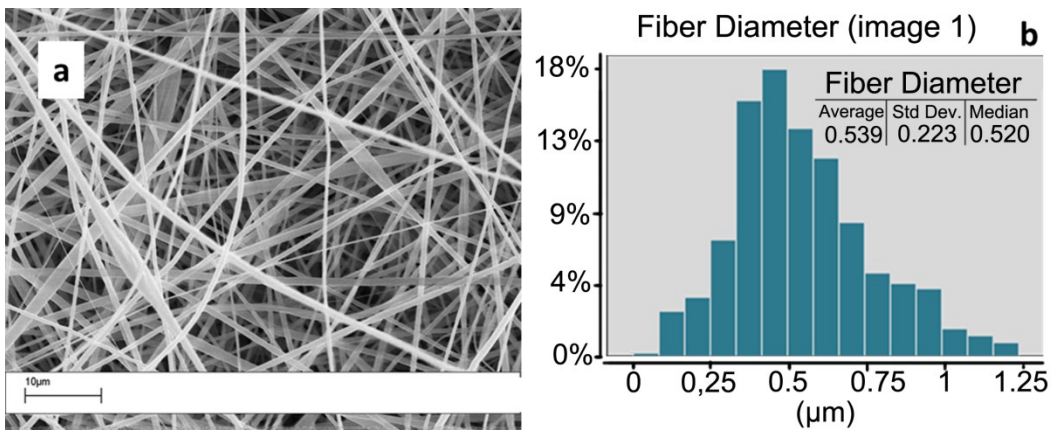

Figure 7.41 SEM images of electrospun and related diameter distributions for undoped VERADEL fibres
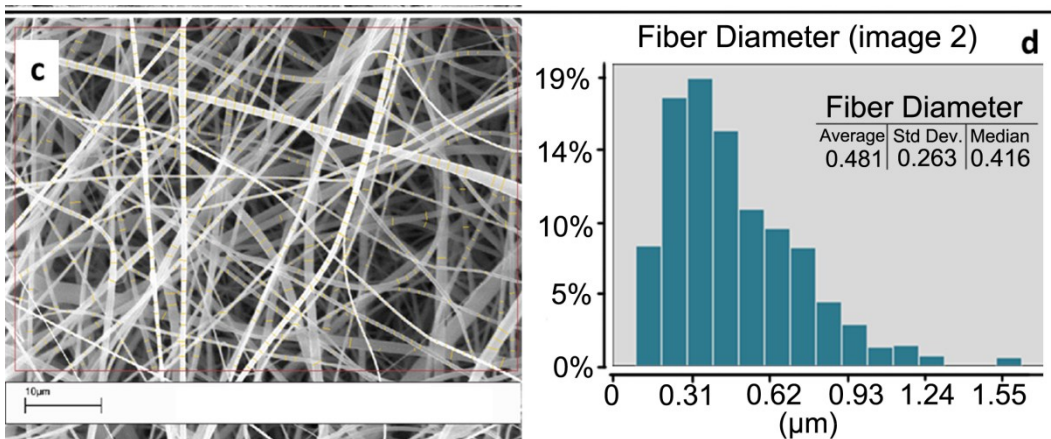
Figure 7.42 SEM images of electrospun and related diameter distributions for Zn(Ac)$_2$ doped VERADEL fibres

It's possible to note that fibre morphology is not significantly affected by the presence of the zinc dopant. The average fibre diameter is 540nm ± 223 nm for undoped VERADEL fibres and 481nm±263 nm for $Zn(AC)_2$ doped fibres.

In order to assess the successful inclusion of $Zn(Ac)_2$ into the polymeric fibers an annealing process at T = 400°C was done. Figure 7.43 shows the pure ZnO nanofibres obtained.
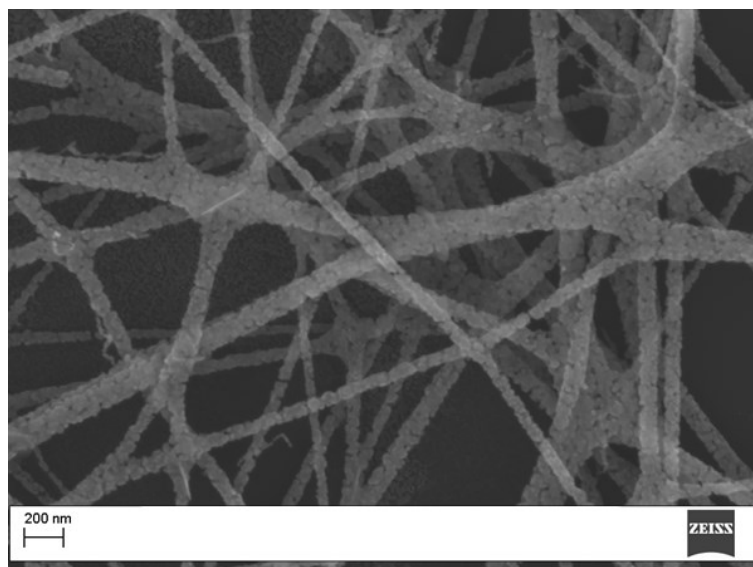

Figure 7.43 ZnO doped PES fibres after annealing at 400°C.

Figure 7.44 shows high magnification details of ZnO nanorods grown on seeded undoped and ZnO doped PES fibres: clearly larger nanostructures grow on seeded ZnO doped VERADEL (Fig.7.44b) than those observed on seeded undoped PES fibres (Fig.7.44a).
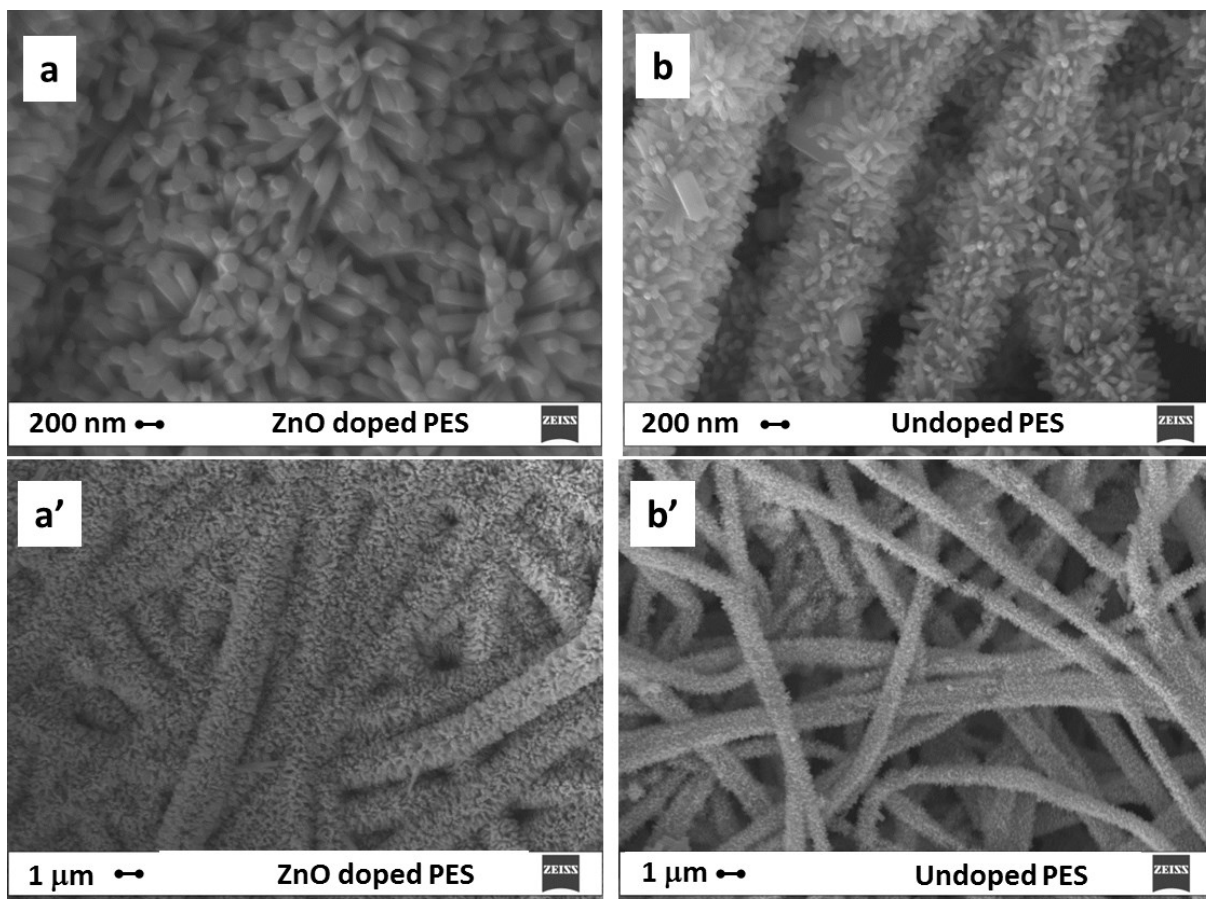
Figure 7.44 ZnOnanorods CBD growth on a) undoped and b) ZnO doped VERADEL fibres after 1 hour seeding.

EDX analysis further confirms the growth of smaller ZnO nanostructures onto undoped PES fibre mat, thus resulting in an external shell thinner than the one grown on the ZnO doped PES fibrous mats. Figure 7.45 shows the EDS spectrum of the fibrous mats after CBD growth: the C and S signals related to PES core are still visible for undoped samples (red line), while for ZnO doped VERADEL fibre mat the thicker ZnO shell hinders the contribution of the internal core and only ZnO related signals are visible in the recorded spectrum (black line).
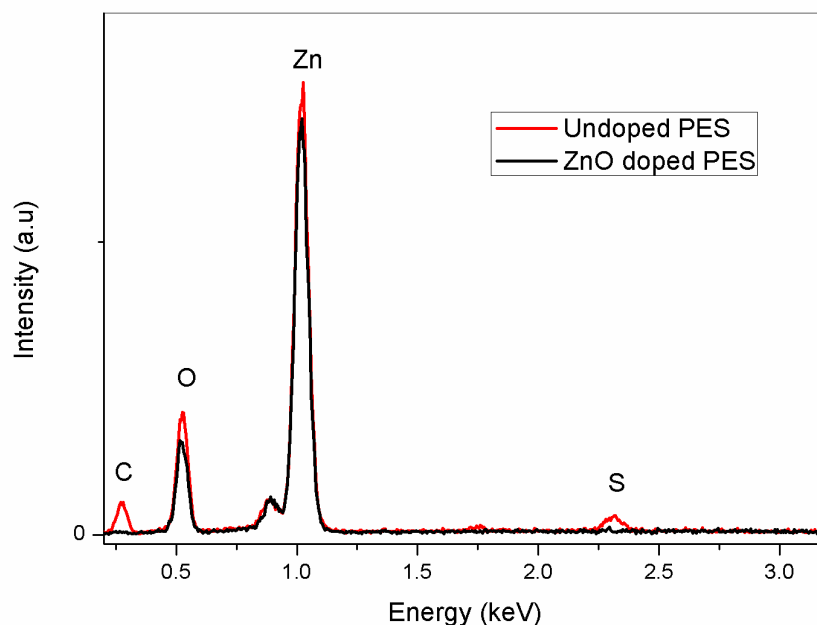
Figure 7.45 EDS spectra of undoped and ZnO doped VERADEL fibre mats after CBD growth.

XRD Analysis

In order to assess the crystallinity of the ZnO nanorods an XRD Analysis was done and results are shown in Figure 7.46. ZnO presence inside VERADEL fibres does not affect the crystallinity of ZnO nanorods in the external shell: in fact XRD patterns of polymeric fibres after CBD growth possess all reflection peaks indexed to hexagonal wurtzite ZnO. These brush-like ZnO nanorods show XRD patterns displaying a more intense(101) diffraction peak than the (002) one due either to the growth of nanostructures with {10-10} planes as basal facets correlated to signal arising from tilted [0001] oriented nanorods with respect to supporting surface orientation [8].
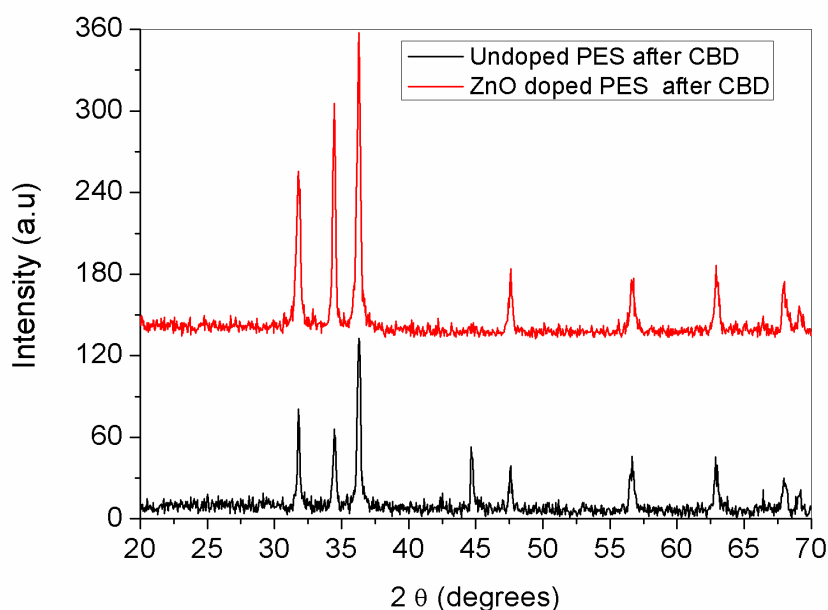
Figure 7.46 XRD patterns of a) undoped and b) ZnO doped electrospun fibre mats after CBD process.

TGA Analysis

A thermogravimetric analysis was done on electrospun fibers as obtained and on electrospun fibers after the CBD process.

Thermal degradations were performed in a Mettler Thermogravimetric Analyzer TGA 1 Star System. The temperature calibration of equipment was made according to the method suggested by Mettler. Samples of about 1mg were put into open alumina crucibles and heated in the temperature range 25-700°C, at the heating rate of 10°C·min^{-1}, in static air atmosphere. In order to correct the error in the mass determination due to the reduction of the buoyancy force on increasing temperature, we used the blank method, recommended by the ICTAC Kinetics Committee. A thermogravimetric (TG) run with an empty pan (blank) was preliminarily performed in the same experimental conditions used for samples. The so obtained blank curve was subtracted from those of samples, so obtaining corrected degradation TG curves. At the end of each experiment these data were used to plot the

percentage of undegraded sample, $(1-D)\%$, as a function of temperature, where $D = (W_\mathrm{o}-W)/W_\mathrm{o}$, and W_o and W were the masses at the starting point and during scanning.

Figure 7.47 shows the results of TGA analysis of the undoped and $Zn(Ac)_2$ doped VERADEL fibers after the electrospinning process.

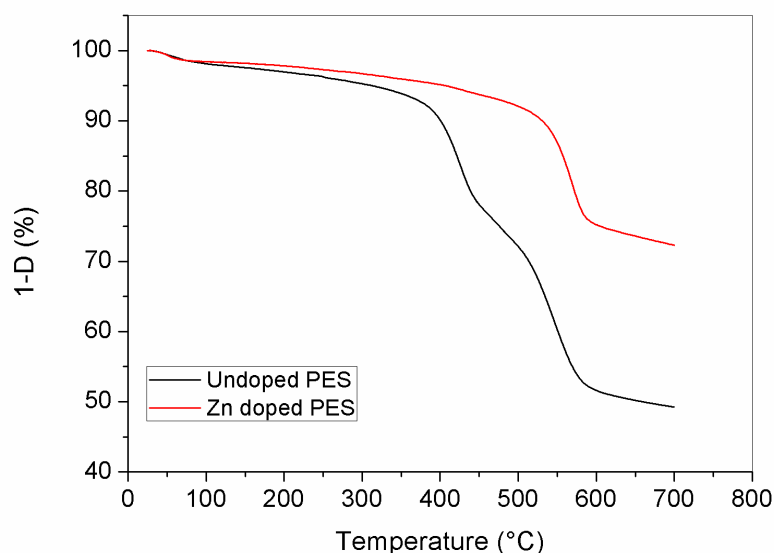**Figure 7.47 TG degradation curves, at 10°C·min^{-1}, in air of undoped and $Zn(Ac)_2$ doped VERADEL fibres.**

In particular, for undoped fibres, degradation starts at ~ 390°C and finishes at ~ 590°C following a two steps pathway. On the contrary, the maximum weight loss of $Zn(Ac)_2$ doped VERADEL fibres occurs in one step between 540°C and 590°C, thus pointing at a delayed degradation of the polymeric component. We can rationalize this effect by considering the high thermal conductivity and heat capacity of the formed ZnO nanofibers (see Fig.7.43), thus responsible for the delay of VERADEL degradation. The residue weight percentage calculated for $Zn(Ac)_2$ doped fibres degraded in air is higher than that obtained for undoped VERADEL fibres, due to formation of ZnO fibres concomitant to VERADEL degradation (see Fig.7.43).

Thermogravimetric analysis (TGA) of VERADEL fibres after CBD growth is reported in Figure 7.48.
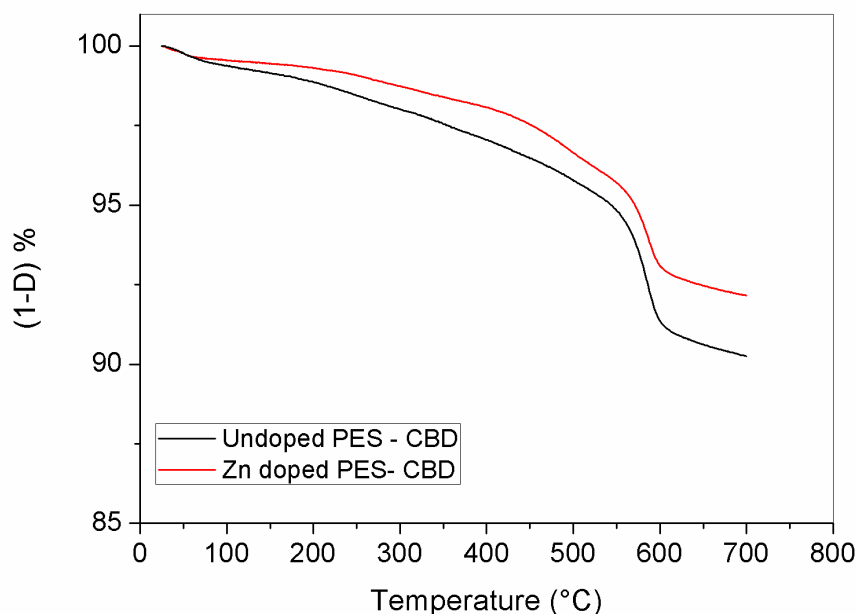

Figure 7.48 TG degradation curves, at 10°C·min⁻¹, in air of undoped (black line) and ZnO doped (red line) VERADEL fibres after CBD growth of ZnO NRs brush-like shell.

ZnO CBD growth further improves thermal stability of polymer: moreover, the massive growth of ZnO nanostructures onto polymeric scaffold is confirmed by the significant decrease of polymeric fraction with respect to ceramic one as indicated by the faint degradation yield, now reduced at less than 10% (see, for comparison, TG data reported in Fig.7.47). From these data we can estimate the weight percentage of the external ZnO shell with respect to the polymeric contribution, important for evaluation of photocatalytic properties of this ceramic-polymeric material.

7.4.5 Photocatalytic test

The use of these hybrid oxide-polymer mats as active materials for water purification has been tested by evaluating their capability to degrade MB aqueous solutions.

Doped and ZnO doped VERADEL mats (7 mg) were dipped in a quartz cuvette containing $1 \times 10-5$ methylene blue aqueous solution (3 ml, pH= 7) and irradiated by UV lamp (Black-RayB-100 A, 365 nm). The cuvette was covered by a box wrapped around by an aluminium foil for reflection of UV light back into cuvette. The irradiated solution was measured at regular time intervals with an UV-VIS spectrophotometer (JASCO V-630) in a wavelength range of 200-800 nm.

The degradation of MB was evaluated by the absorbance peak at 664 nm in the Lambert-Beer regime. The photodegradation rate was calculated from the linear plot of $\ln(C0/C)$ versus the irradiation time. The decomposition of the MB dye in the absence of any photocatalyst materials was checked as a reference. Control experiments in the dark overnight were conducted to clarify the contribution of the adsorption of the MB at the sample surface.

Photodegradation of MB was evaluated by monitoring its absorption spectra as a function of irradiation time in the presence of bare and ZnO NRs decorated fibres: in particular, normalized change in its concentration (C_0/C) upon varying irradiation time is reported to determine the degradation efficiency. The standard procedure used requires to test the MB solution degradation, in presence of photocatalytic material, under dark to evaluate the effect of dye physisorption. Our experiments have been started after running overnight a control test in dark. The MB concentration remains almost unchanged (less than 1% variation of the initial absorbance for 1×10^{-5}M MB solution). It is important to note that the hydrophilicity of ZnO doped VERADEL mats

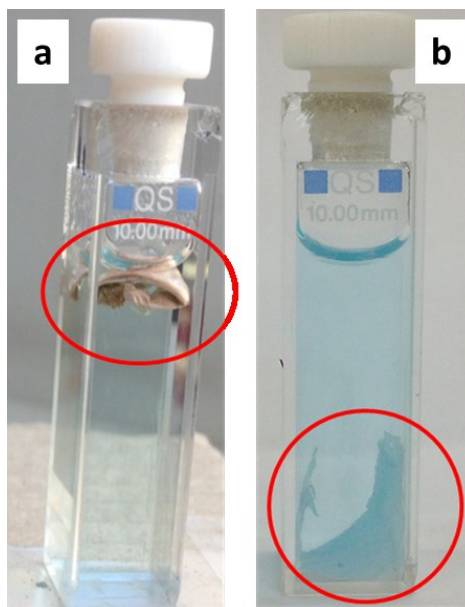changes significantly in presence or in absence of ZnOnanorods external shell, as shown in Figure 7.49.

Figure 7.49 Quartz cuvettes used to irradiate MB aqueous solutions containing a) bare and b) ZnO NRs decorated ZnO doped PES nanofibres.

In fact, as clearly visible in Figure 7.49, in the absence of ZnO shell the hydrophobic mat (measured Water Contact Angle= 128°) remains at solution surface totally crumpled to minimize contact with aqueous solution: consequently, exposed surface area and light absorption are significantly limited. Accordingly, we can expect a reduction of catalytic performances, strongly dependant on exposed surface area. On the contrary, in presence of ZnO nanorods external shell (Figure 7.49b) the mat remains well stretched in solution and can be easily dipped in dye aqueous solution. This behaviour can be related to the increased mat density due to the presence of ZnO NR external shell associated to the improved wettability (measured WCA= 106°).

Figure 7.50 reports the normalized (C/C_0) methylene blue (MB) degradation after exposure to UV light.
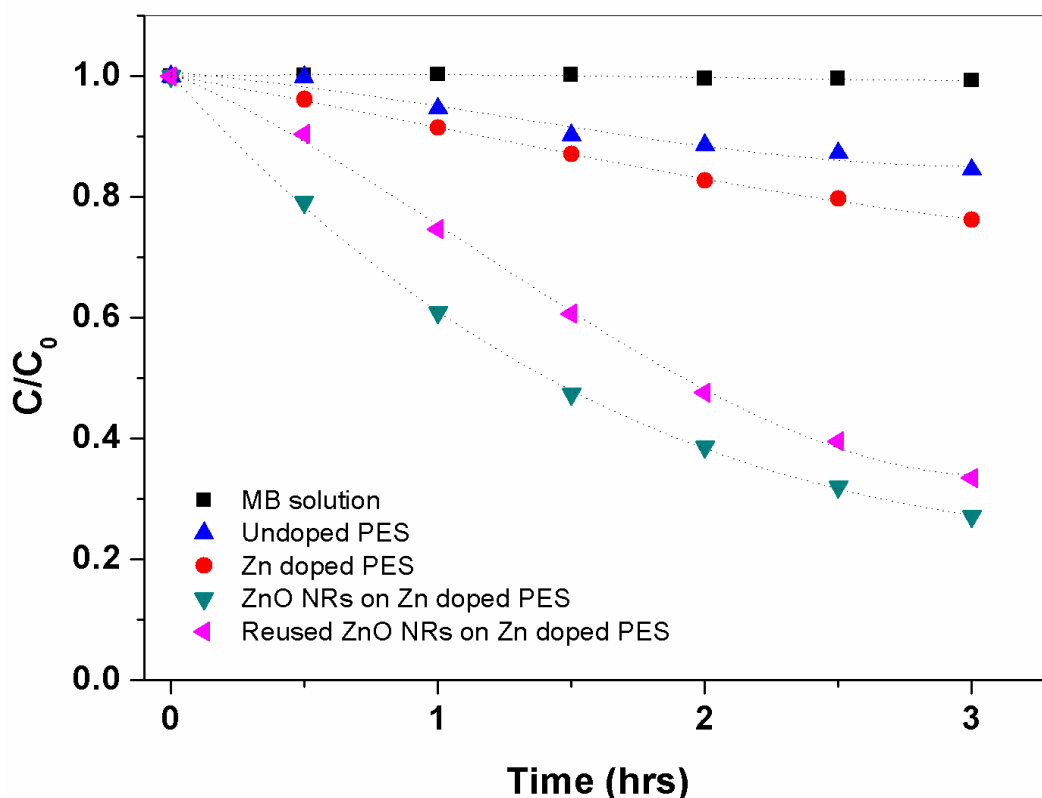
Figure 7.50 Photocatalytic MB degradation under UV light irradiation.

ZnO doped PES mats (red dots) shows an improved photocatalytic activity with respect to undoped PES mats (blue triangles). After ZnO NRs CBD growth, photocatalytic activity increased and a MB degradation of 78% is observed. The obtained results are well reproducible, thus validating the possibility to scale up the solution growth at larger volumes. Noteworthy, MB solution remains clear during the overall degradation experiment and no filtration is required to monitor the photocatalytic dye's degradation.

Another important result attains the possibility to reuse, after washing in water and drying overnight at 100°C, these photocatalytic mats without a significant reduction (about 10%) of their efficiency (Fig.7.50, purple triangles).

7.4.6 Optimization of process conditions for active membrane preparation

As seen in the samples preparation paragraph the procedure used in order to produce the UF membranes is about 18 hours long. For this reason, here a process optimization procedure is proposed. Since the longer step of the procedure is the Seeding one, I tried to reduce the time of this step by increasing the temperature. In Table 7.4 all the tested values, of time and temperature, are listed.

TEMPERATURE (°C)	TIME(h)
110	5
150	1
180	1

Table 7.4

SEM analysis of these samples are presented below.

The first test was to reduce the seeding time to 5h maintaining the temperature at 110°C. Results are shown in Figure 7.51.
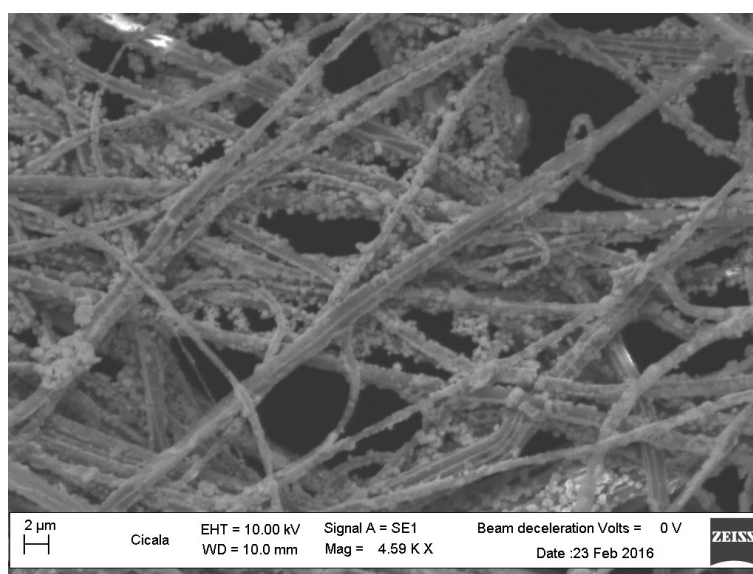

Figure 7.51 ES fibers after CBD seed 5h at 110°C

155

As we can see in this case we don't have brush-like ZnO NRs that cover the fibers but only few structures among the fibers. In the second try I increased the temperature at 180°C and reduced the time to 1h. As shown in Figure 7.52 in this case the fibers are not well defined and no growth of ZnO structures is observed. This can be do the fact that at this temperature polymer degradation phenomena may starts.
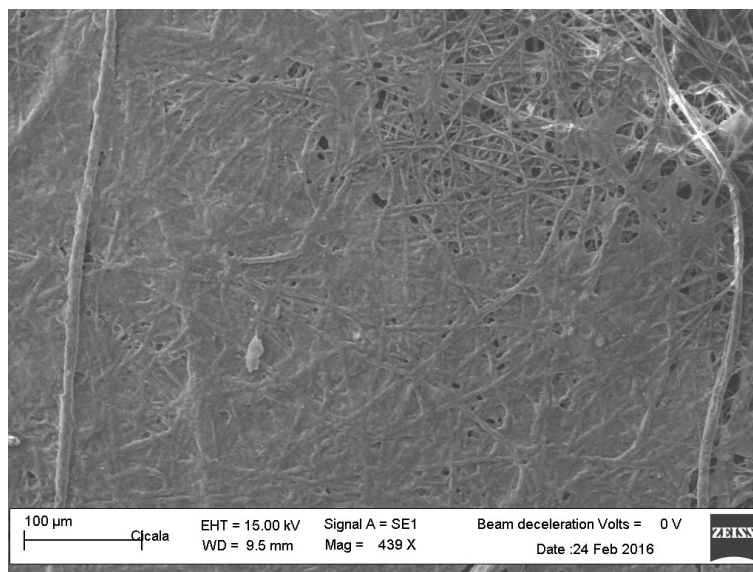

Figure 7.52 ES fibers after CBD seed 1h at 180°C

The last test was to use a temperature of 150°C and a time of 1h. Result of SEM analysis is presented in Figure 7.53. As we can see, in this case, samples quite similar to those obtained whit the standard seeding process have been obtained. So it's possible to conclude that the process has been optimized by using a temperature of 150°C and a time of 1h. This allows to decrease the time of the entire membrane production process of about 11 hours.
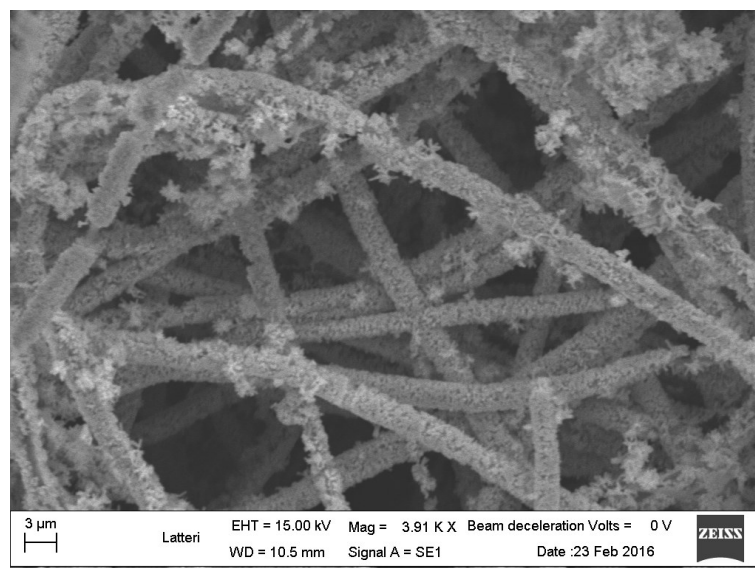
Figure 7.53 ES fibers after CBD seed 1h at 150°C

7.4.7 Characterization of Electrospun fibers for antibacterial UF membranes

In the last part of my PhD I tried to obtain active UF membranes with antibacterial properties. In fact, filtration of microorganisms by conventional membranes leads to the formation of biofilms, which significantly decrease the quality of filtered water.

For this purpose a polymeric solution was prepared as described in *7.2.1* and electrospun. During the electrospinning process, due to the high temperature, the silver precursor is converted into silver nanoparticles[9]. Below the characterization of the obtained membranes is reported.

SEM and EXD Analysis

In Figures 7.54 and 7.55 morphological analysis of fibers electrospun with the two different precursors are shown. The fibers show smooth surfaces and no sign of significant defects is observable.
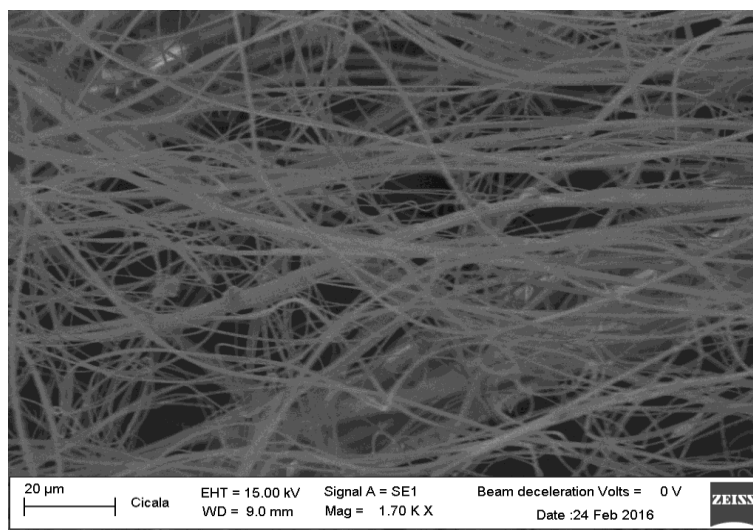
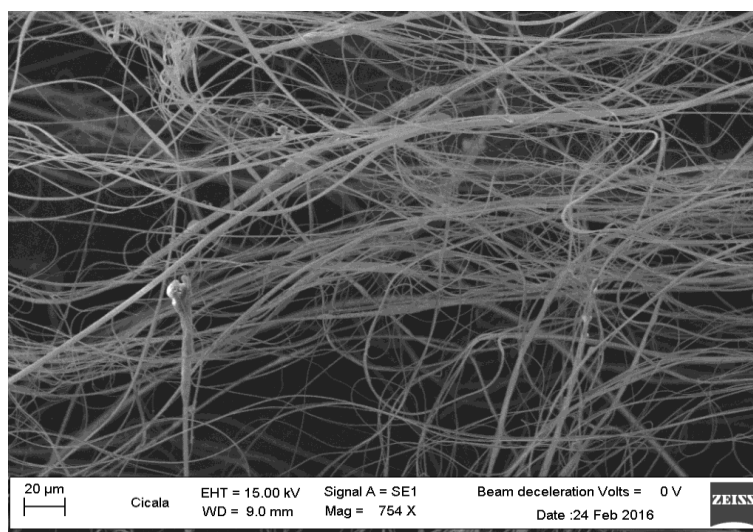**Figure 7.54 ES VERADEL fibers + Ag(hfa)**

Figure 7.55 ES VERADEL fibers + AgNO₃

In order to confirm that silver nanoparticles are present inside the fibers an EDX analysis was done and the result is reported in Figure 7.56 where is possible to distinguish the Ag peak.
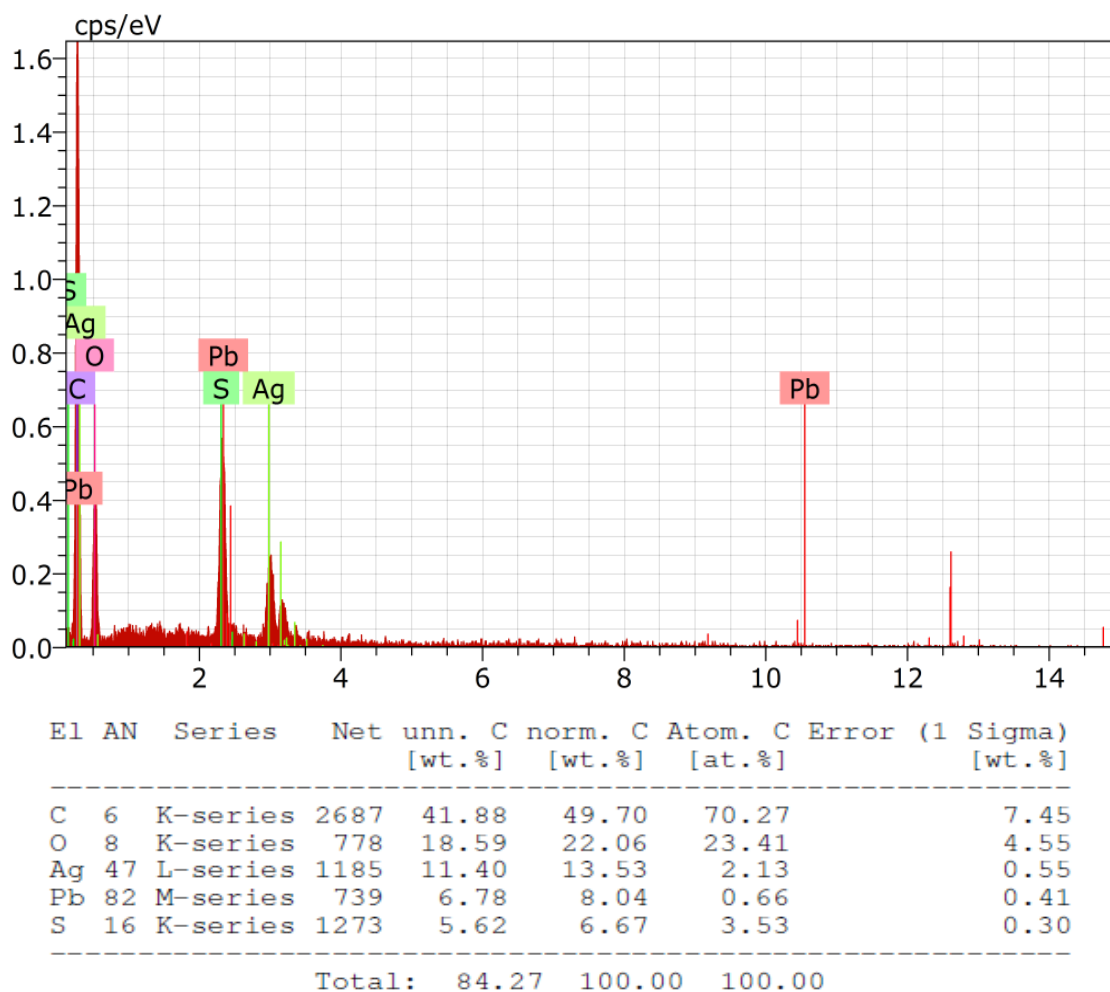
Figure 7.56 EDX Analysis of VERADEL + AgNO₃ fibers

El	AN	Series	Net	unn. C [wt.%]	norm. C [wt.%]	Atom. C [at.%]	Error (1 Sigma) [wt.%]
C	6	K-series	2687	41.88	49.70	70.27	7.45
O	8	K-series	778	18.59	22.06	23.41	4.55
Ag	47	L-series	1185	11.40	13.53	2.13	0.55
Pb	82	M-series	739	6.78	8.04	0.66	0.41
S	16	K-series	1273	5.62	6.67	3.53	0.30
			Total:	84.27	100.00	100.00	

UV Analysis

The last characterization of this fibers was an UV-vis Spectroscopy in order to confirm the conversion of the silver precursors into silver nanoparticles. For this analysis the Plasmon Resonance of the silver nanoparticles was investigated. Plasmons are the collective oscillation of free electrons in a conducting material. When the frequency of the incident light matches the resonant oscillation frequency, the nanoparticles absorb the light efficiently[10]. In particular silver nanoparticles absorbe ligth at λ= 450 nm.

In Figure 7.57 is possible to observe that for the VERADEL fibers with silver precursors the peak at 450nm is present while it's not present for the VERADEL fibers, that confirms the conversion of the silver precursors into silver nanoparticles.
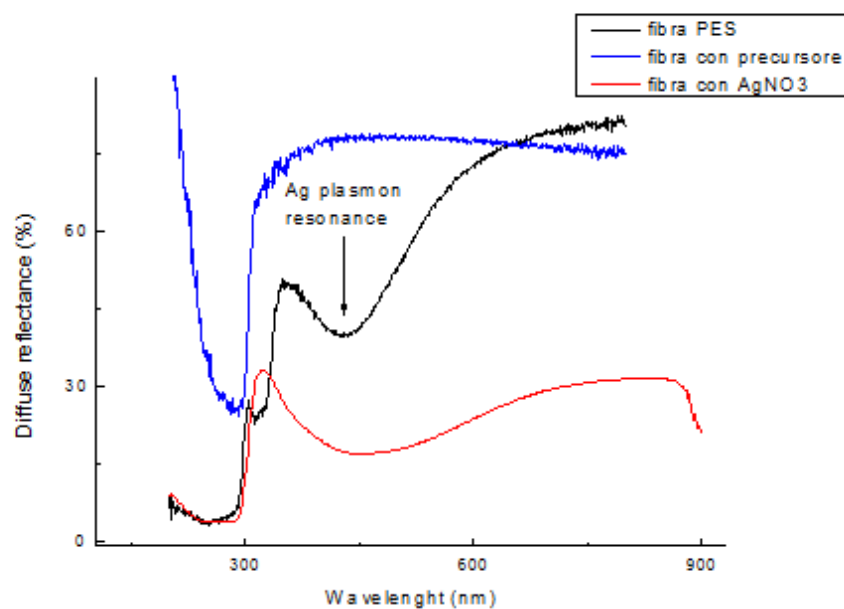

Figure 7.57 UV Spectroscopy characterzation

7.5 Chapter 7 References

[1] C. Puglisi et al., Polymer Elsevier, (2006**).**

[2] I.Blanco et al., J. Therm. Anal. Calorim. 107, 1083-1091 (2012)

[3] Narain, John Wiley & Sons Inc, Hoboken, New Jersey, 2014, pp. 348-351

[4] B. Alvarado-Tenorio et al., *Macromolecules* 44, 5682–5692 (2011)

[5] M.E. Fragalà et al., Chem Mater

[6] W.A.Murray et al., *Nano Lett*. 6:1772-1777,(2006);

[7] Overbeke E. et al., Polymer, 44, 4899 (2003).

[8] M.E.Fragalà et al., *CrystEngComm*, 2009, 11, 2770–2775.

[9]Dhyah Annur et al., Biomacromolecules 2015, 16, 3248−3255

[10] H. Chen et al., Today, 2010, 5, 494–505.

8. Conclusion and Recommendations for Future Works

As seen before, the aim of this PhD project was the development of novel multifunctional composites, based on the use of hierarchical structuring, to use for two different applications: as nano-toughener for composite laminates and as active membranes for water filtration.

The choice of coPESs as thermoplastic polymers to electrospin turned out to work well. The electrospinning process did not show any difficulties in particular boh for the neat coPES and the nanoparticle-filled ones. MWCNT were more difficult to disperse with respect to SiO2 and POSS particle because of MWCNTs tendency to stay agglomerated.

The molar mass of the coPES showed a significant effect on the dissolution behavior of the veils studied. Larger masses led to longer dissolution times. The addition of nanofiller increased dissolution times as well. Their presence inside electrospun nanofibers was confirmed by SME, EDX and TEM analysis.

The addition of nanofillers affected positively the Tgs of the samples and also the elastic moduli for nanofilled-coPES9k veils. A higher Tgs difference for samples prepared with coPES9k veil and their prepreg counterpart were observed for carbon-reinforced samples. The filtering effect of carbon fibers, which altered the diffusion path of coPES9k, explained these differences. The diffusion of coPES9k across the laminate thickness was qualitatively assessed by placing coPES9k in middle layers only. Commercial PESs by Solveay, Virantage® 30500 and Virantage® 10200 were able to be electrospun in the same conditions of coPES9k. They both were totally dissolved in the epoxies composite laminates., increasing the Tg of the epoxy-rich phase.

The results presented are relevant for the correct design of electrospun veils for the toughening of epoxy resin composites.

Recommendations for future work, for the first part of the project are:

- better dispersion of nanoparticles in polymer solutions thus increasing the mass fraction in the elctrospun veil, in order to achieve higher percentages in the finale epoxy matrix;

- to evaluate the functionalities given by the presence of nanoparticles to the final composite laminate.

In the second part of the PhD project, ZnO doped PES fibrous mats are obtained by roll-to-roll electrospinning of polymer solutions doped with zinc acetate.

The choice of commercial PES (VERADEL) as organic part of the membrane to electrospin turned out to work well. Also in this case the electrospinning process did not show any difficulties. The presence of Zn acetate contributes to thermally stabilize the polymeric composite, due to formation of ZnO during thermal treatments. An easy and cost effective seeding strategy allows for a high yield growth of ZnO nanostructures onto the obtained polymeric mats. In particular, brush-like ZnO nanorods are grown on the obtained sub-micrometer PES fibres by Chemical Bath Deposition to obtain highly nanostructured surfaces with a high level of crystallinity. These hierarchical mats are water resistant and photocatalytic actives. Furthermore, an optimization of the process conditions was done. All these aspects, combined with the process simplicity and scalability to larger volumes are extremely important in the perspective of fabrication of active filter for water purification.

The last work of this thesis was about the production of membranes for UF with antibacterial activity. In particular, membranes with silver nanoparticles was produced starting from a precursor solution and by only the electrospinning process. The conversion of silver precursor into silver nanoparticles was confirmed by UV analysis.

Recommendations for future work, for the this part of the project are:

- to test the properties of the membranes with ZnO nanorods as antibiofouling agent;

- to test the real antibacterial activity o of the membranes with AgNPs;

- try to develop a membrane with both ZnO and AgNPs in order to have UF membranes with more funtionalities.